Heat Extraction System for Augmenting the Heating and Peak Shifting Ability of Electrically Heated Floor Residential Buildings

Ying Sun

A Thesis
In the Department
of
Building, Civil and Environmental Engineering

Presented in Partial Fulfillment of the Requirements
For the Degree of
Master of Applied Science (Building Engineering) at
Concordia University
Montreal, Québec, Canada

July 2018

CONCORDIA UNIVERSITY

School of Graduate Studies

This is to certify that the thesis prepared

By: **Ying Sun**

Entitled: **Heat Extraction System for Augmenting the Heating and Peak Shifting Ability of Electrically Heated Floor Residential Buildings**

and submitted in partial fulfillment of the requirements for the degree of

Master of Applied Science (Building Engineering)

complies with the regulations of the University and meets the accepted standards with respect to originality and quality.

Signed by the final examining committee:

Dr. H. Ge Chair / Examiner

Dr. G. Gouw Examiner

Dr. B. Lee Examiner

Dr. F. Haghighat Supervisor

Approved by Dr. F. Haghighat

Chair of Department or Graduate Program Director

Dr. A. Asif

Dean of Faculty

Date July 17, 2018

ABSTRACT

Peak shifting plays a vital role in easing the stress on electrical grids as well as in reducing the electricity bill for consumers by taking benefit of the time-of-use tariff. In cold climates, this can be achieved effectively by storing the heat in thermal energy storage (TES) systems during off-peak periods and releasing the stored heat during peak periods. In this regard, building integrated thermal energy storage (BITES) systems (e.g. ventilated wall, electrically heated floor (EHF) with high thermal mass (e.g. bricks, concrete), hydronic heated floor etc.) can be used. It is worth stating that a well-designed BITES system can completely shift the load from peak periods to other periods. On the other hand, residential buildings in places like North America face practical constraints on incorporating high thermal mass into each envelope and each room. To overcome this limitation and also mainly to increase the percentage of peak load shifting, the present work proposes a forced ventilation system/heat extraction system (HES) to transfer the additional heat from zones with well-designed BITES system to zones with no such provisions.

In this study, a multistory house, in which the BITES system (i.e. EHF) is mainly installed on the basement floor is developed in TRNSYS and validated using the field measurement data. The validated model is then utilized to evaluate the peak shifting potential of the existing EHF under different heating strategies. It is inferred from the simulation results that the existing EHFs almost had the ability to completely shift the heating consumption in the basement from peak period to other periods). Further, the potential of HES to transfer the heat from the basement to the second floor are investigated in terms of its heating performance (effect of air flow rate and outlet location) and ability to extend the peak shifting potential of EHF. The key finding of the present study is that the HES augments the peak shifting potential of EHF up to 19%. Also, it is inferred that the proposed methodology increases the heating energy consumption by 18% but decreases the daily heating cost by 24%. It should be mentioned that the increase in energy consumption is due to the prolonged operation of the basement EHF during the off-peak period and the decrease in energy cost is because of shifting the peak to the off-peak period.

The proposed concept would be a benefit to both supplier and consumer in terms of peak shifting and heating cost saving. Also, the proposed methodology resolves the constraint of incorporating higher thermal mass in each floor of the residential buildings.

ACKNOWLEDGMENTS

First and foremost, I would like to express my deep appreciation to my supervisor, Dr. Fariborz Haghighat. Many thanks for the opportunity he gave me to be a part of his research team. I am and will always be extremely grateful for the support, guidance and trust from him. Because of his kindness and help, I could finish my project on the time.

I would like to appreciate my friends, Dr. Mahmood Mastani Joybari and Dr. Karthik Panchabikesan, for their helpful suggestions for this project. Their generous and patient help to review and modify my reports, paper and thesis was a big assistance for me.

I would also like to thank all those with whom I worked during this project: Alain Moreau and Stéphane Boyer from Laboratoire des téchnologies de l'énergie d'Hydro-Québec, Miguel Robichaud from Ouellet Canada, and my colleagues (Hélène and Dave). Their expertise and patience helped me to be familiar and confident about this project.

I would like to show my appreciation to Dr. Zhun Yu, professor from Hunan University, China. Because of him, I began to be interested in research works and had the opportunity to start Master's program.

I extend my deep thanks to all my colleagues (Behrang, Emilie, Jun, Jianing, Maryam, Soroush) for their kindness, friendliness and selfless help. Working with them was a fantastic experience for me.

Last but not least, I would like to thank my grandma, Yucui Liu, my mother, Xiangzun Cui, my father, Chengzhi Sun, and my brother, Yifan for their understanding and support. I could not have finished this Master's program without their love and encouragement.

CONTRIBUTION OF AUTHORS

Chapter	**2, 3, 4**
Title	Enhancement in peak shifting and shaving potential of electrically heated floor residential buildings using heat extraction system
Authors	Ying Sun, Karthik Panchabikesan, Mahmood Mastani Joybari, Dave Olsthoorn, Alain Moreau, Miguel Robichaud, Fariborz Haghighat
Status	Accepted for publication in Journal of Energy Storage
Description	All the results reported in the paper are included in this thesis. The main contributions of the published paper are listed as below. (1) Integration heat extraction system (HES) into an existing electrically heated floor (EHF) house; (2) Exploration of the peak shifting ability of the existing EHF, and the EHF with HES; (3) Results showed that the integration of EHF and HES decreased the daily heating cost by 24%.

TABLE OF CONTENTS

LIST OF FIGURES

LIST OF TABLES

LIST OF SYMBOLS AND ABBREVIATIONS

Symbols

$A_{i,wall}$	Exterior wall area of zone i [m^2]
A_{wall}	Exterior wall area of the whole house [m^2]
$A_{i,win}$	Exterior door/window area of zone i [m^2]
A_{win}	Exterior door/window area of the whole house [m^2]
A_j	Area of component j [m^2]
c	Global flow coefficient [$m^3.s^{-1}.Pa^{-n}$]
c_j	Flow coefficient for component j [$m^3.s^{-1}.Pa^{-n}$]
$c_{j,AIVC}$	Flow coefficient for component j from the Technical Note AIVC44 (Orme et al., 1994) [$m^3.s^{-1}.Pa^{-n}$]
$c_{j,wdw}$	Flow coefficient for exterior window/door/wall j [$m^3.s^{-1}.Pa^{-n}$]
c_{test}	Global flow coefficient of the whole unit measured by air-tightness test [$m^3.s^{-1}.Pa^{-n}$]
D_{peak}	Duration of peak period [h]
D_{mid}	Duration of mid-peak period [h]
D_{off}	Duration of off-peak period [h]
E_{peak}	Electricity price during peak period [CAD/kWh]
E_{mid}	Electricity price during mid-peak period [CAD/kWh]
E_{off}	Electricity price during off-peak period [CAD/kWh]
F_{ST}	Floor surface temperature [°C]
h_{WW}	Convective heat transfer coefficients at windward exterior surfaces[$W.m^{-2}.K^{-1}$]
h_{LW}	Convective heat transfer coefficients at leeward exterior surfaces[$W.m^{-2}.K^{-1}$]
i	Zone number [-]
j	Component number [-]
m_t	Measured value at time t
$\bar{m}$	Average of the measured values
n	Global flow exponent [-]
$n_{j,AIVC}$	Flow exponent for component j from the Technical Note AIVC44 (Orme et al., 1994) [-]
n_{test}	Global flow exponent of the whole unit measured by air-tightness test [-]
N	The number of data points
p	The number of adjustable model parameters
ΔP	Pressure difference [Pa]
P_{peak}	Power consumption during peak period [kW]
P_{mid}	Power consumption during mid-peak period [kW]
P_{off}	Power consumption during off-peak period [kW]

$P_{peak,basement}$	Power consumed by besement during peak period [kW]
$P_{mid,basement}$	Power consumed by besement during mid-peak period [kW]
$P_{off,basement}$	Power consumed by besement during off-peak period [kW]
$P_{ave,basement}$	Average power consumed by the basement [W]
$P_{nominal}$	Nominal power of EHFs [W]
Q	Global volumetric flow rate [$m^3.s^{-1}$]
Q_i	Infiltration for zone i [$m^3.s^{-1}$]
$Q_{j,75Pa}$	The maximum leakage value for component j at 75Pa ("National Energy Code of Canada for Buildings, 2015," 2015) [$m^3.m^{-2}.s^{-1}$]
s_t	Simulated output at time t
T_{in}	Interior air temperature [°C]
$T_{in,i,t}$	The air temperature of zone i on that floor or house at time t [°C]
$T_{ave,mean}$	Average mean second floor air temperature [°C]
$T_{max,mean}$	Maximum mean second floor air temperature [°C]
T_{max}	Maximum room temperature within the second floor [°C]
$T_{mean,t}$	The area weighted mean temperature of one floor or the whole house at time t [°C]
T_{min}	Minimum room temperature within the second floor [°C]
$T_{min,mean}$	Minimum mean second floor air temperature [°C]
$T_{min,mean}$	Minimum mean second floor air temperature [°C]
U	Wind speed [$m.s^{-1}$]

Abbreviations

abs(*NMBE*)	Absolute value of NMBE [%]
ASHRAE	The American Society of Heating, Refrigerating and Air-Conditioning Engineers
ANSI/BPI	American National Standards Institute/ Building Performance Institute
CAD	Canadian Dollar
CFM	Cubic feet per minute [$ft^3.\ min^{-1}$]
CV(*RMSE*)	Coefficient of Variance of the Root Mean Square Error [%]
EHF	Electrically Heated floor
FEMP	Federal Energy Management Program
HES	Heat Extraction System
HHF	Hydronic Heated Floor
IPMVP	International Performance Measurement and Verification Protocol

NMBE	Normalized Mean Bias Error [%]
NRS	Night-Running Strategy
PCM	Phase Change Materials
PSS	Peak Shifting Strategy
TES	Thermal Energy Storage
TRNSYS	TRaNsient SYstems Simulation program

INTRODUCTION

1.1. BACKGROUND AND MOTIVATION

In Canada, space heating accounted for 55% of the total energy consumption in commercial and institutional sectors in 2013, while the energy spent for space heating was 63% for residential sector (NRCAN, 2016). Since heating demand mainly occurs in cold season, the energy consumption gets further intense during winter. Besides, due to occupant living habits and climatic factors, daily peaks of energy consumption generally occur during the morning (e.g. 6 a.m. to 10 a.m.) and/or late afternoon (e.g. 4 p.m. to 10 p.m.) (Lanoue and Mousseau, 2014; Thieblemont et al., 2017). Note that, electricity consumption of a single house during peak periods could be 20 times higher than the average consumption ((Freris and Infield, 2013). This high electricity demand during the peak period further increases the stress on the electricity grid. If the energy consumption during the peak period exceeds the normal demand, utility providers should spend additional costs to either generate the additional load or purchase power at higher prices from neighboring grids (Hydro-Québec, 2017). As a result, time-of-use tariffs are commonly adopted worldwide (Guerassimoff and Maïzi, 2012; Yang et al., 2013). This means that changing the energy consumption pattern or developing procedure to reduce peak demand will not only release the stress on the electrical grid but also enable the consumers to save their electricity bill.

To decrease the peak demand, the following suggestions/solutions have been proposed in the literature:

(1) Encouraging consumers to change their energy consumption habits (e.g. postponing the use of the dishwasher and hot water from peak periods to off-peak periods). However, the anticipated reduction of peak demand in this case might be negligible (M. Crawley, 2016).

(2) Increasing the thermal resistance of building envelopes, thus decreasing the heating/cooling demand of the building (Olsthoorn et al., 2017). However, the initial investment/renovating cost of this solution is usually significant. Besides, in some regions, due to the large thermal resistance, heat released due to occupant behavior may not be lost to the ambient

during summer. Thus, cooling load will get increased. Thus, this solution might result in negative effect on peak demand reduction.

(3) Storing the energy during off-peak periods or during periods with availability of solar energy and utilizing it later during peak periods (Romaní, Belusko, et al., 2018). It needs to be noted that although this solution is effective in peak load shifting, it may increase the daily energy consumption due to the prolonged operation of charging process during off-peak periods. If the consumed energy mainly comes from electricity, which is produced from fossil fuels, the increased energy consumption would lead to more greenhouse gas emission. However, this issue can be negligible for buildings in Québec, Canada, where the energy is mainly produced from the renewable resources (i.e. hydroelectricity) (Hydro-Québec, 2017).

Considering the uncertainty in the performance of the first suggestion and initial investment/renovating cost of the second solution, shifting peak power consumption using thermal energy storage (TES) systems is worth investigating from a sustainability standpoint.

Envelopes (i.e. walls, ceilings and floors) constructed with materials which have the ability to store energy (e.g. materials with high thermal mass or phase change materials (PCM)) could be considered as one way to incorporate TES into buildings (Navarro et al., 2016). This kind of system has been defined as building-integrated thermal energy storage (BITES) system (Y. Chen et al., 2014). Significant research has been done to investigate the heating/cooling ability of BITES systems, which will be reviewed in Chapter 2.

However, in reality, due to the design and/or cost constraints, BITES systems are usually installed in a specific part of a building. For instance, majority of residential houses in North America are built in wood, while basement is the only place that has the provision for having concrete slabs. This constraint in the structure of buildings limits the application of concrete slabs as BITES into all rooms. Further, the peak shifting potential of BITES is limited by their scope of action (i.e. the area could be heated by releasing the stored energy of BITES). One way to extend the peak shifting ability of partially installed BITES system is to extract the stored energy to heat other areas (which has no provision for employing TES system). This method is called heat extraction system (HES) in this thesis.

Before implementing HES, it must be ensured that the BITES system has the ability to store and supply the additional energy within it. Besides, before practicing a new proposed system to real practice, it must be evaluated and considered as theoretically applicable. This can be done by performing the parametric analysis through simulation. Pan et al. (2007) illustrated that building simulation is helpful to analyze and evaluate the energy performance of potential energy saving methods. Considering the need/potential of peak shifting in reducing the residential buildings heating cost and the structural constraints of residential buildings in places like North America, this present work focuses on investigating the peak shifting potential of partially installed BITES system and further an HES is proposed to extend its peak shifting ability based on simulation study.

1.2. OBJECTIVES

The main objective of the present research work is to explore the possibilities of extending the heating and peak shifting capacity of a BITES system/electrically heated floor (EHF) in residential buildings through the integration of forced ventilation system or also called heat extraction system. To achieve the primary objective, the following specific objectives are proposed and carried out.

- To develop a multi-zone building model with EHF in basement (similar to the experimental house) to predict the inter-zone temperature and heating energy consumption.
- To validate the prediction made by the developed model with the field measured data.
- To investigate the peak shifting potential of existing EHF installed in the basement under different heating strategies utilizing the validated model.
- To investigate the potential of the proposed heat extraction system towards transferring the heat from the basement to the second floor in terms of its heating performance as well as its ability to extend the peak shifting potential of EHF.
- To analyze the heating cost saving potential of the proposed integrated system (EHF and HES) by considering the time-of-use tariff in Ontario, Canada

1.3. THESIS OUTLINE

In **Chapter 1,** general introduction regarding the role of TES, BITES in peak shifting along with the background and motivation of the present study is presented. Then, the main objective and specific objectives of this thesis is proposed, followed by the thesis outline.

In **Chapter 2,** previous research works that focused on reporting the peak shifting ability of BITES in terms of passive or active system are reviewed in detail. Later in this chapter, major inference from the literature is summarized.

In **Chapter 3,** the description of the residential house based on which the simulation study was carried out is given. Then, the details over the data collected and monitored from the house as well as the function of these data are presented. Subsequently, the methodologies applied to carry out the three research tasks: (1) developing and validating the multi-zone models, (2) exploring the peak shifting potential of EHF, (3) investigating the heating and peak shifting extending performance of a proposed HES are briefed in detail.

In **Chapter 4,** the results of the three aforesaid tasks are presented discussed in detail.

In **Chapter 5,** the major conclusions arrived based on investigations carried out in the present study are summarized. Later in this chapter, the scope for future work and recommendations are made.

CHAPTER TWO: LITERATURE REVIEW

In this chapter, detailed literature review is carried out for building-integrated thermal energy storage (BITES) systems applied for peak shifting or peak shaving. BITES systems utilize thermal mass of building fabric (e.g. concrete walls and slabs, etc.) as thermal energy storage (TES) system (Y. Chen et al., 2014). Through storing energy during off-peak periods or during periods with availability of solar energy and releasing it later during peak period, BITES systems are widely utilized to meet gaps between thermal energy supply and demand in buildings (Alva et al., 2018). The gaps mainly include the time difference between generation and consumption as well as cost difference between peak and off-peak periods of a day. This advantageous of BITES has been evaluated by Romanchenko et al. (2018). They compared the decrease of heat load variation when implementing BITES or hot water tank to multi-family residential buildings (i.e. a district heating system). The results showed that BITES were efficient for short-term energy storage and it decreased the daily net load variations by 20%. Moreover, the investment cost of BITES was 10-fold lower than that of hot water tank system. More works focusing on the peak shifting capability of BITES are summarized later in this chapter. They are reviewed in the order of storage mechanisms, i.e. passive or active. Passive BITES systems store energy without any mechanical input, while active BITES systems are charged or discharged by a mechanical forced source (i.e. air, water or electricity) incorporated within building fabric.

2.1. PASSIVE BITES

In the passive BITES system, energy is stored/released by natural heat transfer. Therefore, no maintenance cost for mechanical devices and convenience in its implementation encouraged researchers to practice it for peak shifting or peak shaving. Zhu et al. (2009) reported that exterior wall with high thermal mass had the ability to store sufficient heat during the daytime and release it during night. During heating season, the heating demand in a room with concrete wall was lower than a room with conventional wood frames. Besides, variations in the internal surface temperature of the investigated concrete wall was less than the wood wall.

Ip and Miller (2009) analyzed the seasonal thermal storage ability of earth-rammed thermal mass based on data collected from the Brighton Earthship in which a rammed earth-sheltered wall was located. The inference from their study is that the thermal mass in the wall could store heat during summer and release it during winter to keep a higher indoor temperature. However, additional heating was still required to maintain thermal comfort in winter.

Hollow walls with air flowing through their channels (due to stack effect) can also be considered as passive BITES. Alaidroos and Krarti (2016) proposed a passive cooling strategy in which a ventilated wall cavity was coupled with spray evaporative cooling system, as shown in Figure 2.1. The principle was that outdoor air was cooled by the spray system initially, then, flew down through the cavity and supplied to the indoor. Through an optimized control strategy, the ventilated wall reduced the cooling energy consumption by 23% or 100% for long term (one season or one year) or short term (one hour or one-day), respectively, compared with conventional concrete wall (Alaidroos and Krarti, 2017). Besides, thermal performance of a novel ventilated brick wall has been studied by Buratti et al. (2018).

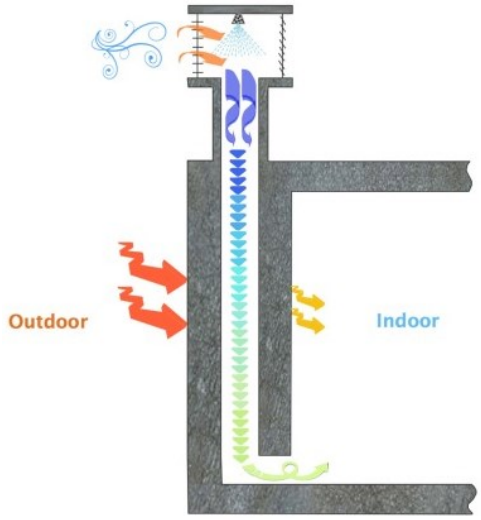

Figure 2.1: Schematic diagram of the ventilated wall cavity (Alaidroos and Krarti, 2016)

In terms of applying sensible passive BITES to the whole building, a two-story experimental passive house has been investigated through simulation by Robillart et al. (2018). In this house, most constructions (e.g. exterior walls, ground floor and intermediate floor, etc.,) were made of concrete with high thermal mass. A model predictive control has been proposed to

enhance the peak load shifting capability of the house. Their study showed that when exterior temperature fluctuated between -14 °C and 11.3 °C, the model predictive control completely shifted the heating load from peak period to off-peak period. On the other hand, energy consumed during the peak period represented 55% (if there was 1 occupancy) or 33% (if there were 2 occupancy) of the total energy consumption in reference case with a constant set-point temperature (19 °C). The reason for the high percentage of peak shifting is that the high thermal mass of envelopes stored the heat during off-peak period and released it later during peak-period. Note that the house was assumed as one zone during simulation.

To offer or increase TES density to building envelopes, PCM could be integrated into conventional construction. Zhang et al. (2005) compared the performance of PCM-integrated exterior wall and typical residential frame wall by incorporating them into two test houses, shown in Figure 2.2. Result showed that the reduction of average space cooling load was around 8.6% and 10.85% when 10wt% and 20wt% PCM was applied, respectively. Similar experimental set up has been utilized by Cabeza et al. (2007) : two house-like cubicles (one was constructed with conventional concrete, and the other one was structured by concrete and micro-encapsulated PCMs) were built. Results indicated that energy storage of concrete walls incorporated with micro-encapsulated PCMs would result in a two hour delay of peak indoor temperature in summer and also a lower indoor temperature fluctuation. Lee et al. (2015) utilized similar set up to evaluate the heat flux reduction and time delay of residential building walls integrated with a thin PCM layer. The maximum peak heat flux reduction in the test house integrated with PCM layer was around 57 % and the time delay was around 6 h, compared to the test house with traditional walls. They did further experiments using the same set up and found that the PCM-enhanced walls reduced the peak space cooling load of a test house by 26.75% compared to the house with typical residential frame wall (Lee et al., 2018). Also, integrating PCM into walls resulted in the time delay of peak heat fluxes by about 1.5 hour.

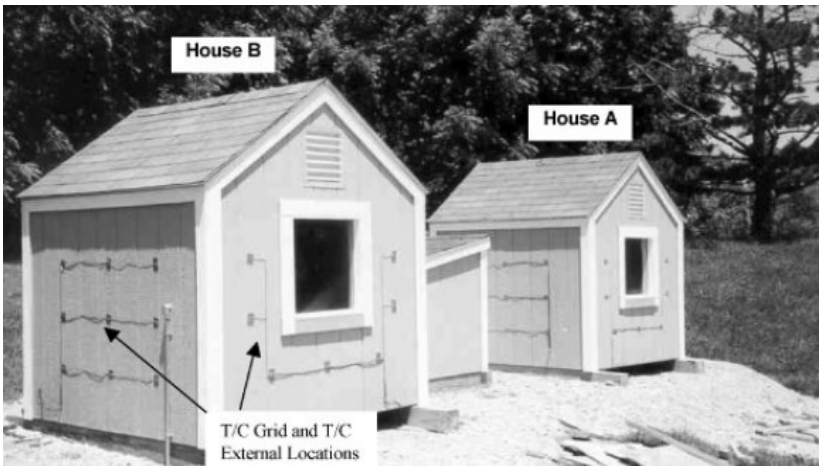

Figure 2.2: Test houses in the experiment of Zhang et al. (2005)

Kosny et al. (2012) found that a south oriented vertical frame wall, within which the PCM-enhanced insulation was placed, could reduce about 20% - 35% peak-hour load and delay the heat flow rate oscillations about three hours. Besides, Fateh et al. (2017) presented that placing a PCM insulation layer in the middle of a typical wallboard could result in a maximum cooling load reduction of 15% and delay the occurrence of peak heat flux about 2 hours.

Barzin et al. (2015) compared the space heating demand of two test huts which were constructed using lightweight materials. The difference between these huts was that in the first hut, the interior walls and ceiling were furnished with ordinary 13 mm gypsum wallboards and in the second hut, 10mm gypsum board plus a layer of 5.2 mm PCM sheet was used. The application of PCM incorporated wallboards shifted the heating demand from early evening peak period (between 5 pm and 8 pm) to off-peak period – midnight, because of thermal stored from solar irradiation and off-peak period heating. Note that the ambient temperature nearly never dropped below 10 °C during the experiment.

Guarino et al. (2017) investigated the peak load shifting capability of an interior passive PCM wall in a test room with 2.80×1.30×2.44 m dimensions, shown in Figure 2.3. The PCM layers were installed on the interior surface, which was facing a large window with 2.0×2.0 m dimensions (60% window to wall ratio). Results showed that after storing heat through absorbing solar radiation during daytime, the discharge phase of these PCM layers was prolonged 6-8 h after the end of solar irradiation. Besides, the peak heating load and peak cooling load could be decreased by 40% and 17% during high solar irradiation days in winter and summer, respectively. Also, the

proposed passive TES wall was effective to decrease the yearly heating and cooling energy consumption.

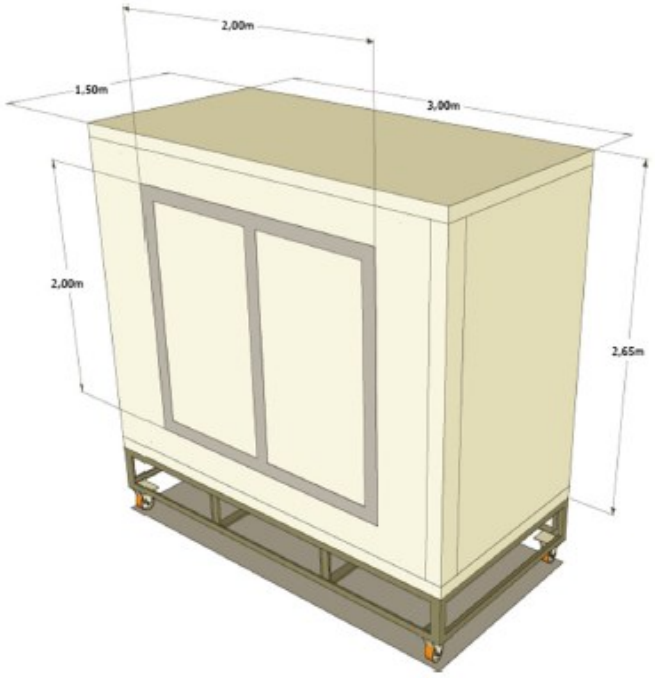

Figure 2.3: Schematic diagram of the test room in the study of Guarino et al (2017)

Integrating PCMs into residential buildings for passive thermal control has been reviewed by Kenisarin and Mahkamov (2016). They summarized and compared seventeen projects, which aimed at analyzing thermal performance of construction elements with PCM through small model and real size rooms. Descriptions of these projects are reorganized in Table 2.1. Conclusions from this review were that integrating PCM into residential building envelopes for passive thermal energy storage could effectively (1) decrease the variation of room air temperature; (2) shift the peak heating or cooling load of lightweight building by several hours; (3) decrease energy consumed to maintain thermal comfort in residential buildings.

Table 2.1: Descriptions of projects that investigated TES performance of passive BITES with PCM in residential buildings

No.	Reference(s)	Project Location	Experiment set up		Result(s) and Inferences
			Room Dimensions, Length × Width × Height, m	**Control parameter(s)**	
1	(Rudd, 1993)	Building Science Corporation, USA	3.35×3.35×2.44	Standard wallboard	The thermal storage capacity of the PCM wallboard was averagely 2.1 times greater than that of the standard wallboard.
			3.35×3.35×2.44	PCM wallboard	
2	(Scalat et al., 1996)	Concordia University, Canada	2.29×2.27×2.45	Conventional gypsum boards	Integrating PCM into gypsum wallboards doubled the heat storage capacity of the traditional one.
			2.29×2.27×2.45	PCM impregnated gypsum wallboards	
3	(Athienitis et al., 1997)	Concordia University, Canada	2.82×2.22×2.24	PCM gypsum boards	Incorporating PCM into inside wall lining caused a 4 °C decrease of maximum room temperature during summer. Passive BITES system is effective to store solar gain and improve thermal comfort.
4	(Ismail and Castro, 1997)	University of Campinas, Brazil	1.25×1.80×1.70	Removable roof (fibrous cement with or without PCM layer); side wall (bricks with or without PCM layer)	The integration of PCM into walls and roof resulted in a stable indoor temperature, a decreased (around 34%) and displacement of peak load.
5	(Kondo et al., 2001)	Kanagawa University, Japan	3.60*2.70*2.60	Plasterboards	PCM wallboard decreased fluctuation of the indoor air temperature, reduced the peak electricity consumption, and shifted peak load from peak period to off-peak period.
			3.60*2.70*2.60	PCM wallboards	

Table 2.1: Descriptions of projects that investigated TES performance of passive BITES with PCM in residential buildings

No.	Reference(s)	Project Location	Experiment set up		Result(s) and Inferences
			Room Dimensions, Length × Width × Height, m	**Control parameter(s)**	
6	(Schossig et al., 2005)	Fraunhofer Institute for Solar Energy System, German	Two full-size test rooms	PCM plaster	The maximum room temperature during summer in the test room with PCM plaster was around 4 °C lower than in the room without PCM.
				Plaster	
7	(Principi et al., 2005)	Polytechnic University of Marche, Italy	3.00×3.00×3.00	Standard layers of plaster, mineral wool, clipboard etc.	Implementation of PCM layer reduced the inner surface temperature of the south wall.
			3.00×3.00×3.00	Standard layers with an additional PCM layer	
			3.00×3.00×3.00	Standard layers with an additional air and PCM layers	
8	(Shilei, Guohui, et al., 2007; Shilei, Neng, et al., 2006)	Shenyang, China	5.00×3.30×2.80	PCM wallboards	For heating mode, implementation of PCM wallboards decreased energy consumption by factor of 1.68, compared to that of conventional wallboards. For cooling mode, PCM wallboards significantly decreased the peak cooling load (around 30%)
9	(Luisa F Cabeza, Cecilia Castellon, et al., 2007; Luisa F Cabeza, Marc Medrano Martorell, et al., 2007)	Universitat de Lleida, Spain	2.00×3.00×2.00	Conventional concrete	Concrete walls incorporated with micro-encapsulated PCMs would result in a two hour delay of peak indoor temperature in summer and also a lower indoor temperature fluctuation.
			2.00×3.00×2.00	Concrete incorporated with micro-encapsulated PCMs.	
10	(Khudhair and Farid, 2009)	The University of Auckland, New Zeeland	2.60×2.60×2.60	Conventional gypsum wallboards	The application of PCM wallboards maintained a more comfortable interior environment.
			2.60×2.60×2.60	PCM wallboards	

Table 2.1: Descriptions of projects that investigated TES performance of passive BITES with PCM in residential buildings

No.	Reference(s)	Project Location	Experiment set up		Result(s) and Inferences
			Room Dimensions, Length × Width × Height, m	**Control parameter(s)**	
11	(Voelker et al., 2008)	Bauhaus University –Weimar, Germany and Czech Republic	4.43×2.50×2.95	Conventional wallboards	The application of PCM wallboards decreased the maximum interior temperature by 3°C during summer.
			4.43×2.50×2.95	PCM wallboards	
			4.43×2.50×2.95	Plasterboards	
			4.43×2.50×2.95	PCM wallboards and salt heat storage elements	
12	(Kuznik and Virgone, 2009a, 2009b; Kuznik et al., 2008)	Thermal Sciences Center of Lyon Project, France	3.10×3.10×2.50	Conventional gypsum wallboards	The application of phase change panels decreased overheating during summer. However, it did not improve the minimum interior temperature during winter.
			3.10×3.10×2.50	Composite phase change panel	
13	(Konuklu and Paksoy, 2009)	Çukurova University, Turkey	2.70×2.00×1.50	PCM sandwich panels	Summer: The application of PCM sandwich panel as inner walls decreased the maximum average interior temperature and cooling load by 2.5 °C and 7%, respectively. Winter: The increase of the average temperature and decrease of heating load was 2.2 °C and 17%, respectively.
14	(Castell et al., 2010; Castellón et al., 2009)	Universitat de Lleida, Spain	2.40×2.40×2.40	Bricks with/without PCM elements	The application of PCM elements decreased the maximum interior temperature by 1 °C during summer and delayed its occurrence by 2 hours. Besides, its application achieved 14% - 17% reduction of cooling load.

Table 2.1: Descriptions of projects that investigated TES performance of passive BITES with PCM in residential buildings

No.	Reference(s)	Project Location	Experiment set up		Result(s) and Inferences
			Room Dimensions, Length × Width × Height, m	**Control parameter(s)**	
15	(Bragança et al., 2011)	University of Minho, Portugal	Summer: 4.24×2.58×3.00	Gypsum-PCM mixture	Summer: The integration of PCM decreased the maximum interior temperature by 5 °C and increased the minimum temperature by 1.5 °C. Besides, the occurrence of maximum temperature was delayed 2-3 hours by its application. Winter: The room temperature was lower than PCM's melting temperature, thus, the effect of PCM was not significant.
				Gypsum plaster.	
			Winter: Two houses with two rooms	-	
16	(Bečkovský et al., 2011; Ostrý et al., 2011)	Brno University, Czech Republic	26.7 m^3	Conventional gypsum wallboards	Summer: The application of PCM decreased the interior temperature fluctuation. Winter: If the interior temperature could not reach phase change temperature, the effect of PCM was not obvious.
			26.7 m^3	Aluminum panels with a phase change composition	
17	(Mandilaras et al., 2013)	National University of Athens, Greece	A typical two-story residential house	All external walls and internal partitions were constructed by PCM gypsum boards.	The variation of room air temperature was not significant over a 24 h day-night cycle. However, the collected data was not enough to determine the influence of PCM panels on the thermal characteristics of the building.

From previous studies, the advantages and disadvantages of utilizing passive BITES to shift load could be summarized as following.

Advantages:

- Decreases both peak heating and cooling loads.
- Reduces temperature swing inside the room over a day.
- Does not required energy from the external source (e.g. electricity or fuel).

Disadvantages:

- The amount and duration of peak load shifting (for heating) highly depends on local weather conditions.
- The process of charging and discharging of TES system is often hard to control.
- The potential of peak shifting cannot be fully utilized most of time due to the uncertainty in weather condition and the process of charging and discharging.

Limited by above disadvantages, passive BITES applied in cold areas without high solar radiation can be inefficient to shift peak heating load during winter. This issue has been verified by Fallahi et al. (2010). They compared energy efficiency of naturally ventilated double-skin façade (passive) and mechanically ventilated double-skin façade (active) in a room with 3.60×1.50×2.50 m dimensions. The simulation results of developed numerical model indicated that the energy saving achieved in winter through applying this passive BITES was negligible. However, the active BITES resulted in 21% - 26% and 41% - 59% energy saving in summer and in winter, respectively. Therefore, in order to effectively utilize the thermal storage capacity of BITES to shift peak load, active systems have been investigated.

2.2. ACTIVE BITES

For active BITES systems, energy storage mediums are charged or discharged by a mechanical forced source (i.e. air, water or electricity). Unlike the passive BITES systems, which are usually integrated in exterior walls, active BITES can be conveniently integrated into most of envelopes. In following subsections, the application of active BITES to shift peak load would be reviewed in the order of locations (i.e. walls, ceilings and floors, and other locations).

2.2.1. INTEGRATION IN WALLS

The mechanical ventilated wall, shown in Figure 2.4, is one of the common ways to integrate active BITES in walls (Yu et al., 2018). Airflow is pumped through channels in the wall and exchanges heat with BITES, then enters the room to mix with the room air or returns to outdoor. Therefore, during off-peak periods or sunny days, hot air passes through the wall to charge it, and then during peak-periods, stored heat could be released to heat air. As a result, the peak load could be shifted or reduced. Chen et al. (2016) indicated that air circulated through hollow-core space of hollow-core masonry block walls could assist space heating and cooling. They proposed three configurations to enhance the thermal coupling between the ventilated active BITES and its zone, and thus enhance the heat exchange between them. However, their study did not apply the proposed BITES to shift peak load.

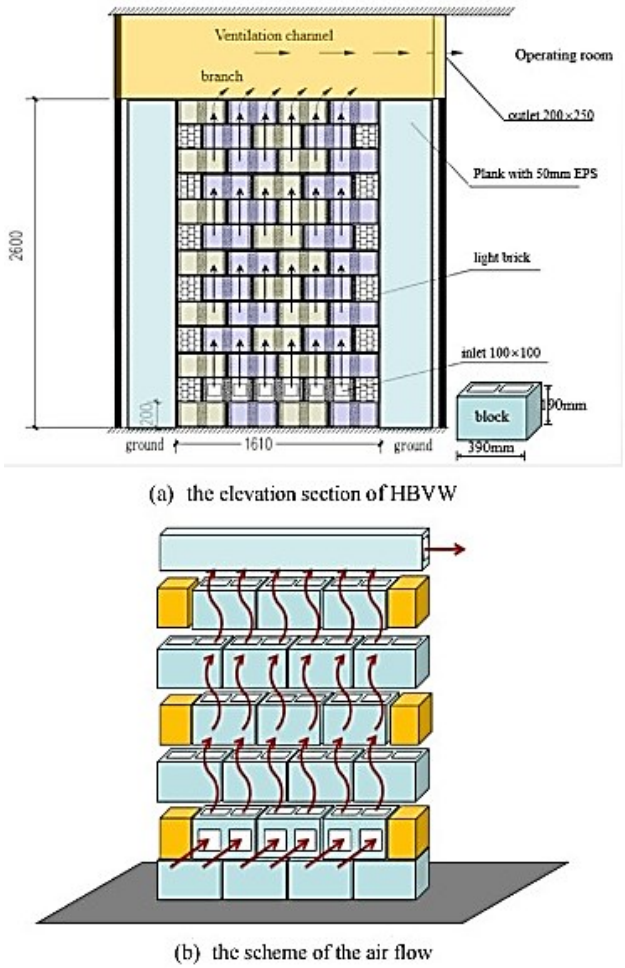

Figure 2.4: Schematic diagram of ventilated wall (Yu et al., 2018).

Thermal performance of a ventilation wall with PCM has been investigated by Chen et al (2016) and Chen et al. (2018). Compared with conventional walls without air channel as well as PCM, the proposed ventilation wall enhanced its heat storage capacity and release capacity by 35% - 48% and 50% - 60%, respectively.

Krzaczek and Kowalczuk (2011) proposed a thermal barrier system (shown in Figure 2.5) to heat or cool a space through supplying energy into the external walls instead of into the internal air directly. Simulation illustrated that exterior walls with the thermal barrier system decreased the heating and cooling demands of a residential detached house three times compared to the traditional exterior wall. However, the proposed system was not applied to shift peak load. The peak shifting performance of a similar cooling radiant wall coupled to a ground heat exchanger was evaluated by Romaní et al. (2016). In their study, the radiant wall and air-to-air heat pump was utilized to supply cooling to two house-like cubicles with dimensions of 5.25×2.7×2.7 m, respectively. Experimental results showed that after operating cooling from 0 am to 8 am at set-point 22 °C, the interior temperature of the cubicle cooled by radiant wall could be kept within an acceptable range all day, while the temperature of the other room exceeded the comfort limits 20.18 % of time. It means that cooling stored in the radiant wall during night could be released to the space and meets the cooling demand during daytime (peak period). A 2D numeric model was developed and validated for this radiant wall by Romaní et al. (2018). The simulated radiant wall was utilized as TES system and incorporated with a heat pump coupled to a PV array for peak load shifting (Romaní, Belusko, et al., 2018).

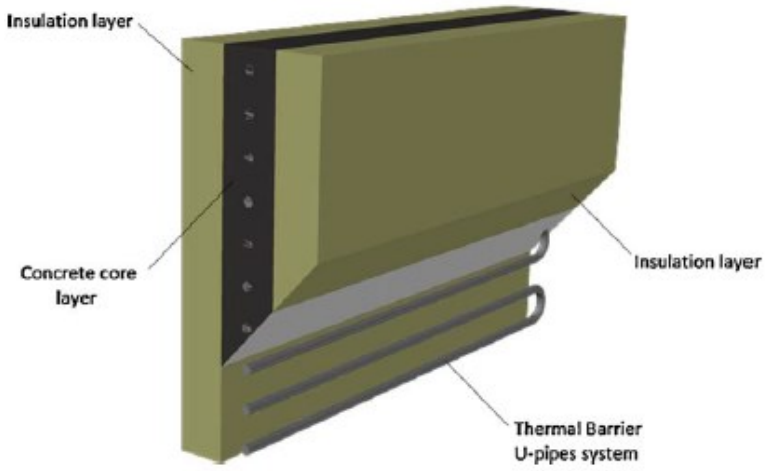

Figure 2.5: Schematic diagram of thermal barrier system proposed by Krzaczek and Kowalczuk (2011)

2.2.2. INTEGRATION IN CEILINGS AND FLOORS

Turner and Tovey (2006) analyzed the energy performance of an educational office building, the main part of which served by the hollow core ventilation system, shown in Figure 2.6. In this system, concrete hollow core ceiling slabs were utilized as supply air dusts and their high thermal mass was used to store thermal energy. Through monitored data, the annual heating for the main part of this experimental building could be decreased below good practice energy benchmarks if proper control strategy was operated. On the other hand, unlike the main part, the top floor was constructed by low thermal mass materials. Although the top floor only accounts for 10% of the total conditioned floor area, it consumed 53% and 74% of the building's total heating demand and cooling demand, respectively. This illustrated that high thermal mass effectively reduced energy consumed by maintaining the indoor environment within thermal comfort.

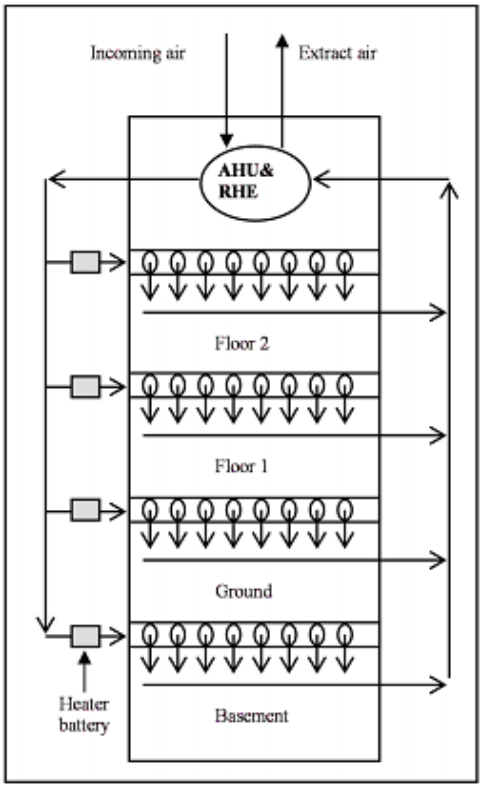

Figure 2.6: The operation of the main part of experimental building proposed by Turner and Tovey (2006)

The ventilated concrete slab, which was located in the basement of a residential house, was coupled with a building-integrated photovoltaic/thermal (BIPV/T) system to store the solar thermal

energy and meet heating demand during winter (Y. Chen et al., 2010; Y. Chen et al., 2016). During summer, cool outdoor air at night passes through the ventilated concrete slab to cool the house (Y. Chen et al., 2012; Y. Chen et al., 2016). Although the ventilated slab was considered as a kind of active BITES, the amount of peak load it could shift and the duration of peak period it could delay were not studied. Furthermore, note that this system was not designed to shift peak load through taking advantage of time-of-use tariff. Chae and Strand (2013) simulated the effect of placing ventilated slabs in the ceiling and floor on energy performance of an office building using EnergyPlus. Taking advantage of free cooling with night cool air, the application of ventilated slab reduced the peak-cooling load by 28%. Navarro et al. (2015) implemented similar system which had PCM inside its hollow to a cubicle with 2.4×2.4×5 m dimensions. During days with higher solar radiation in winter, the stored heat during daytime was sufficient to keep the interior temperature within a specified range during night. Note that the exterior temperature during the investigated winter periods varied from 1 °C to 26 °C. On the other hand, during summer (exterior temperature fluctuated between 14 °C and 36 °C), the coupling of ventilated slab and night cool air kept the interior air temperature under 25 °C during all day.

Prívara et al. (2011) tested a model predictive controller on the concrete ceiling radiant heating and cooling system of a real eight-story university building. Hot water was pumped into the pump, which was embedded into the ceiling. The presented model predictive controller achieved 17% – 24% overall savings during heating season, compared to a well-tuned weather-compensated controller. Besides, the presented controller could further reduce the peak-heating load because it effectively decreased the maximum inlet water temperature to the ceiling.

Koschenz and Lehmann (2004) proposed a hydronic activated PCM-ceiling panel which was beneficial for meeting the heating and cooling load of office and industrial buildings through utilizing renewable energy. Their simulation calculations helped to determine the required thermal properties and materials of the ceiling panel. However, the effect of energy storage of this ceiling panel on the peak load shifting was not studied. Pomianowski et al. (2012) numerically studied the dynamic heat storage and cooling capacity of a hydronic concrete slab with a PCM layer utilized as ceiling in a building. However, their study also did not focus on the peak shifting.

In terms of heating, a floor assembly can be integrated with a hydronic heated floor (HHF) system or electrically heated floor (EHF) system (Thieblemont, Haghighat, and Moreau, 2016).

The HHF provides heat by pumping hot water through pipes, which are usually laid under the flooring, while the EHF system works with electric cables or mats incorporated into the floor. The main determining factor of their peak shifting potential is thermal mass when just sensible storage is considered.

Lin et al. (2006) compared the peak shifting flexibility between a HHF and a fan-coil heating system. It was reported that when the exterior temperature was around 10°C, turning OFF heating systems resulted in indoor temperature dropping rate of 0.214 °C/h and 1.57 °C/h for the HHF system and the fan-coil heating system, respectively. It means once turning OFF, the HHF system could maintain the interior temperature within a comfort range for a longer period (around 7 times longer) than the fan-coil heating system. Similar comparison between a HHF system and a conventional baseboard heating system was done by Le Dréau and Heiselberg (2016). Their study was based on simulation through two building models developed in EnergyPlus. They found that the HHF system showed better peak shifting potential while maintaining the indoor air temperature within a comfortable range.

Jin and Zhang (2011) analyzed the peak shifting capability of a HHF with 10 mm wood and 30 mm concrete on top of the water pipes. Under specific boundary conditions, during the peak period (8am to 5pm), the heating system was turned OFF and the average heat-releasing rate was found to be about 55 W/ m^2. It means that once the heating demand was lower than the heat-releasing rate, the tested HHF system could completely shift the heating load from peak periods to off peak periods.

In order to enhance the heat storage capacity of a conventional HHF system, PCM was integrated into the concrete layer of the slab by Mazo et al. (2012). The simulation result found that the energy stored in HHF integrated with PCM during off-peak period met the heating demand of a cubicle during peak-period most of time. However, note that the cubicle in their study was located in a mild winter weather zone, which means the same HHF system integrated with PCM might not enough to completely shift the peak load when applying it to colder region. Moreover, Zhou and He (2015) compared the effect of different heat storage materials on the thermal performance of a HHF system. The discharge time of floor heating system integrated with PCM (9-11 hours) was about two times longer than that of floor using sand (5-6 hour). Besides, the heat supplied from the PCM integrated floor to the experimental room was nearly always higher than

from the floor utilizing sand. It means that the PCM could store more heat than sand. Thus, a novel hydronic floor system with two PCM layers has been proposed by Xia and Zhang (2016) to shift energy consumption from peak period to off-peak period during summer and winter.

As mentioned earlier, EHF heats the building directly by electric cables or panels placed under the floor surface. Thus, unlike the HHF, additional heating device, e.g. hot water tank, and hydraulic balance are not required for EHF. This means the installation of EHF is easier than the HHF. Besides, the operation pattern (ON/OFF) of EHFs could be flexibly adjusted according to occupants' desirable interior set-point temperature as a function of time. However, the response time of hydronic heated floors would be longer due to the complexity of changing fluid temperature and flow rate (HeavenlyHeat, 2018). Therefore, it is easier to achieve the set-point temperature difference between off-peak and peak period in the EHF system than in the hydronic heated floor system.

Barrio et al. (1992) indicated that the concrete mass in EHFs was widely utilized to store the useful sensible heat energy during the off-peak period. Thieblemont et al. (2016) proposed a method to integrate EHFs (shown in Figure 2.7) into TRNSYS by considering the thermal mass of concrete layers and carried out a parametric study to analyze the effect of floor assembly on the EHF performance. Their simulation results showed that the thickness of concrete layer below or above the EHF, and thickness of the insulation layer have significant influence over the peak shifting ability of the EHF system. To guarantee an acceptable indoor environment thermal comfort, Thieblemont et al. (2016) studied the peak shifting potential of an EHF in a multi-room house by using a partial night-control strategy. It was reported that EHF could shift 84% of building loads to the off-peak period. However, the building model developed in their study was validated using the data collected from the house with baseboards and not with EHF. The same drawback exists in the recent study of Thieblemont et al. (2018), where a self-learning predictive control strategy for EHF was proposed to reduce the energy demand during peak periods.

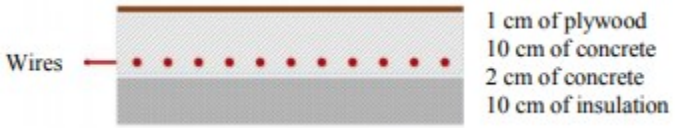

Figure 2.7: Schematic diagram of EHF in the study of Thieblemont et al. (2016)

However, incorporation of phase change materials (PCMs) into EHFs achieved high-energy storage density by latent heat storage. Lin et al. (2004) developed a model to simulate the thermal performance of an EHF system constructed using shape-stabilized PCM plates. Their model was verified by data collected from a single experimental room. El Mays et al. (2017) investigated the performance of an EHF incorporated with PCM in an insulated house. The results indicated that the hybrid EHF possessed the ability to maintain the room temperature above a minimum desired temperature for about 6 hours after turning OFF when the average ambient temperature was 14 °C. However, in their study, the indoor air temperature was allowed to reach 28 °C, which sacrificed the thermal comfort.

2.2.3. OTHER LOCATIONS

Ünalan et al. (2014) proposed a novel sensible thermal energy storage system – a concrete column which is charged by hot air flowing through the pipes (placed inside the column). This novel system was incorporated into a multi-story residential building in Kayseri city, Turkey, where the design winter temperature was -15 °C. 1-dimensional and time dependent model was developed to investigate its heating performance. Results indicated that with proper airflow rate and temperature, charging period of 8 hours and discharging period of 16 hours could keep the indoor temperature above 20 °C.

In summary, earlier studies showed that some active BITES systems could completely reduce energy consumed by heating or cooling during peak period through shifting peak load to off-peak period or period with solar irradiation. However, very few studies focused on shifting peak heating load of residential house with multi rooms during winter with exterior temperature lower than 0 °C in cold region, like Canada.

2.3. SUMMARY

The studies of passive BITES were mainly based on house-like cubicles or single room houses, while very few of them were implemented to a real building. Its application mainly limited by (1) the processes of charge and discharge as well as peak shifting are hard to control; (2) its performance highly depends on solar irradiation during heating season and it cannot effectively store other forms of heating, such as heating from electrical heater. Due to the ability of overcoming previous issues, active BITES system has been studied by many researchers. Even if

it attracted concentration of research, few studies focused on the implementation of active BITES in real multi-zone residential house, which is located in cold region, to shift peak load. Moreover, for the investigations for active BITES based on simulation, assuming the investigated building as single zone is usually utilized. However, the simplified model would affect the accuracy of investigation result and some details of energy and temperature distribution after implementation maybe lost.

Furthermore, both passive and active systems could completely shift peak load. It means that if BITES is partially installed in specific room of a building and it completely shifts peak load of that room while maintaining the room within thermal comfort, excessive energy can be extracted and thus the BITES shows excessive peak shifting potential. It is noted that, in North America, most residential houses are made of wood structure and have a basement. Therefore, the concrete slabs in the basement usually possess the highest thermal mass to store heat in these buildings. Therefore, like above mentioned, if these concrete slabs can be utilized as active BITES and it shows excessive energy storage capability, further peak shifting ability can be extracted. To achieve this aim, enhancing the thermal coupling between BITES and interior air can be useful. Several air-forced BITES (i.e. ventilated slabs) has been carried out to enhance thermal coupling, however, the enhancement effect has not been quantitatively studied.

Due to above mentioned limitations of previous studies, the present research work aims to investigate and extend the peak shifting potential of an existing active BITES system (i.e. EHF system) installed in the basement of an experimental house located in Québec, Canada. To do this study through simulation, multi-zone building models are developed. The prediction accuracy of models is compared and validated. The validated model is then utilized to investigate the peak shifting potential of EHF. Later, a heat extraction system (HES) which aimed at extending the heating and peak shifting capacity of existing BITES is proposed in this study.

CHAPTER THREE: METHODOLOGY

In this chapter, methodologies adopted in the present study are illustrated in detail. Initially, the description of the experimental house such as floor plan, types of heating system used along with its installed location are reported. Then, the details pertaining to data collection and monitoring of the experimental house are listed and classified based on its function. Later, brief explanations on i) modeling the experimental house in TRNSYS, TRNSYS-CONTAM model, ii) investigating the peak shifting potential of EHF under different heating strategies and iii) investigating the heating performance of HES are made.

3.1. DESCRIPTION OF THE EXPERIMENTAL HOUSE

The experimental house (shown in Figure 3.1) investigated in this study is located in Boischatel, Québec, Canada.

Figure 3.1: Front view of the experimental house

This residential house was constructed in the year 2009. It has one semi-underground floor (basement), and two floors (ground floor and the second floor) above the ground. Floor plans for the experimental house are shown in Figure 3.2. The details of the experimental house (such as elevation view, building envelope materials and their properties) are given in Appendix A.

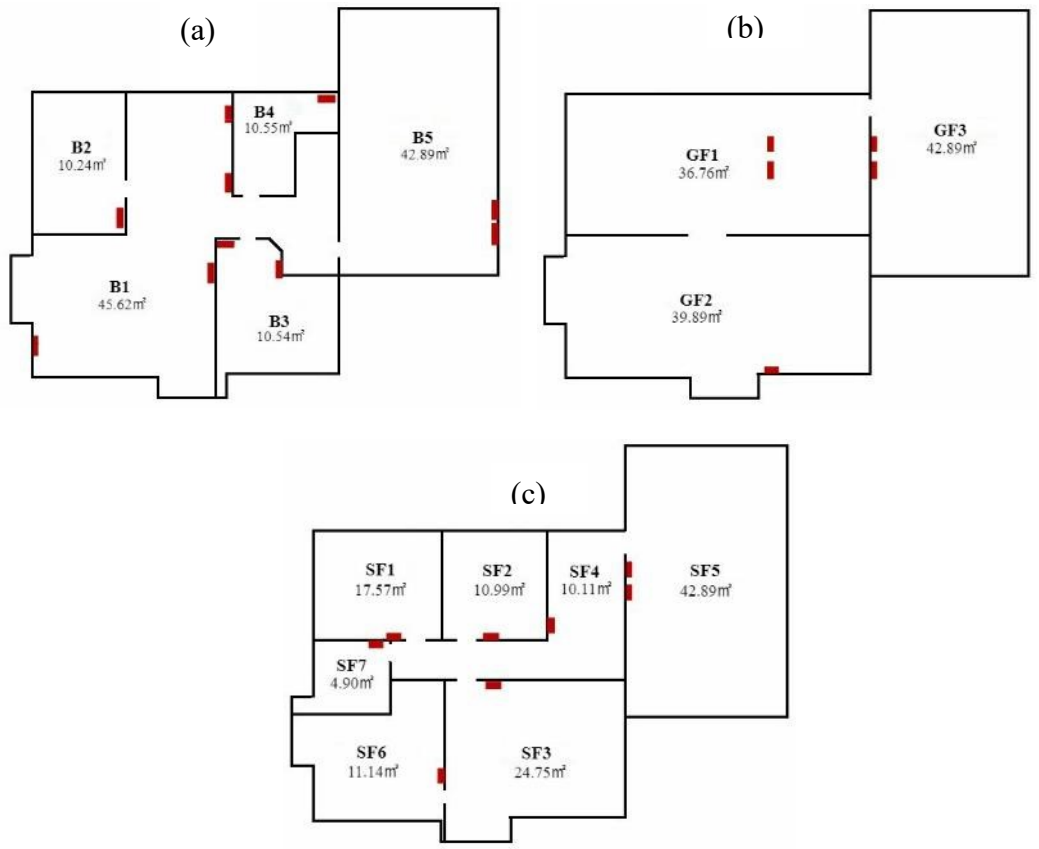

Figure 3.2: Floor plan of the house (a) basement, (b) ground floor and (c) second floor

There are three types of heating systems used in the house:

(1) **Buried EHF system**: electrical heating wires are buried in the middle of 23 cm concrete slab. This can be used for peak load shifting by storing energy in the surrounded concrete;

(2) **Surface EHF system**: electrical heating wires are installed below the floor cover directly. Under this system, a 0.6 cm layer of self-leveling concrete is placed. This means that this type of system is mainly used for maintaining the occupant thermal comfort and has no significant thermal mass for thermal storage;

(3) **Conventional heating system**: electrical baseboard heaters are placed a certain distance from the wall and the floor.

All the heating devices are controlled by thermostats as shown by red blocks in Figure 3.2. The mentioned heating systems are distributed in the experimental house, as shown in Table 3.1.

Table 3.1: The distribution of heating systems in the experimental house

Heating System	Location
Buried EHF	*Basement:* B1, B2, B3, B4, B5
	Ground floor: GF3
Surface EHF	*Ground floor:* GF1
	Second floor: SF6, SF7
Baseboard	*Basement:* B1, B3
	Ground floor: GF2
	Second floor: SF1, SF2, SF3, SF4, SF5

3.2. DATA COLLECTION AND MONITORING

All data utilized in this work is presented in this section, in terms of the process (i.e. model development or model validation) in which it was applied. Note that, there were two types of data: steady and dynamic data. Steady data was collected before developing models for just once, while dynamic data was monitored during the heating season from March 1st, 2017 to April 30th, 2017. All interior doors in this experimental house remained opened during the data collection period

3.2.1. DATA COLLECTED FOR MODEL DEVELOPMENT

(1) Building assembly details

Information regarding the assemblies of the experimental house and the building material properties were collected. The assemblies mainly include basement slabs, floor assemblies with/without EHF, foundation walls, exterior walls, interior walls, ceiling, and roof, etc. The U-value of all these assemblies is summarized in Table 3.2. The collected data of the assembly materials consists of dimensions, density, specific capacity and thermal conductivity.

Table 3.2: U-value of envelopes

Envelope description	U-value (W/m^2K)	Envelope description	U-value (W/m^2K)
Basement slab below heating wires	0.55	Foundation wall in contact with earth	0.61
Basement slab above heating wires	7.91	Foundation wall adjacent to exterior	0.60
Floor of room GF1	0.71	Uninsulated exterior wall	2.79
Floor of room GF2	0.73	Insulated exterior wall	0.16
Floor of room GF3	0.82	Structural concrete wall	2.63
Floor of room SF6 and SF7	0.85	Interior wall	1.79
Floor of the second floor except rooms SF6 and SF7	0.90	Cathedral ceiling	0.11
Attic floor	0.015	Attic roof	11.82

(2) Weather data

Weather data (i.e. dry bulb temperature, wet bulb temperature, relative humidity, horizontal solar radiation, cloud cover and wind speed) was obtained from the closest weather station, Jean Lesage International Airport, Québec City, Canada. The dry bulb ambient temperature during the monitoring period (March 1st, 2017 to April 30th, 2017) is shown in Figure 3.3. The figure shows that the exterior air temperature varied from -24.4 to 19.6 °C and thus the heating demand occurs for most of the period. Therefore, the considered period could represent the situations during winter.

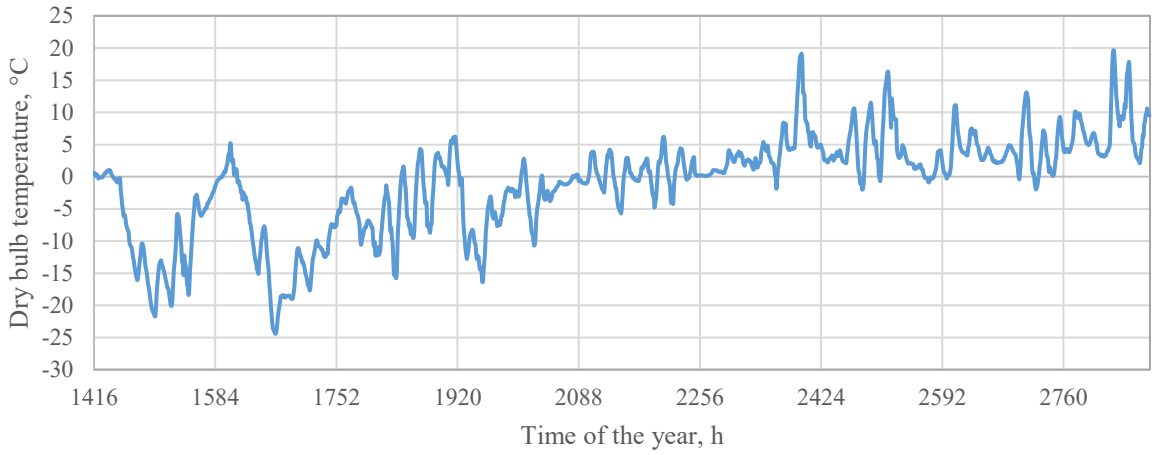

Figure 3.3: Dry bulb ambient temperature during the monitoring period

(3) Air infiltration

In the present study, global exterior air leakage characteristics was used to determine the global air leakage rate based on the power law (Equation 3.1). To do this, a fan depressurization test was conducted based on ASTM-E1827 standard (1999). The global flow exponent (n) and flow coefficient (c) were found to be 0.378 and 0.164 $m^3.s^{-1}.Pa^{-n}$, respectively.

$$Q = c * (\Delta P)^n \tag{3.1}$$

where, Q is the global volumetric flow rate [$m^3.s^{-1}$], c is global flow coefficient [$m^3.s^{-1}.Pa^{-n}$], ΔP is the pressure difference [Pa] and n is global flow exponent.

(4) Occupancy presence or behavior

The occupancy was not monitored due to the high price of instrumenting. Therefore, it was not considered during simulation. However, the amount of energy consumed by occupancy behavior (e.g. cooking, watching TV and lighting, etc.) in simulation was assumed to be the same as the real case while analyzing the model accuracy.

3.2.2. DATA MONITORED FOR MODEL VALIDATION

(1) **Temperatures**

Temperatures of each zone (i.e. air temperature, set-point air temperature and floor surface temperature) were recorded using thermostats (red blocks in Figure 3.2) at a 5-minutes interval.

(2)**Energy performances of heating devices**

Energy performances (i.e. nominal power, heat level, instant power consumption, energy consumption)of each heating device (electricity wiring and baseboards) were recorded with 5-minute intervals by thermostats. Note that heat level in the present study means the percentage of nominal power of the heating device during a specified time interval.

(3) **Total building electricity consumption**

The total energy consumption was collected through smart meters installed by Hydro-Québec at 15-minutes interval.

3.3. TASK A: MODELING

3.3.1. TASK A.1: MODEL DEVELOPMENT

TRNSYS (TRaNsient SYStems simulation program) is a commonly used tool to analyze the transient and detailed building simulation problems. It has many built-in mathematical modules called “types” (D. B. Crawley et al., 2008) which are displayed by a graphical user interface. By linking appropriate input and output of different types, performance of a system could be studied .Therefore, TRNSYS is highly flexible and makes modeling much faster (Saelens et al., 2011).

In this study, a TRNSYS model of the experimental house was developed to exclusively predict its temperature/energy performance. Note that there are no appropriate options in TRNSYS to assume or predict the dynamic inter-zonal airflow. However, in reality, the inter-zonal airflow will not be static and hence reliable prediction of dynamic airflow is necessary for calculating the actual heat transfer among the zones due to the mass transfer (Dols et al., 2016; Haghighat et al., 1991). It means that consideration of a constant value for inter-zonal airflow might predict the temperature and energy consumption of a multi-zone building with more deviations compared to the measured data. To consider the effect of inter-zonal airflow on the model accuracy, a multi-zone airflow model needed to be developed to predict the dynamic airflow between the zones. In this regard, an attempt is made to develop an integrated TRNSYS-CONTAM model, which incorporates the CONTAM model (a common tool to determine the dynamic airflow by considering the variation in wind pressures and subsequent temperature change) into TRNSYS.

The following subsections will introduce the methods adopted to develop the previously mentioned two models: i) TRNSYS model without considering inter-zonal airflow and ii) integrated TRNSYS-CONTAM model with considering the dynamic inter-zonal airflow.

3.3.1.1.TRNSYS model

The TRNSYS model in the present study can be split into four blocks as shown in Figure 3.4.

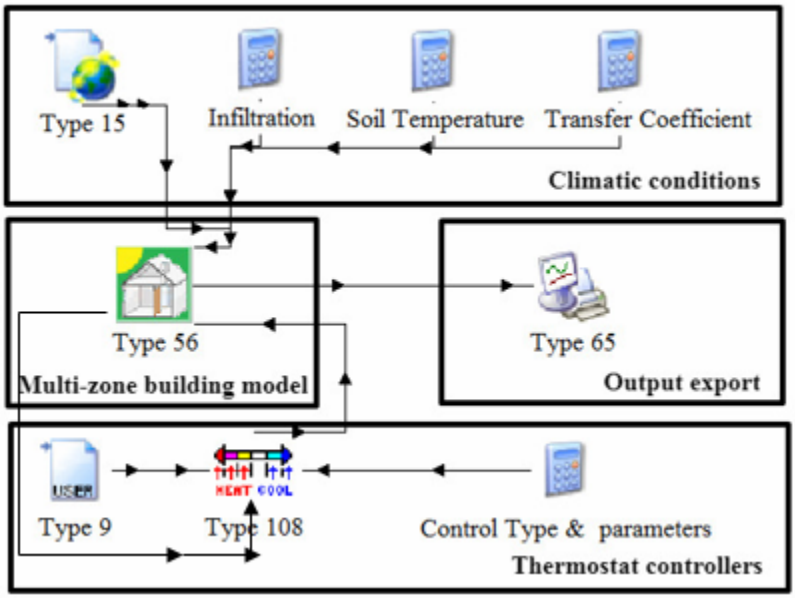

Figure 3.4: Schematic diagram of the TRNSYS model

The description of each block is described below.

(1) Climatic conditions and others

Type 15 (weather data reading and process model) in TRNSYS was used to import the Weather data.

The calculation panel denoted by “Infiltration” in Figure 3.4 provided the infiltration rate of each zone to the multi-zone building model. The infiltration of each zone was calculated by distributing the whole air leakage rate through separating the global flow coefficient to each zone based on the component area (shown in Equation 3.2) and retaining the flow exponent for each zone the same as the global value (Haghighat and Megri, 1996; Jiang, 1990).

$$Q_i = \frac{Q}{2} * \frac{A_{i,win}}{A_{win}} + \frac{Q}{2} * \frac{A_{i,wall}}{A_{wall}} \quad (3.2)$$

where Q_i is infiltration for zone i [$m^3.s^{-1}$], $A_{i,win}$ and A_{win} are exterior door/window area [m^2] of zone i and the whole house, respectively. Besides, $A_{i,wall}$ and A_{wall} are exterior wall area [m^2] of zone i and the whole house, respectively. Q is the global volumetric flow rate [$m^3.s^{-1}$].

It is to be noted that the soil temperature at different ground depths is affected by the exterior air temperature, rainfall, and snowfall (Qian et al., 2011). For this study, the depth of soil connected to the experimental house ranged from 0 to around 2 m. In the present study, soil temperatures at 1 m and 2 m underground were assumed to be the boundary temperatures connected to exterior walls and insulated floors, respectively. Besides, there is a driveway heating system at the outside of GF3 and a sunshield roof and wooden floor at the outside of GF1; therefore, for subzero exterior temperatures, the soil temperature at the depth of 1 m under these locations would be higher than the temperature at the same depth under other locations. The calculation of soil temperature was contributed by 'Soil Temperature' panel.

The exterior surface convective heat transfer coefficient was supplied by the 'Transfer Coefficient' panel as shown in Figure 3.4. It was calculated based on Equations 3.3 and 3.4 (Defraeye et al., 2010):

$$h_{WW} = 5.01 * U^{0.85} \text{ (Windward)} \quad (3.3)$$

$$h_{LW} = 2.27 * U^{0.83} \text{(Leeward)} \quad (3.4)$$

where h_{WW} and h_{LW} are convective heat transfer coefficients [$W.m^{-2}.K^{-1}$] at windward and leeward exterior surfaces, respectively and U is wind speed provided by Type 15 [$m.s^{-1}$].

(2) Multi-zone building model

Type 56 (the multi-zone building model) was utilized to predict the zonal temperature or zonal energy demand. To develop this type, several data such as room volume, envelopes and their constituting materials and properties, inter-zonal airflow (assumed to be zero in this TRNSYS model) and parameters from 'Climatic conditions' and 'Thermostat controllers' are fed as the input. In the present study, the EHF was modeled based on a procedure suggested by Thieblemont et al. (Thieblemont, Haghighat, and Moreau, 2016) with consideration of the floor thermal mass.

In this procedure, the EHF system was simulated as a zone with top and bottom slabs. Heating power consumed by EHF was represented by surface gain of the top surface of its bottom slab.

(3) Thermostat controllers

The calculation panel denoted by 'Control Type & Parameters' selected either simulated power consumption from Type 108 (5-stage room thermostats) or measured power consumption from Type 9 (data reader). The selected power consumption was fed into the developed Type 56 module to meet the heating demand.

Note that Type 108 calculated the required power consumption to keep Type 56 meeting the set-point for interior temperature and limitation for floor surface temperature (i.e. no more than 28°C). Therefore, simulated zone air temperature and floor surface temperature were the feedback from Type 56. However, Type 9 did not require feedback from Type 56 and it could directly send measured power consumption to Type 56 when 'Control Type & Parameters' panel was set to validate the temperature prediction.

(4) Output export

All simulation results were exported to text files by Type 65 (online plotter with the file), which could also display selected results while the simulation is in progress. The exported results were further processed and analyzed in MATLAB and Microsoft Excel.

3.3.1.2. Integrated TRNSYS-CONTAM model

To develop the integrated TRNSYS-CONTAM model firstly, a multi-zone airflow model should be developed in CONTAM, then, the developed multi-zone air flow model should be integrated into the developed TRNSYS model. By this mean the integrated model can predict the interior temperature/energy consumption with considering the influence of inter-zonal airflow. Detailed description of these two steps are described as below:

Step 1: Development of CONTAM model

To develop the multi-zone airflow model, information about the exterior and interior envelopes is required to determine the infiltration rate for each zone and inter-zonal airflow rate, respectively.

For exterior envelopes, the distribution of cracks and gaps for each zone as well as their air leakage characteristics are needed. However, it should be noted that during data collection, only air leakage characteristics for the whole house was obtained. Besides, the flow exponent cannot be lower than 0.5 in CONTAM model (Dols and Polidoro, 2015), which means the infiltration distribution method adopted in subsection 3.2.1.1 could not be applied here, because it kept the flow exponent for each zone as the same as the global one (0.378). Effective ways are needed to convert the global air leakage characteristics to the air leakage characteristics of each crack/gap and obtain a flow exponent (higher than 0.5) for each crack/gap.

Li (2002) reported an effective way to select the flow exponent for each component from the Technical Note AIVC44 (Orme et al., 1994), and normalize flow coefficient for each component based on Equation 3.5.

$$c_j = c_{j,AIVC} * [c_{test}(\Delta P)^{n_{test}}] / \sum c_{j,AIVC}(\Delta P)^{n_{j,AIVC}} \quad (3.5)$$

where c_j is the flow coefficient for component j [$m^3.s^{-1}.Pa^{-n}$]; $c_{j,AIVC}$ and $n_{j,AIVC}$ are the flow coefficient [$m^3.s^{-1}.Pa^{-n}$] and flow exponent [-] for component j from the Technical Note AIVC44 (Orme et al., 1994), respectively. Besides, c_{test} and n_{test} are the global flow coefficient [$m^3.s^{-1}.Pa^{-n}$] and flow exponent [-] of the whole unit measured by air-tightness test, respectively.

Note that, the building was constructed by following the highest energy efficiency standard of Québec and thus the air leakage along some components would meet the National Energy Code of Canada for Buildings ("National Energy Code of Canada for Buildings, 2015," 2015). Therefore, in this study, the flow component for each component was selected from the Technical Note AIVC44 (Orme et al., 1994). Besides, the process of calculating c_j was modified as:

1) Getting c_j for exterior windows/doors/walls, through which the air leakage value has been limited by the National Energy Code of Canada for Buildings ("National Energy Code of Canada for Buildings, 2015," 2015) as:

$$c_{j,wdw} = A_j Q_{j,75Pa}/(\Delta P)^{n_{j,AIVC}} \quad (3.6)$$

where $c_{j,wdw}$ the is flow coefficient of exterior window/door/wall j [$m^3.s^{-1}.Pa^{-n}$], A_j is the area of component j [m^2], $Q_{j,75Pa}$ is the maximum leakage value [$m^3.m^{-2}.s^{-1}$] for component j at 75Pa ("National Energy Code of Canada for Buildings, 2015," 2015). The value of ΔP (Pressure difference) is 75Pa, and the values for $n_{j,AIVC}$ are 0.6 for the exterior window/door and 0.82 for the exterior wall (Orme et al., 1994).

2) Calculating c_j for other components based on Equation 3.5. In this case, ΔP = 10Pa, because it is very close to the actual air conditions (Nirvan, 2011). Besides, $c_{j,AIVC}$ and $n_{j,AIVC}$ were selected from the median of AIVC 44 (Orme et al., 1994). $c_{test}(\Delta P)^{n_{test}}$ was modified according to Equation 3.7 to the global air leakage at 10 Pa minus the air leakage along exterior window/door/wall at 10 Pa:

$$c_{test}(\Delta P)^{n_{test}} = c * (\Delta P)^n - \sum c_{j,wdw}(\Delta P)^{n_{j,AIVC}} \quad (3.7)$$

where ΔP is pressure difference of 10 Pa.

The result of calculating c_j for each component is listed in Appendix B, while the comparison of infiltration rate at 10 Pa pressure difference for each zone between normalization methods used in previous TRNSYS model and this TRNSYS-CONTAM model was listed in Appendix C. It shows that if the stack effect is neglected and the pressure difference between ambient and each zone is assumed to be uniform at 10 Pa, the total infiltration rate is the same between these two models. That means the simulated total energy consumed by heating the house would not get affected by the different kind of normalization methods. However, the air leakage rate of all rooms in basement and some part of rooms in ground floor and second floor would be different between different methods. Note that CONTAM would consider stack effect, therefore, there will be more air leakage to basement than to the second floor. Besides, the pressure difference between ambient and interior environment would change because of orientation and height, and the interior temperature would be different between zones for different heating set-point.

Therefore, the influence of normalization methods on the infiltration rate of each zone and the simulation accuracy was considered as negligible in this study.

To simulate the interior doors with known dimensions, two-way flow model in CONTAM was selected. For flow coefficient of these doors, the default value of this model was used. For staircases simulation, the stairwell model was selected.

Step 2: Integrating CONTAM into TRNSYS model

Type 56 (TRNSYS multi-zone building model) and Type 97 (CONTAM multi-zone airflow model) were applied in TRNSYS 17 to combine multi-zone heat transfer with multi-zone airflows. A simplified description of this incorporated TRNSYS-CONTAM model is shown in Figure 3.5. Note that the real link between TRNSYS and CONTAM models is more complicated than the presented one.

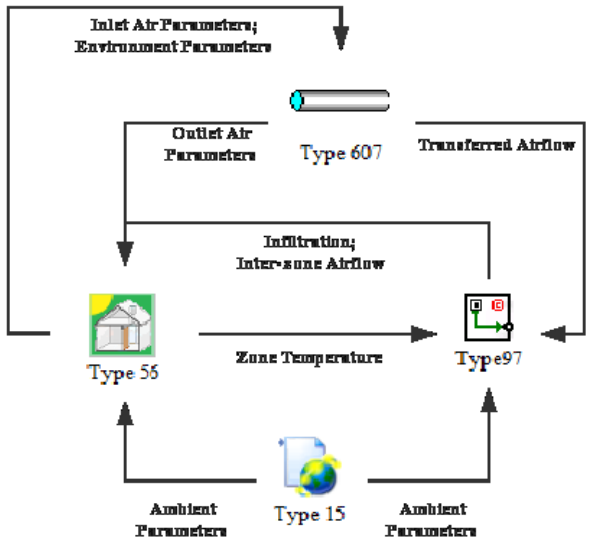

Figure 3.5: Schematic diagram of TRNSYS-CONTAM model

In the TRNSYS-CONTAM model, Type 15 provided the ambient parameters as inputs to Type 56 and Type 97. Type 56 supplies interior zone air temperature to Type 97, while Type 97 returns infiltration of each zone and inter-zonal airflow to Type 56.

In Figure 3.5, Type 607 represents the duct of the HES, which would be presented later in Section 3.5. The inlet air parameters and environmental parameters of HES were supplied from Type 56 to Type 607, while the outlet air parameters (e.g. temperature, humidity ratio, pressure) and the heat loss from the duct are returned from Type 607 to Type 56. The transferred airflow rate of the heat extraction system is set in Type 607 and then sent to Type 97 for simulating the inter-zonal airflow and infiltration.

3.3.2. TASK A.2: MODEL VALIDATION

Model validation is an essential part of developing a model from a real building (Nirvan, 2011). Validation process and criteria utilized in model validation varies based on the aim of study. This section shows the selection of criteria and the design of validation process.

3.3.2.1.Criteria selection

Normalized Mean Bias Error (NMBE) and Coefficient of Variance of the Root Mean Square Error (CV(RMSE)), shown in Equations 3.8 and 3.9, are indices commonly selected to compare the difference between data simulated by building models, especially building energy models, and data collected from experiment.

$$NMBE = \frac{\sum_{t=1}^{N}(m_t - s_t)}{\bar{m}(\mathrm{N-p})} \times 100\ (\%) \tag{3.8}$$

$$CV(RMSE) = \frac{\sqrt{\sum_{t=1}^{N}(m_t - s_t)^2 / (N-p)}}{\bar{m}} * 100\ (\%) \tag{3.9}$$

where m_t and s_t denote the measured value and simulated output at time *t.* Besides, *N* is the number of measured data points whereas *p* is the number of adjustable model parameters, which is suggested to be zero for *NMBE* and one for *CV*(*RMSE*) during calibration (Robertson et al., 2013; Ruiz and Bandera, 2017). Finally, $\bar{m}$ is the average of the measured values.

Positive *NMBE* values mean that the model under-predicts the measured data, while negative values mean over-prediction (Ruiz and Bandera, 2017). The sum of positive and negative values would reduce the value of *NMBE*. This means that it is subject to cancellation errors, thus,

using *NMBE* alone is not recommended for validation purposes (ASHRAE, 2014; Ruiz and Bandera, 2017). On the other hand, *CV*(*RMSE*) measures the variability of the errors between measured and simulated values and is not limited by cancellation errors (Ruiz and Bandera, 2017). Therefore, *NMBE* and *CV*(*RMSE*) are often applied together to verify the accuracy of models.

Several standards have been reported for choosing the calibration criteria for entire building energy prediction, as shown in Table 3.3. From the table, it can be inferred that acceptance criteria suggested by ASHRAE (2014) and FEMP (2015) were the same. Their thresholds for hourly energy consumption were more generous than for monthly, which is more reasonable than the converse situation in IPMVP (2001). Thus, the criteria selection suggested by ASHRAE (2014) and FEMP (2015) is considered in the present study for hourly or monthly energy validation.

Table 3.3: Acceptance criteria (in %) for energy model validation

Index \ **Standard**	ASHRAE (ASHRAE, 2014)	FEMP (FEMP, 2015)	IPMVP (IPMVP, 2001)	ANSI/BPI (ANSI/BPI, 2015)
$NMBE_{hour}$ (%)	±10	±10	±5	-
$NMBE_{month}$ (%)	±5	±5	±20	-
$NMBE_{bill}$ (%)	-	-	-	±5
$CV(RMSE)_{hour}$ (%)	30	30	20	-
$CV(RMSE)_{month}$ (%)	15	15	5	-
$CV(RMSE)_{bill}$ (%)	-	-	-	20

In this study, NMBE and CV(RMSE) were selected as indices to evaluate the prediction accuracy of the developed models (i.e. TRNSYS and TRNSYS-CONTAM models).

3.3.2.2. Validation process

Multi-zone airflow models are usually validated by (1) comparing simulated tracer gas concentration with filed measured data (Lansari et al., 1996) or experimental measured data (Emmerich et al., 2004); (2) comparing simulated interior zone pressure with the measured one (Li, 2002). Multi-zone heat transfer models are commonly validated by (1) comparing simulated interior zone temperature (by considering the same energy consumption) with filed measurement data (Olsthoorn, 2017; Wang and Xu, 2006); (2) comparing simulated energy consumption (by

considering the same set-point temperature) with measured data (ASHRAE, 2002; Olsthoorn, 2017; Pan et al., 2007). Since the aim of this study is to investigate and enhance the thermal performance of EHF, the temperature profiles and energy consumption simulated by the developed TRNSYS and TRNSYS-CONTAM models were compared to the monitored data.

The detailed validation process included:

a) Temperature validation:

The power consumption, which was the same as data measured from the experimental house (see Section 3.2.2), was fed as input to TRNSYS and TRNSYS-CONTAM models. The transient temperatures i.e. air temperature of each room, area weighted mean air temperature of each floor and the house (calculated using Equation 3.10), were selected as the outputs which needed to be compared with the monitored temperature. Note that the area weighted mean air temperature is the same as volume weighted mean air temperature if the height of each zone is the same. The reason for choosing this type of mean temperature is to respect the average energy content of each floor or the whole house under the assumption of constant air density and specific heat capacity.

$$T_{mean,t} = \frac{\sum(A_i * T_{i,t})}{\sum A_i} \tag{3.10}$$

where $T_{mean,t}$ is the area weighted mean temperature of one floor or the whole house at time t [°C], $T_{i,t}$ is the air temperature of zone i on that floor or house at time t [°C], A_i is the floor area of zone i [m^2].

b) Energy consumption validation:

The set-point temperature was used as the input. The heating consumption of each floor, the total heating consumption (basement and the second floor) and the total energy consumption of the entire house were selected as outputs, which would be compared with the collected data.

Validation was carried out on hourly, half-daily, daily, and monthly data. The main reason for considering the half-daily and daily data for validation is to ensure the accurate prediction of half-daily and daily energy consumption in order to analyze the peak shifting methods. The hourly

and monthly energy consumption validation are needed due to the criteria set by different standards (Table 3.3).

Since the status of exterior doors (open/closed) on the ground floor cannot be monitored, validating the floor is complicated. Moreover, the ground floor was not subject to the HES study. Consequently, there was no need to validate the ground floor and during the validation process, air temperatures and floor surface temperatures on the ground floor were kept the same as the measured data. Hence, during validation, the simulated ground floor temperature and heating consumption was assumed as the same as the measured one.

Note that during modeling, occupancy behavior was not considered, which means that the energy consumed by cooking, lighting and domestic hot water could not be predicted. In order to obtain the total simulated energy consumption, consumption related to occupancy was considered as the same as the measured one, shown in Figure 3.6.

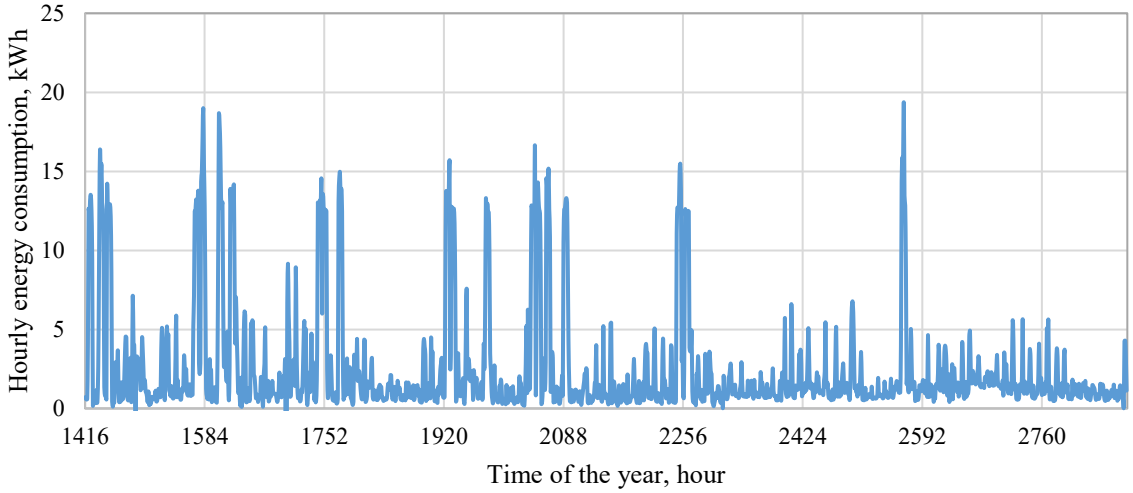

Figure 3.6: The hourly energy consumption related to occupancy

3.4. Task B: Investigation on Peak Shifting Potential of EHF in Basement

The buried EHF in the experimental house can be charged/discharged through turning ON/OFF the electrical wires. The ON/OFF status of the electrical wires is controlled through changing interior set-point temperature. Therefore, proper set-point temperature during different

periods not only keeps the interior environment within thermal comfortable, but also achieves the aim of peak shifting. In this study, an attempt is made to investigate the peak shifting ability of buried EHF in the basement at different heating strategies and set point temperatures. If the investigated EHF could completely decrease the power consumption of basement, it shows the possibility to supply heat to other rooms and shift more heating load from peak periods to off-peak periods.

The duration of peak, mid-peak and off-peak period for Québec, Canada adopted in this study is based on the work done by Thieblemont et al. (2017) as shown in Figure 3.7.

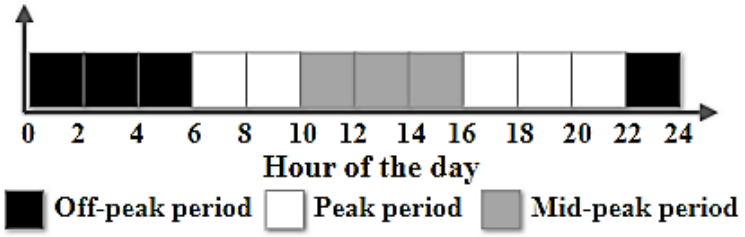

Figure 3.7: Duration of peak, mid-peak and off-peak periods (Thieblemont et al., 2017)

Many heating (control) strategies have been proposed in previous studies. Among them, night-running strategy (NRS) and peak shifting strategy (PSS) were commonly used. NRS shifts heating load from daytime to nighttime through heating only at night (Amir et al., 1999; Farid and Chen, 1999; Navarro et al., 2015; Thieblemont, 2017), while PSS proposed by Thieblemont et al. (2017) has a higher set-point temperature during off-peak period and mid-peak period than during peak period. The reason for the higher set-point temperature during off-peak period is to take advantage of the cheaper electricity price, while the reason for higher set-point temperature for mid-peak period is to recharge the EHF system during afternoon and avoid heating consumption during the early evening (4 pm – 10 pm) of peak period. It should be noted that the experimental house considered in the work of Thieblemont et al. (2017) was also located in Québec, Canada. Therefore, similar strategies (i.e. night-running strategy and peak shifting strategy) were operated to the basement in which buried EHF was installed in the experimental house. The set-point for different periods of these two heating strategies are summarized in Table 3.4.

Table 3.4: The set-point for different periods in night-running strategy and peak shifting strategy

Heating strategy / Period	Night-running strategy	Peak shifting strategy
Off-peak	$T_{in,set}$	$T_{in,set}$
Mid-peak	20 °C	21.5 °C
Peak		20 °C

Note: $T_{in,set}$ means set-point during off-peak period, which is discussed in Table 3.5 in detail.; EHF will be turned OFF once the interior temperature reached the set-point or the floor surface temperature (F_{ST}) was higher than 28 °C.

Note that, the set-point temperature during off-peak period affects the amount of stored heat and the duration of discharge. Therefore, several scenarios were designed to investigate the effect of set-point temperature during off-peak periods on the amount of shifted load, room temperature and the heating cost for both night-running strategy and peak shifting strategy. Table 3.5 briefs these scenarios during the period from March 1st to April 30th, 2017.

Table 3.5 Scenarios for EHF peak shifting potential study based on different strategies at different set point temperature during off-peak periods

Investigated Strategy	Scenario names	$T_{in,set}$ °C	Constant parameter(s)
Night-running strategy (NRS)	NRS (22 °C)	22	The ground floor and the second floor were heated at 21 °C.
	NRS (23 °C)	23	
	NRS (24 °C)	24	
Peak shifting strategy (PSS)	PSS (22 °C)	22	
	PSS (23 °C)	23	
	PSS (24 °C)	24	
-	Reference scenario	21.5	

Note: For reference scenario, the set-point temperature for basement was 21.5 °C all day. The investigated strategies were implemented to the basement.

A simple economical analysis was conducted to account the benefit of peak shifting. Note that there is no time-of-use tariff applied in Québec, therefore, the implemetation of these strategies might increase the heating cost. This is due to the higher set-point temperature during off-peak periods during which the exterior temperature was usually lower among one day. However, heating cost saving might achieved if there was electricity price difference between peak and off-peak

periods. Rettino-Parazelli (2017) reported that time of use tariff is planned to be applied in Québec from winter 2018/2019. Therefore, in the present study, the effect of peak shifting on heating cost was estimated by considering the time-of-use electricity price applicable to Ontario (2017), the province which is next to Québec. The considered time-of-use tariff is 0.18 CAD/kWh for peak period, 0.132 CAD/kWh for the mid-peak period and 0.087 CAD/kWh for the off-peak period. Note that the considered price was applied for weekdays in Ontario. However, it was utilized for all days in this study because the aim was to investigate if peak shifting could result in heating cost saving through taking benefits from time-of-use tariff. The daily heating cost was calculated by:

$$Daily\ heating\ cost\ (CAD) = (P_{peak}*E_{peak}*D_{peak})+(P_{mid}*E_{mid}*D_{mid})+(P_{off}*E_{off}*D_{off}) \quad (3.11)$$

where P_{peak}, P_{mid}, P_{off} is the power consumption [kW]; D_{peak}, D_{mid}, D_{off} is the duration [h] ; E_{peak}, E_{mid}, E_{off} is the electricity price [CAD/kWh] during peak, mid-peak and off-peak period, respectively. Like above mentioned, E_{peak}, E_{mid}, E_{off} is 0.18, 0.132 and 0.087 CAD/kWh, respectively.

3.5. TASK C: INVESTIGATION ON THE HEAT EXTRACTION SYSTEM

The schematic diagram of HES is shown in Figure 3.8. The idea of using the HES is to transfer hot air from the rooms (called source rooms), which have BITES, to other rooms (called object rooms) lacking this kind of thermal storage system. The objective of the HES for the existing experimental house is extracting heat from EHFs and thus making the best utilization of its peak shifting potential. It is proposed to extract heat from rooms with higher set-point temperatures to rooms with lower air temperature. In this way, temperature difference between source rooms and

object rooms is ensured which in turn enhances the heating effect of the transferred air on object rooms.

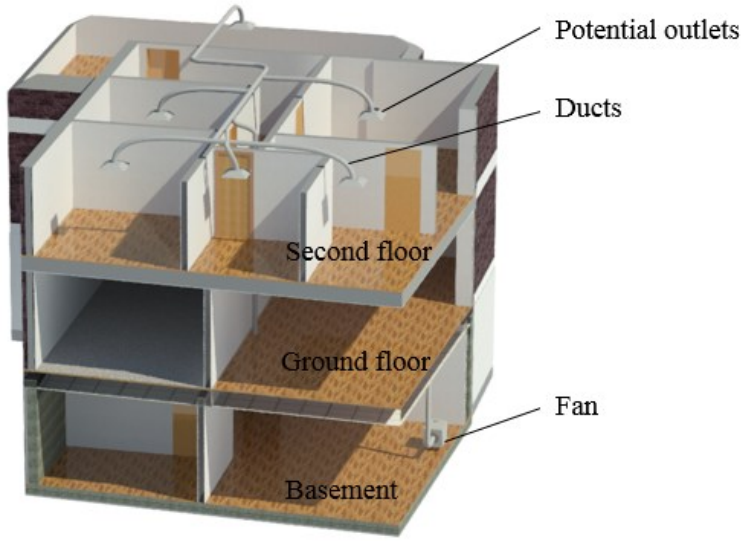

Figure 3.8: Schematic diagram of the experimental house with HES

In residential buildings, due to thermal comfort issues, the set-point temperature for living rooms should usually be higher than bedrooms (Raymer, 2009). Therefore, for the HES considered for this experimental house, hot air can be transferred from the living room in the basement (B1) to the second floor where most of bedrooms are located. In this study, both heating performance and peak shifting performance of the HES were investigated.

3.5.1. TASK C.1: HEATING PERFORMANCE OF HES

The effect of airflow rate and outlet location on the heating performance of HES are investigated while keeping the source room at the set point temperature, 24 °C (the acceptable temperature for living rooms (Raymer, 2009)) with the aim of making sure the heating potential of EHF.

For the investigation on the effect of airflow rate on the heating performance of HES, the effect of transferred airflow rate in the range of 0 to 0.28 $m^3.s^{-1}$ (i.e. 0 to 600 CFM) was studied. During simulation, an existing duct system, which extends between the basement and second floor, was utilized to transfer the air from B1 directly to SF6 and SF7. The outlet airflow through SF6 and SF7 were assumed to be identical, being half of the total transferring airflow. All heating

devices on the second floor were turned OFF, while the source room (i.e. B1) was heated with a set-point at 24 °C and all other rooms in the basement were heated with set-points at 20°C. Interior air temperature of the ground floor were kept at 21 °C (its set-point temperature). The period of simulation was from March 1st to April 30th, 2017.

To study the effect of outlet location, rooms in the second floor, except SF2, which is used as the locker room, were selected and studied as potential outlet locations. A constant value of 0.14 $m^3.s^{-1}$ (i.e. 300 CFM) was used as the total transferring airflow rate. This means that airflow for each outlet was 0.07 $m^3.s^{-1}$ (150 CFM) when there were two outlets or 0.05 $m^3.s^{-1}$ (100 CFM) when there were three outlets. The set-point temperature for all heating devices and simulation periods were the same as the investigation for airflow rate.

The investigated parameters for HES heating performance study are summarized in Table 3.6 based on above description.

Table 3.6: Investigated parameters for HES heating performance study

Investigated parameter: Variable range	**Constant parameter**
Air flow rate ($m^3.s^{-1}$): 0; 0.05; 0.09; 0.14; 0.19; 0.24; 0.28 (i.e. 0; 100; 200; 300; 400; 500; 600 CFM)	Two outlets: SF6 and SF7
Outlet locations: SF1; SF3; SF4; SF5; SF6; SF7; SF6,7; SF5,6,7	Air flow rate: 0.14 $m^3.s^{-1}$ (i.e. 300 CFM)

Note: CFM means cubic feet per minute [$ft^3.\ min^{-1}$] which is commonly used in North America.

3.5.2. TASK C.2: PEAK SHIFTING EXTENDING PERFORMANCE OF HES

To study the ability of HES to extend the peak shifting performance of EHF, PSS with set-point at 24 °C during off-peak periods was applied to the basement. Table 3.7**Error! Reference source not found.** briefs the scenarios considered in the present study to analyze the peak shifting extending performance of HES during the period from March 1st to April 30th, 2017.

Table 3.7: Scenarios to study the ability of HES to extend peak shifting potential of EHF

Cases	Scenarios	Explanation
Case I (with HES)	**Scenario 1:** Peak_HES_SF6,7	• Basement was heated by EHF based on the peak shifting strategy. • The second floor was heated by the hot air transferred from basement using HES with two outlets (SF6, SF7).
	Scenario 2: Peak_HES_SF5,6,7	• Basement was heated by EHF based on the peak shifting strategy. • The second floor was heated by hot air transferred from basement using HES with three outlets (SF5, SF6, SF7).
Case II (without HES)	**Scenario 3**: Peak _SF6,7	• Basement was heated by EHF based on the peak shifting strategy. • The second floor was heated by existing baseboards. • Temperature of each zone in the second floor was kept same as in the Scenario 1.
	Scenario 4: Peak_ SF5,6,7	• Basement was heated by EHF based on the peak shifting strategy. • The second floor was heated by existing baseboards. • Temperature of each zone in the second floor was the same as Scenario 2.
Reference Case	**Scenario 5**	• Basement was heated at 21.5 °C by EHF regardless the time of the day. • The second floor is heated by existing baseboards. • Temperature of each zone in the second floor was the same as Scenario 2.

It should be noted that, during the simulation, airflow rate of HES for Case I was considered to be 0.28 $m^3.s^{-1}$ (600 CFM). This is due to the fact that set-point temperature of the source room is lower than 24°C in peak and mid-peak periods and this relatively high air flow rate would be more reliable to keep the second floor within thermal comfort. Besides, for all scenarios, the ground floor was kept at 21 °C.

CHAPTER FOUR: RESULTS AND DISCUSSION

In this chapter, the results obtained by comparing the simulated temperature and energy consumption with measured data, respectively are reported initially. Then, based on the validated TRNSYS-CONTAM model, the investigation results for the peak shifting potential of the existing EHF are reported and discussed in detail. Finally, results obtained through the investigations carried out on the heating and peak shifting extending performance of HES are reported.

4.1. MODEL VALIDATION

4.1.1. TEMPERATURE PREDICTION

Temperature validation results of TRNSYS and TRNSYS-CONTAM models are compared in Table 4.1.

Table 4.1: Temperature validation results of TRNSYS and TRNSYS-CONTAM models

Room/floor	*T model NMBE (%)*	*T-C model NMBE (%)*	*T model CV(RMSE) (%)*	*T-C model CV(RMSE) (%)*
Basement				
B1	0.57	1.42	5.06	3.11
B2	12.50	2.33	14.23	3.33
B3	4.94	0.17	12.34	3.93
B4	-0.52	0.35	5.66	3.08
B5	-1.08	-0.72	4.87	4.43
Second floor				
SF1	8.57	2.76	10.47	4.54
SF2	2.25	-2.34	12.03	6.00
SF3	-8.07	-1.88	15.65	6.29
SF4	11.49	2.50	15.84	4.82
SF5	3.32	-2.89	9.76	6.30
SF6	2.24	-2.36	11.46	7.11
SF7	6.23	-1.05	10.56	4.25

Note: T model means TRNSYS model. T-C model means TRNSYS-CONTAM model.

The inference from Table 4.1 is that for the basement temperature prediction, TRNSYS model provided a greater absolute value of NMBE (*abs*(*NMBE*)) for most of the rooms except room B1 when compared to TRNSYS-CONTAM model. Especially for B2, the *NMBE* obtained from TRNSYS model even reached 12.50%, which means the temperature of B2 was underestimated by the TRNSYS model simulation. However, the *NMBE* of room B2 was 2.33% in the TRNSYS-CONTAM model, which indicates that the underestimation of TRNSYS model

was caused by the fact that the TRNSYS was not able to consider the inter-zonal air movement (hot air from B1 to B2). Besides, TRNSYS model always resulted in higher *CV*(*RMSE*) for each room in the basement when compared to TRNSYS-CONTAM model. This indicates that the temperature for rooms in the basement predicted by TRNSYS-CONTAM model is in good agreement with the real measured data most of time, compared to the TRNSYS model's prediction.

In the second floor, TRNSYS model has high *abs(NMBE)* (more than 5%) for the temperature prediction of five rooms (SF1, SF3, SF4, SF6 and SF7). Particularly, in SF4, the *NMBE* is 11.49 %, which means the TRNSYS model underestimated the room air temperature. Meanwhile, in TRNSYS model, *CV*(*RMSE*) values for most rooms in the second floor were higher than 10%. By contrast, in the TRNSYS-CONTAM model, the *abs*(*NMBE*) values for rooms in the second floor was always lower than 5%, and the *CV*(*RMSE*) values for these rooms were always lower than 10%.

Based on the above analysis, it is construed that the TRNSYS-CONTAM model had better temperature prediction for both the basement and the second floor. Furthermore, due to the low *abs(NMBE)* and *CV(RMSE)* shown in Table 4.1, TRNSYS-CONTAM model was considered as temperature validated and can be used to predict temperature distribution within the experimental house, while the TRNSYS model was not validated because of the unacceptable high value of indices.

Although Table 4.1 shows the overall prediction accuracy of these two models and it did not represent the prediction results graphically. The comparison between predicted temperature and measured data over time should be further presented by figures. However, the illustration of this comparison for each room would be extremely complicated. Thus, the difference between the results predicted by these two models and the measured data are compared by means of area-weighted mean temperatures (i.e. mean basement temperature, mean second floor temperature, and mean temperature of basement and second floor) as shown in Figure 4.1.1(a), 4.1(b) and 4.1(c) respectively.

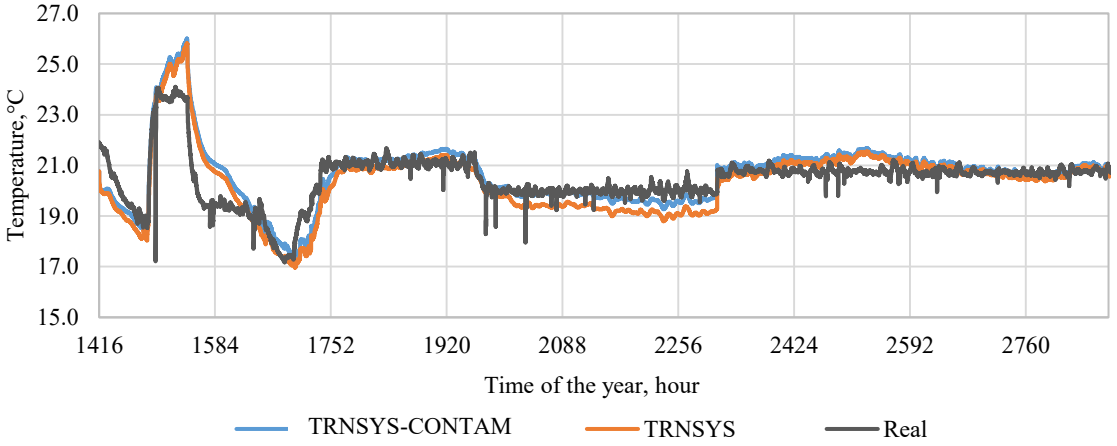

(a)

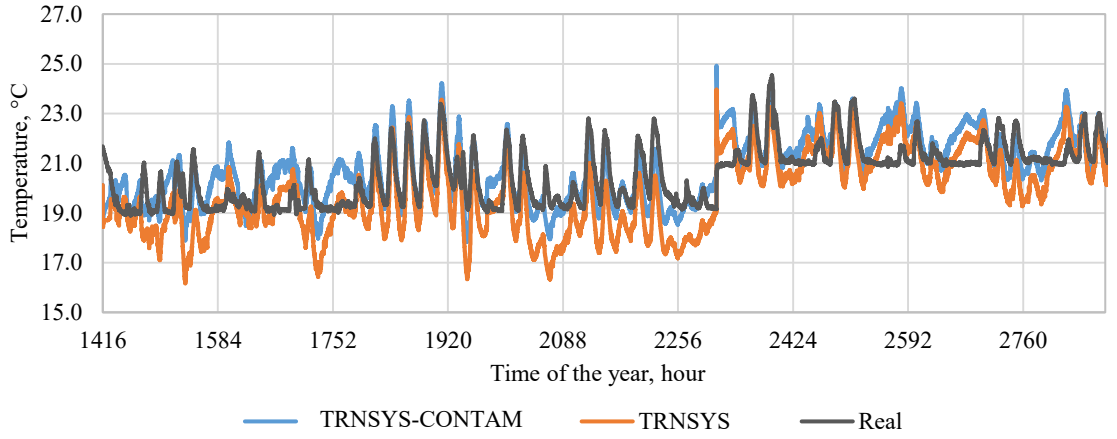

(b)

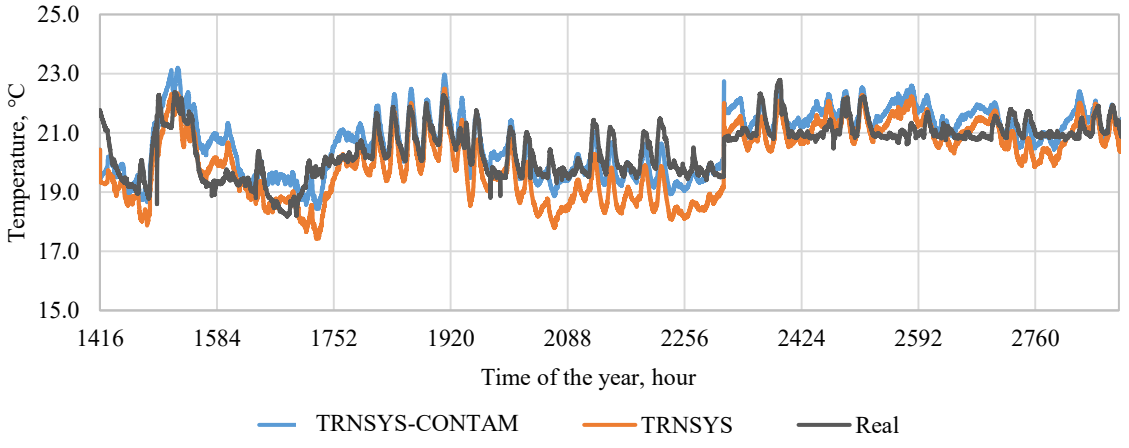

(c)

Figure 4.1: Comparison between TRNSYS model, TRNSYS-CONTAM model and real data in terms of (a) mean basement temperature; (b) mean second-floor temperature; (c) mean temperature of the basement and second floor

Figure 4.1.1(a) shows that the variability of errors between measured mean basement temperature and predicted one by TRNSYS-CONTAM model is smaller than that between measured one and predicted mean temperature by TRNSYS model most of time. Furthermore, Figure 4.1.1(b) depicts that the mean second-floor temperature predicted by TRNSYS-CONTAM is closer to measured data compared with the result of TRNSYS model most of the time. Moreover, TRNSYS-CONTAM model slightly overestimates the second-floor temperature, while TRNSYS model underestimates it most of the time. The reason for overestimation of TRNSYS-CONTAM model is that the real exterior temperature was lower than the temperature from the closest weather station, while the reason for underestimation of TRNSYS model is that the hotter air naturally transferred from the ground floor to the second floor (inter-zonal airflow) was totally neglected.

From Figure 4.1.1(c), trend of the mean basement and second-floor temperature predicted by these two models and the measured data are nearly the same. Although sometimes, from this figure it can be inferred that, TRNSYS-CONTAM model presented slightly inaccuracy prediction, however in overall, TRNSYS-CONTAM model still shows better temperature prediction than TRNSYS model. Table 4.1 also confirms this conclusion.

4.1.2. ENERGY CONSUMPTION PREDICTION

Energy consumption validation results of TRNSYS and TRNSYS-CONTAM model are compared in Table 4.2, while comparisons between these two models in terms of proximity to real measured data during the validation period are shown in Figure 4.2.

Table 4.2: Energy validation result of TRNSYS and TRNSYS-CONTAM models

Floor	Hourly				Half-daily				Daily				Monthly			
	T model NMBE (%)	*T-C model NMBE (%)*	*T model CV(RMSE) (%)*	*T-C model CV(RMSE) (%)*	*T model NMBE (%)*	*T-C model NMBE (%)*	*T model CV(RMSE) (%)*	*T-C model CV(RMSE) (%)*	*T model NMBE (%)*	*T-C model NMBE (%)*	*T model CV(RMSE) (%)*	*T-C model CV(RMSE) (%)*	*T model NMBE (%)*	*T-C model NMBE (%)*	*T model CV(RMSE) (%)*	*T-C model CV(RMSE) (%)*
Basement	-4.50	-1.68	60.59	56.06	-4.50	-1.68	29.01	29.03	-4.50	-1.68	23.39	22.04	-4.50	-1.68	6.40	2.37
Second floor	-24.02	3.77	62.61	58.98	-24.02	3.77	39.45	33.71	-24.02	3.77	36.48	28.03	-24.02	3.77	35.08	5.90
Total heating	-9.07	-0.40	50.64	46.95	-9.07	-0.40	26.46	25.52	-9.07	-0.40	22.10	19.23	-9.07	-0.40	13.08	0.80
Whole house	**-3.86**	**-0.17**	**21.54**	**19.97**	**-3.86**	**-0.17**	**11.26**	**10.90**	**-3.86**	**-0.17**	**9.40**	**8.18**	**-3.86**	**-0.17**	**5.54**	**0.19**

Note: T model means TRNSYS model. T-C model means TRNSYS-CONTAM model. Total heating means total energy consumed by heating the basement and second floor. Whole house means the energy consumed by the whole house.

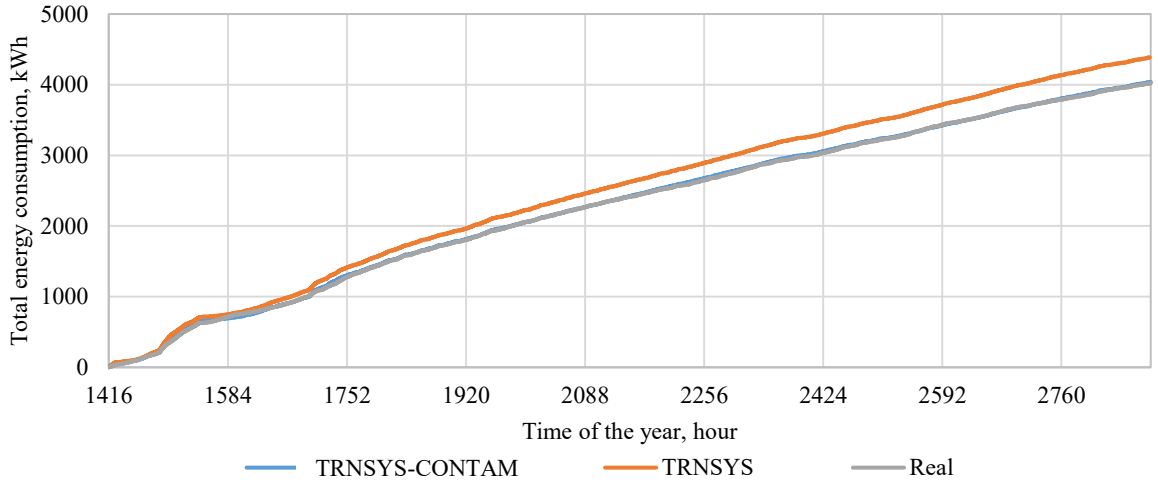

Figure 4.2: Comparison between TRNSYS model, TRNSYS-CONTAM model and real data in terms of total heating consumption during the validation period

From Table 4.2, the energy validation results of TRNSYS-CONTAM model was found to be better than TRNSYS model, in terms of both *abs(NMBE)* and *CV(RMSE)*. Better energy consumption prediction performance of TRNSYS-CONTAM model could also be observed in Figure 4.2. Compared to the measured data, TRNSYS model overestimated around 9.16% of the total heating consumption during the validation period, while the difference between TRNSYS-CONTAM model and the measured data is negligible.

Table 4.2 also shows that the energy consumption pattern predicted by TRNSYS model for the second floor is not in good agreement with the measured data. The *CV*(*RMSE*) is always higher than 30% regardless of the period, i.e. hourly, half-daily, daily, or monthly. The *NMBE* of the second floor even reached -24.02%, which means the TRNSYS model overestimated the energy consumed by the heating devices on the second floor. The reason for this situation is that the TRNSYS model is not able to consider the inter-zonal air movement (movement of hot air from the ground floor to the second floor).

The application of TRNSYS-CONTAM model effectively solved the abovementioned issues in TRNSYS model by considering the inter-zonal air movement in the multi-zone building. The monthly *CV*(*RMSE*) of the second-floor energy prediction is 5.90%, which is much lower than the threshold value (15%) suggested by standards (Table 3.3). However, the *CV*(*RMSE*) of half-daily prediction of the second-floor heating consumption was 33.71%, which was relatively high. Since the energy consumed by the second floor comprised a small percentage of the total heating consumption, this *CV*(*RMSE*) of half-daily in the second floor was acceptable.

Meanwhile, in terms of hourly or monthly energy prediction of the whole house, both TRNSYS-CONTAM model and TRNSYS model can be considered as validated, as it meets the threshold values suggested in Table 3.3. However, most half-daily, daily *CV*(*RMSE*) values of TRMSYS/CONTAM model were always lower than 30% and smaller than these values in TRNSYS model. Besides, half-daily and daily *abs*(*NMBE*) values of TRNSYS-CONTAM model were always lower than 5%. Therefore, the developed TRNSYS-CONTAM model are recommended to conduct the detailed parametric study due to the more accuracy energy prediction, while the TRNSYS model was not. The result also indicated that accurate inter-zonal airflow would affect the accuracy of energy prediction.

4.2. INVESTIGATION FOR PEAK SHIFTING POTENTIAL OF EHF

The operation status (ON/OFF) of heating system would affect the interior temperature. Hence it is important to analyze the effect of heating strategies on the interior temperature, mean basement temperature during coldest day (March 10th, 2017) and warmest day (April 27th, 2017) under different scenarios and the respective results are compared in Figure 4.3 and Figure 4.4, respectively. Note that the coldest day and warmest day were selected from March and April, 2017.

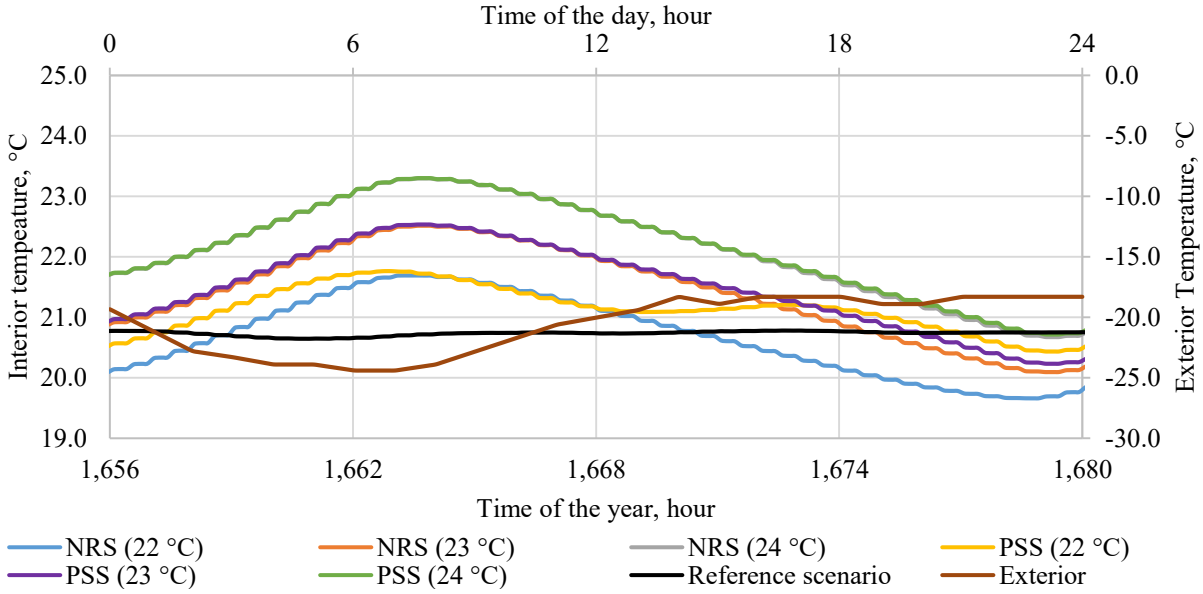

Figure 4.3: Mean basement temperature during coldest day (March 10th, 2017)

Figure 4.3 shows that for the coldest day, the mean basement temperature of all scenarios did not reach the set-point temperature during off-peak period. However, higher set-point temperature during off-peak period could guarantee a higher mean basement temperature at 6 a.m. (the end of off-peak period), which means more energy was stored and could be released during peak and mid-peak periods. Besides, all scenarios based on PSS kept the mean basement temperature above 20°C all day long. However, NRS with set-point at 22 °C for off-peak periods resulted in the mean basement temperature lower than the set-point (i.e. 20°C) at the end of late afternoon peak period (i.e. 4 p.m. – 10 p.m.). Therefore, during extremely cold days, PSS would be recommended to be applied to the existing EHF system to shift power consumption of peak period with considering the interior thermal comfort.

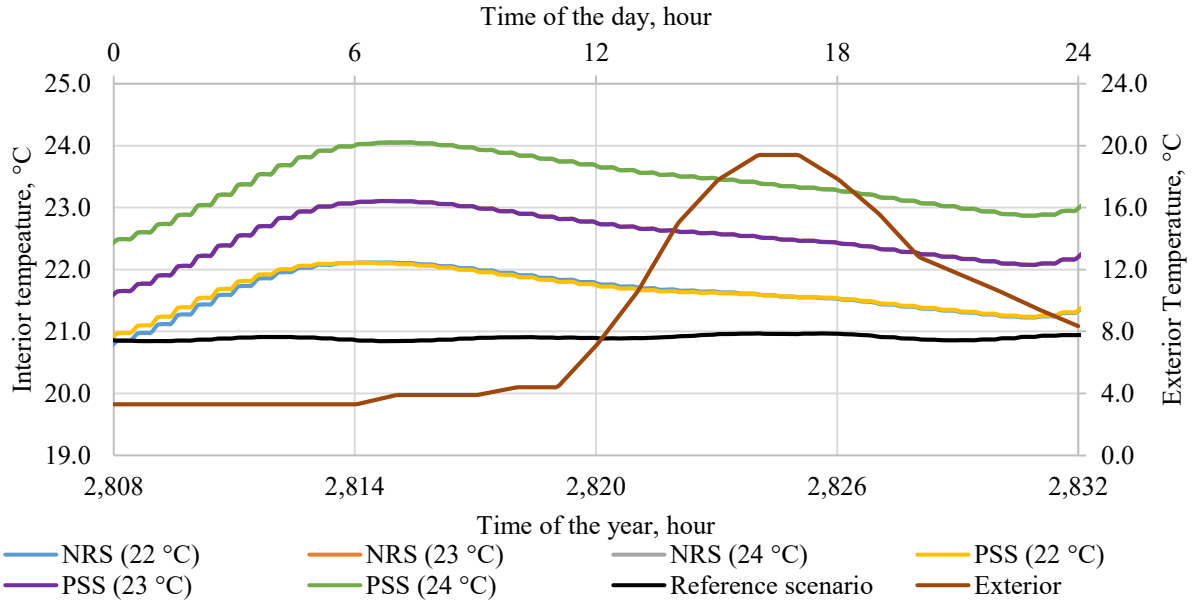

Figure 4.4: Mean basement temperature during warmest day (April 27th, 2017)

Figure 4.4 illustrates that when the ambient was warm enough, the mean basement temperature was nearly the same if the off-peak period set-point temperature was the same between NRS and PSS. Therefore, PSS is recommended to shift peak load while making sure thermal comfort during extremely cold season.

The average heating power consumption of the basement during different periods based on scenarios given in Table 3.5 is compared in Figure 4.5 (left axis).

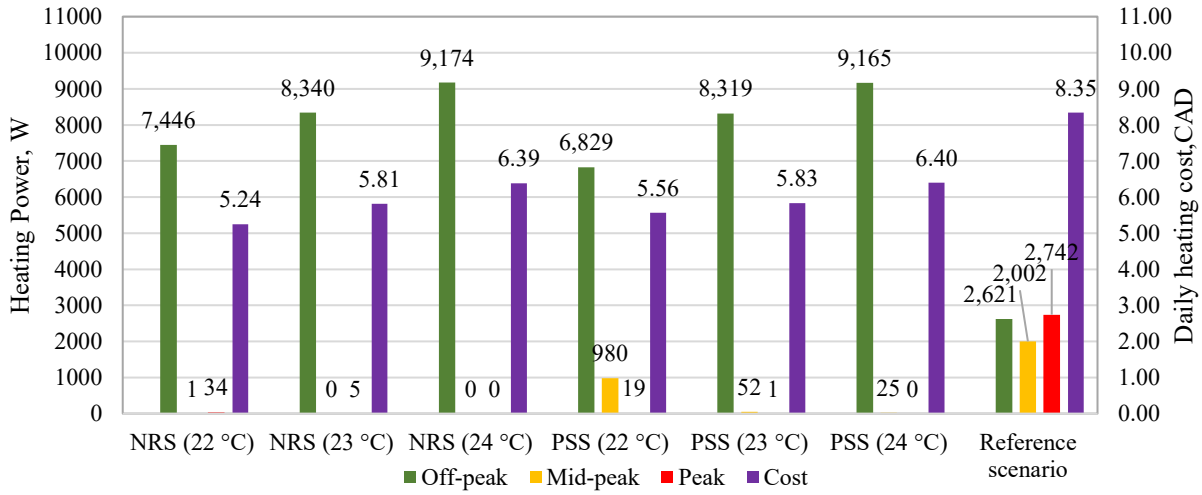

Figure 4.5: Average heating power consumed by the basement during different periods (left axis) and daily heating cost of basement (right axis) under different heating strategies

Figure 4.5 shows that both NRS and PSS has the ability to completely shift the peak load of basement for the considered set point temperatures. However, the effect of PSS on the basement heating power consumption during mid-peak period was depended on the set-point temperature of off-peak period: if the basement set-point for off-peak period was 22 °C (Scenario: PSS (22 °C)), the mid-period consumption could be decreased by 51.5% compared to the reference scenario; otherwise, if the set-point during off-peak period was 23 °C (Scenario: PSS (23 °C)) or 24 °C (Scenario: PSS (24 °C)), the basement power consumption during mid-peak period could be decreased by 97.40% or 98.75%, respectively. One the other hand, the NRS could completely decrease the mid-period power consumption of basement.

In terms of off-peak period power consumption, the value in NRS was slightly higher than that in PSS when the basement set-point temperature for off-peak period was 24 °C. However, the converse situation occurred when the set-point was 22°C or 23 °C. This is because in Scenario: PSS (22 °C), the set-point temperature difference between off-peak period and mid-peak period was small (i.e. 0.5 °C), thus, once stored energy released during early peak period (i.e. 6 a.m. – 10 a.m.) and the air temperature dropped, the EHF would have to be turned ON to recharge the slabs during mid-peak period.

It should be mentioned that both NRS and PSS can be applied to shift peak load as well as mid-peak load. However, their peak shifting abilities were affected by the set-point temperature during off-peak period: the higher the off-peak period set-point temperature, the more heating load was shifted from peak period to off-peak period. If thermal comfort was not considered and the aim was to shift both mid-peak and peak consumption, NRS would be recommended. However, if the main concern was shifting peak load as much as possible with consideration thermal comfort during extremely cold days, then PSS is recommended. Besides, the existing EHFs in the basement showed the ability to completely shift the heating consumption of the room in the basement from peak period to other periods.

Despite of the advantages, applying both strategies, which had a higher set-point temperature (23 °C or 24 °C) during off-peak period lead to higher daily energy consumed by heating the basement. If there was no time-of-use tariff in the implementation area, the heating

cost would be increased. Therefore, the effect of different heating strategies on the daily heating cost based on time-of-use tariff was worth investigated.

Figure 4.5 (secondary Y axis) compares the daily heating cost of basement under the afore-said scenarios. For NRS, increasing the set-point temperature during off-peak period increased the daily heating cost. Compared with the reference scenario, the daily basement heating cost was decreased by 37.16%, 30.34%, and 23.48% when the set-point of NRS for off-peak period was 22 °C, 23 °C and 24 °C, respectively. Also, PSS was effective to decrease the heating cost. Compared with the reference, the reduction of daily basement heating cost caused by PSS was 33.34%, 30.10% and 23.32% when the set-point temperature for off-peak period was 22 °C, 23 °C and 24 °C, respectively. Through comparison of daily basement heating cost between NRS and PSS under the same set-point temperature for off-peak period, NRS was more cost saving and recommended than PSS if thermal comfort was not considered.

Considering the energy consumed by basement and the second floor, the power consumption during different periods and the daily heating cost of these scenarios are compared in Figure 4.6. The results from this figure were consistent with that from Figure 4.5, which are not repeated here. Note that the power consumption difference between this figure and Figure 4.5 indicates the power consumed by the second floor as shown in Figure 4.7.

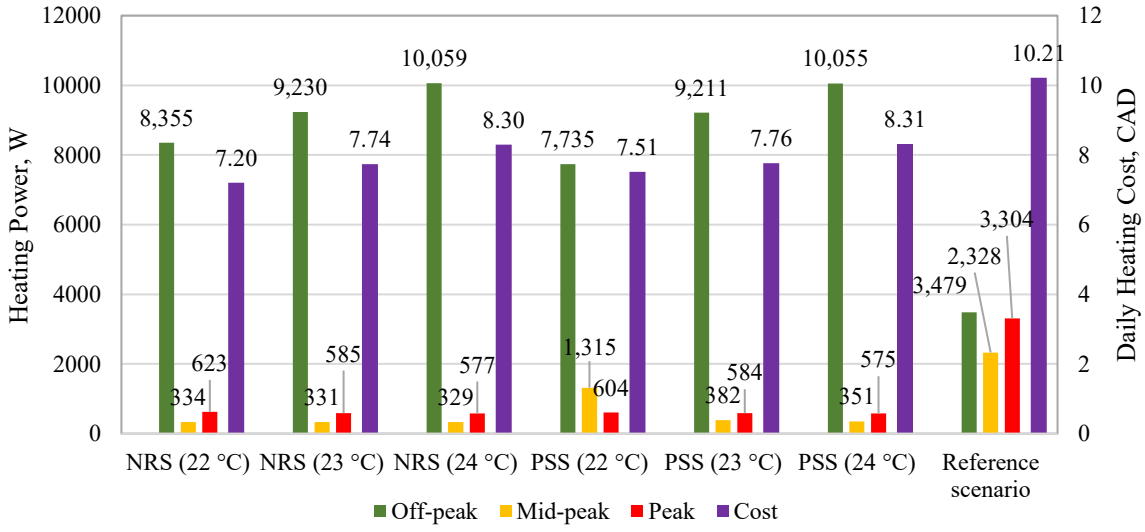

Figure 4.6: Average heating power consumed by the basement and the second floor during different periods (left axis) and daily heating cost (right axis) under different heating strategies

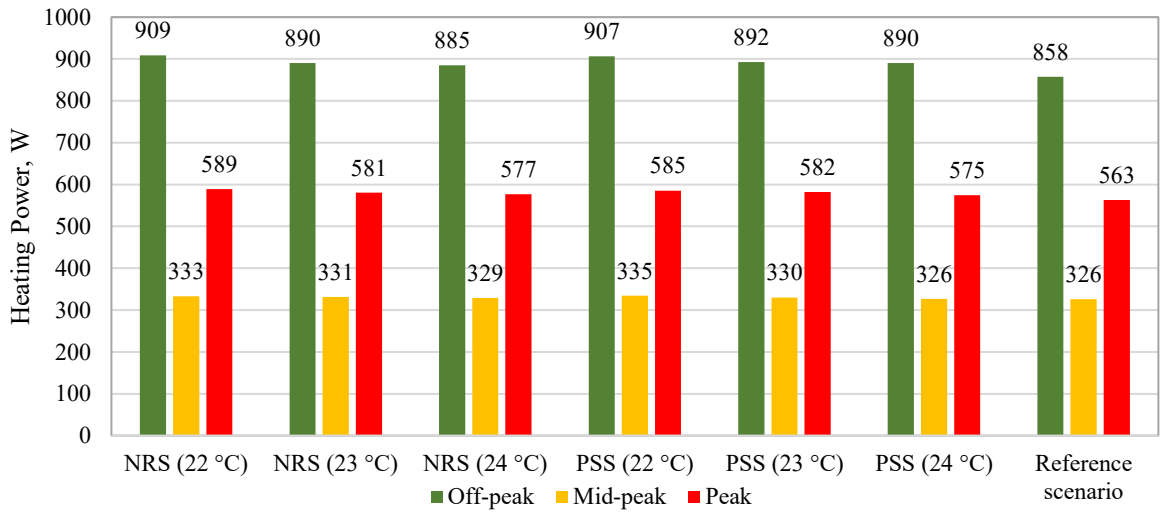

Figure 4.7: Average heating power consumed by the second floor during different periods under different heating strategies

Figure 4.7 shows that the power consumed by the second floor was not affected by the heating strategies applied to the basement. Besides, under constant set-point temperature during all day, heating demand of the second floor was lowest during mid-peak period and highest during off-peak period. This is mainly because that the exterior temperature during off-peak period was lowest during the day, while the higher exterior temperature and heat gain due to solar radiation during mid-peak period would decrease the heating demand. Because of the relatively low heating demand during mid-peak and peak period, proper strategy may be found to extract a small part of stored energy from the existing EHF to meet the heating demand of the second floor during daytime.

4.3. INVESTIGATION OF HES

4.3.1. HEATING PERFORMANCE OF HES

4.3.1.1. The effect of airflow rate

The airflow rate of HES would affect the temperature of source room which has a constant set-point temperature at 24 °C, because of the temperature difference between the source room and

air returned from the ground floor. The effect of airflow rate on the source room (B1) temperature during the coldest day and warmest day are shown in Figure 4.8 and Figure 4.9, respectively.

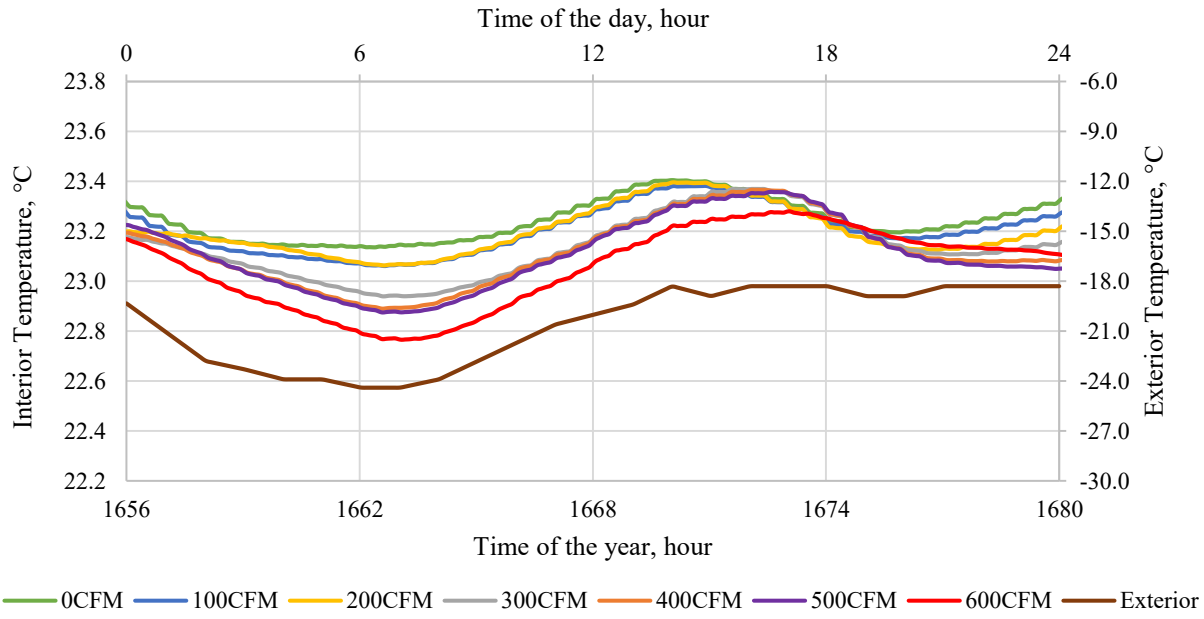

Figure 4.8: The effect of airflow rate on the temperature of source room (B1) during the coldest day (March 10th, 2017)

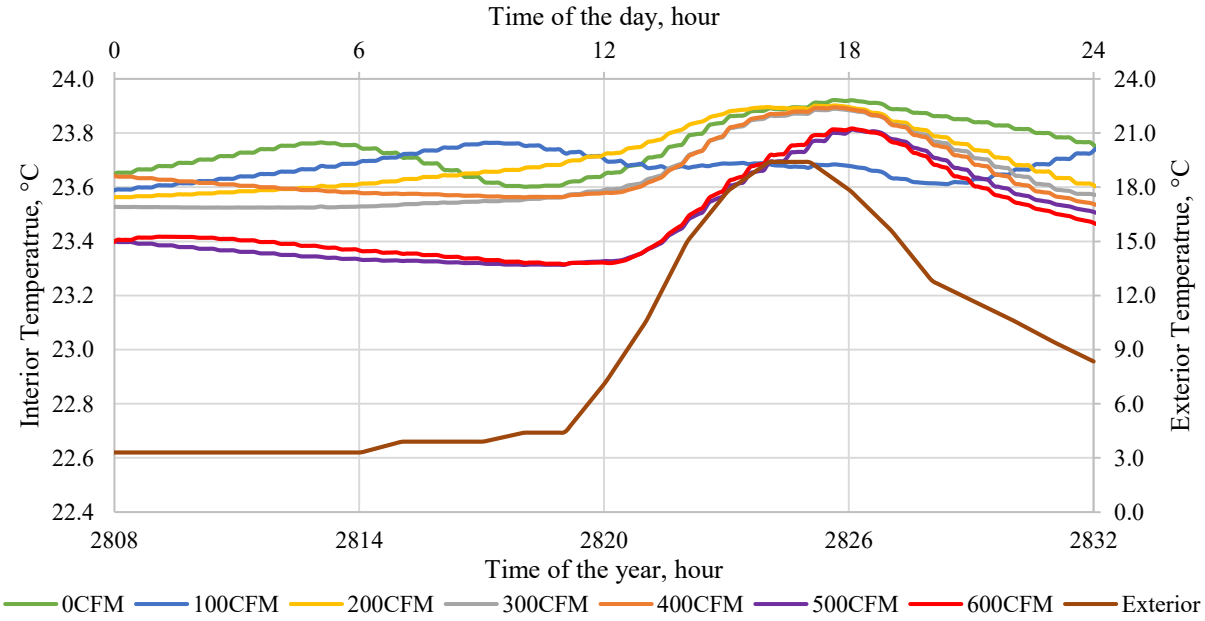

Figure 4.9: The effect of airflow rate on the temperature of source room (B1) during the warmest day (April 27th, 2017)

Figure 4.8 shows that during the coldest day, increasing the airflow rate of HES would decrease the temperature of room B1. For example, compared with no operation of HES (0 CFM), turning ON the HES at 600 CFM (i.e. 0.28 $m^3.s^{-1}$) resulted in a 0.4 °C temperature decrease at 6 a.m. Besides, it indicates that when the airflow rate was higher than 300 CFM (i.e. 0.14 $m^3.s^{-1}$), the occurrence of maximum interior temperature among the coldest day could be delayed from about 2 p.m. to around 5 p.m. The decrease of maximum temperature of room B1 was negligible when the airflow rate was lower than 500 CFM (i.e. 0.24 $m^3.s^{-1}$).

Similarly, increasing the airflow rate of HES decreased the interior temperature of room B1 during the warmest day as shown in Figure 4.9. Except 100 CFM (i.e. 0.05 $m^3.s^{-1}$), the tendency of source room temperature followed the trend of exterior temperature under all other airflow rates. Besides, the air temperature of room B1 never reached the set-point temperature (i.e. 24 °C), no matter during the coldest day or warmest day, mainly due to heat transfer with other rooms in the second floor which had a lower set-point temperature (20°C).

The temperature of rooms in the second floor as a result of different airflow rate during March 10th and April 27th are shown in Figure 4.10 and Figure 4.11, respectively.

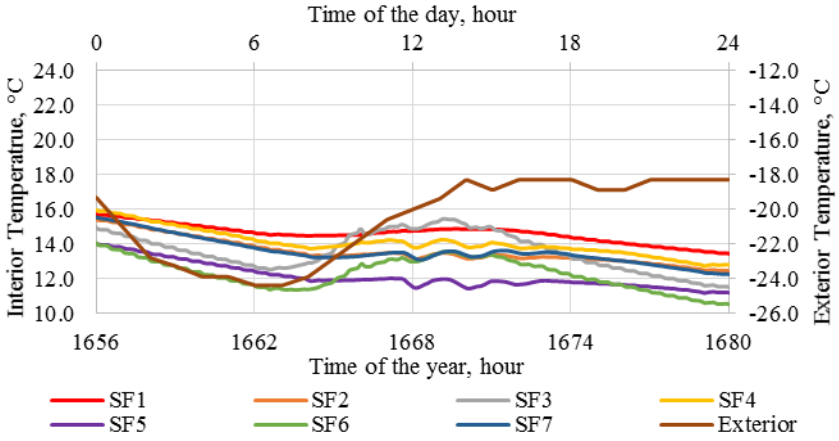
Time of the day, hour
0
6
12
18
24
Interior Temperatrue, °C
Exterior Temperature, °C
24.0
22.0
20.0
18.0
16.0
14.0
12.0
10.0
-12.0
-14.0
-16.0
-18.0
-20.0
-22.0
-24.0
-26.0
1656
1662
1668
1674
1680
Time of the year, hour
SF1
SF2
SF3
SF4
SF5
SF6
SF7
Exterior

(a)

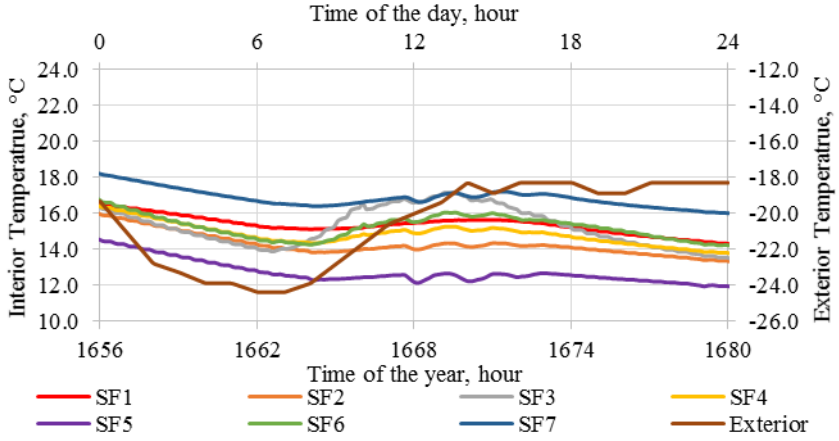
Time of the day, hour
0
6
12
18
24
Interior Temperatrue, °C
Exterior Temperatrue, °C
24.0
22.0
20.0
18.0
16.0
14.0
12.0
10.0
-12.0
-14.0
-16.0
-18.0
-20.0
-22.0
-24.0
-26.0
1656
1662
1668
1674
1680
Time of the year, hour
SF1
SF2
SF3
SF4
SF5
SF6
SF7
Exterior

(b)

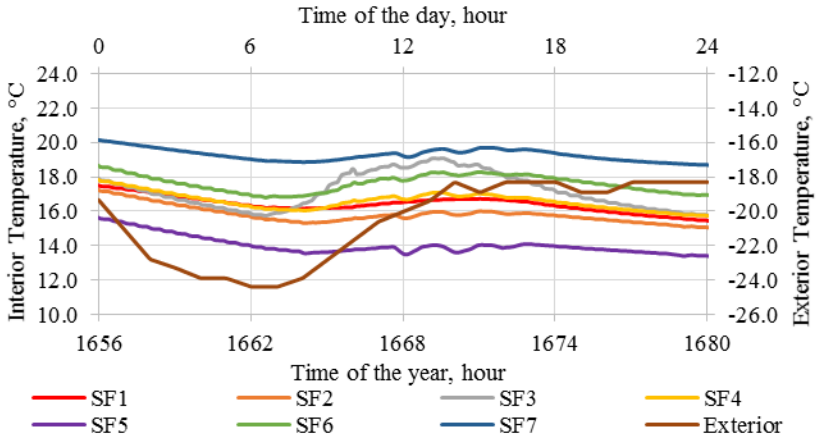
Time of the day, hour
0
6
12
18
24
Interior Temperature, °C
Exterior Temperature, °C
24.0
22.0
20.0
18.0
16.0
14.0
12.0
10.0
-12.0
-14.0
-16.0
-18.0
-20.0
-22.0
-24.0
-26.0
1656
1662
1668
1674
1680
Time of the year, hour
SF1
SF2
SF3
SF4
SF5
SF6
SF7
Exterior

(c)

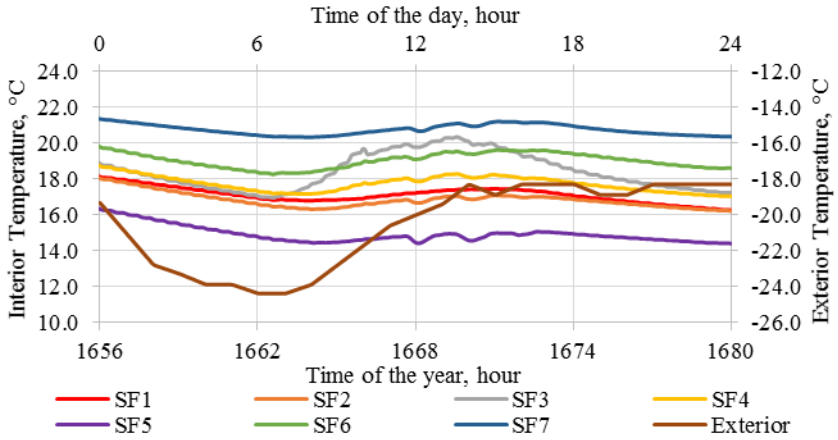
Time of the day, hour
0
6
12
18
24
Interior Temperature, °C
Exterior Temperature, °C
24.0
22.0
20.0
18.0
16.0
14.0
12.0
10.0
-12.0
-14.0
-16.0
-18.0
-20.0
-22.0
-24.0
-26.0
1656
1662
1668
1674
1680
Time of the year, hour
SF1
SF2
SF3
SF4
SF5
SF6
SF7
Exterior

(d)

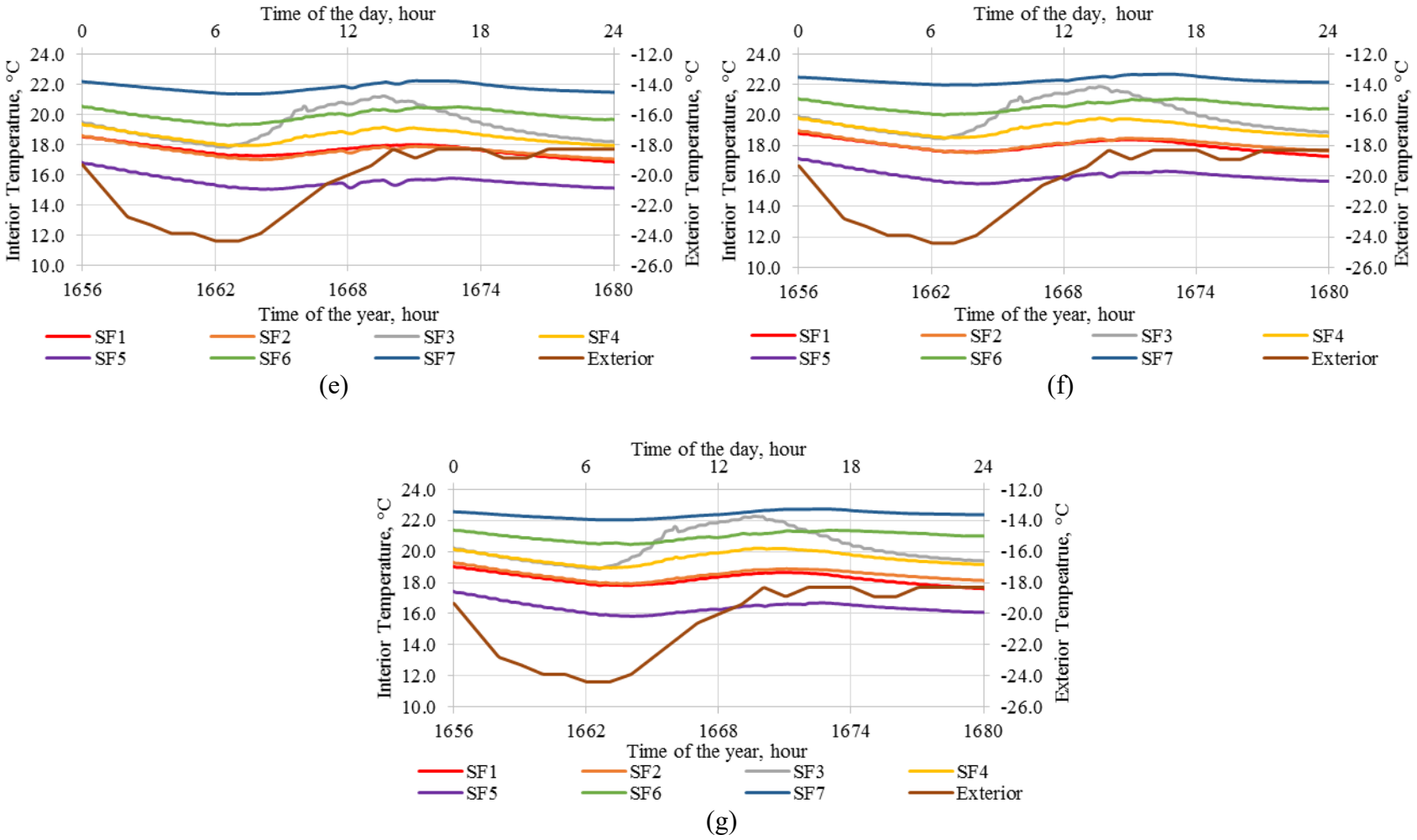

Figure 4.10: The air temperature of rooms in the second floor during the coldest day (March 10th, 2017) with the airflow rate of HES at (a) 0 CFM, (b) 100 CFM, (c) 200 CFM; (d) 300 CFM; (e)400 CFM; (f) 500 CFM; (g) 600 CFM

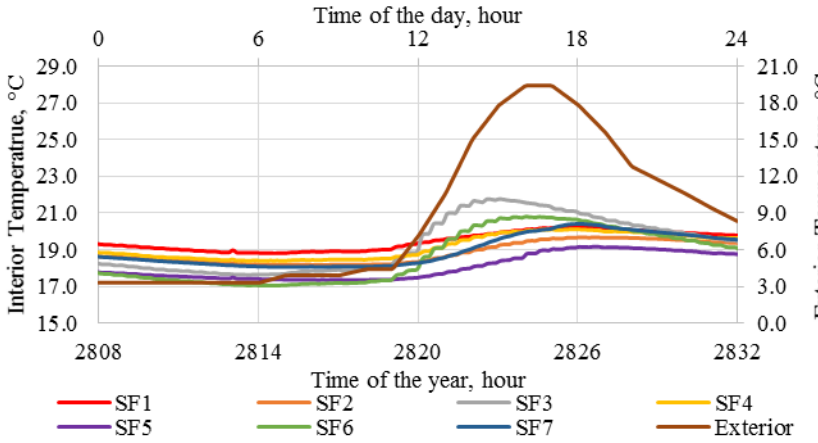
Time of the day, hour
0
6
12
18
24
Interior Temperatrue, °C
29.0
27.0
25.0
23.0
21.0
19.0
17.0
15.0
Exterior Temperatrue, °C
21.0
18.0
15.0
12.0
9.0
6.0
3.0
0.0
2808
2814
2820
2826
2832
Time of the year, hour
SF1
SF2
SF3
SF4
SF5
SF6
SF7
Exterior

(a)

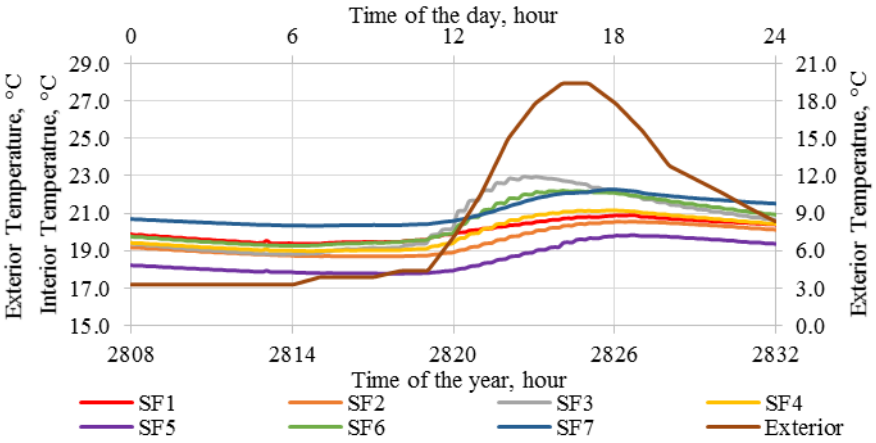
Time of the day, hour
0
6
12
18
24
Interior Temperatrue, °C
29.0
27.0
25.0
23.0
21.0
19.0
17.0
15.0
Exterior Temperatrue, °C
21.0
18.0
15.0
12.0
9.0
6.0
3.0
0.0
2808
2814
2820
2826
2832
Time of the year, hour
SF1
SF2
SF3
SF4
SF5
SF6
SF7
Exterior

(b)

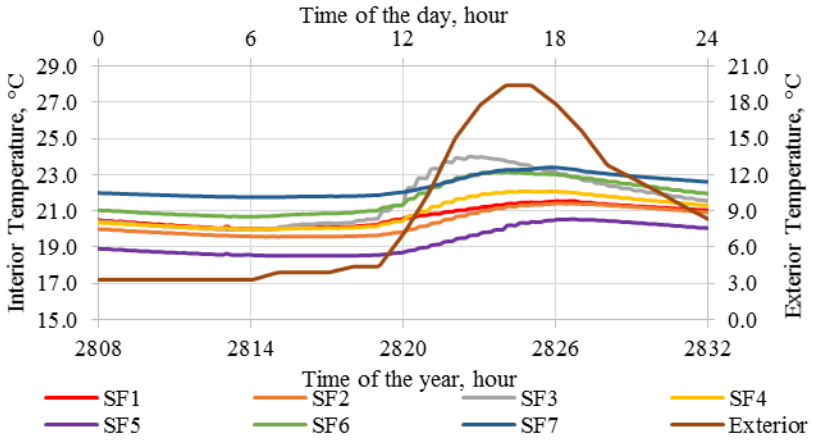
Time of the day, hour
0
6
12
18
24
Interior Temperature, °C
29.0
27.0
25.0
23.0
21.0
19.0
17.0
15.0
Exterior Temperature, °C
21.0
18.0
15.0
12.0
9.0
6.0
3.0
0.0
2808
2814
2820
2826
2832
Time of the year, hour
SF1
SF2
SF3
SF4
SF5
SF6
SF7
Exterior

(c)

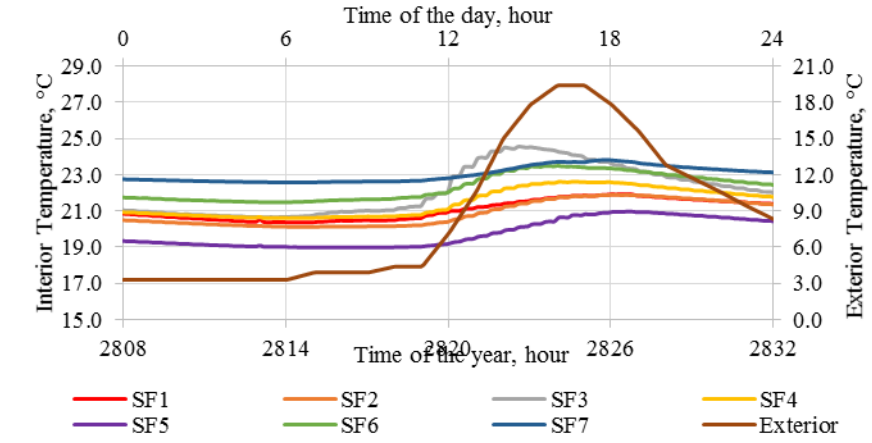
Time of the day, hour
0
6
12
18
24
Interior Temperature, °C
29.0
27.0
25.0
23.0
21.0
19.0
17.0
15.0
Exterior Temperature, °C
21.0
18.0
15.0
12.0
9.0
6.0
3.0
0.0
2808
2814
2820
2826
2832
Time of the year, hour
SF1
SF2
SF3
SF4
SF5
SF6
SF7
Exterior

(d)

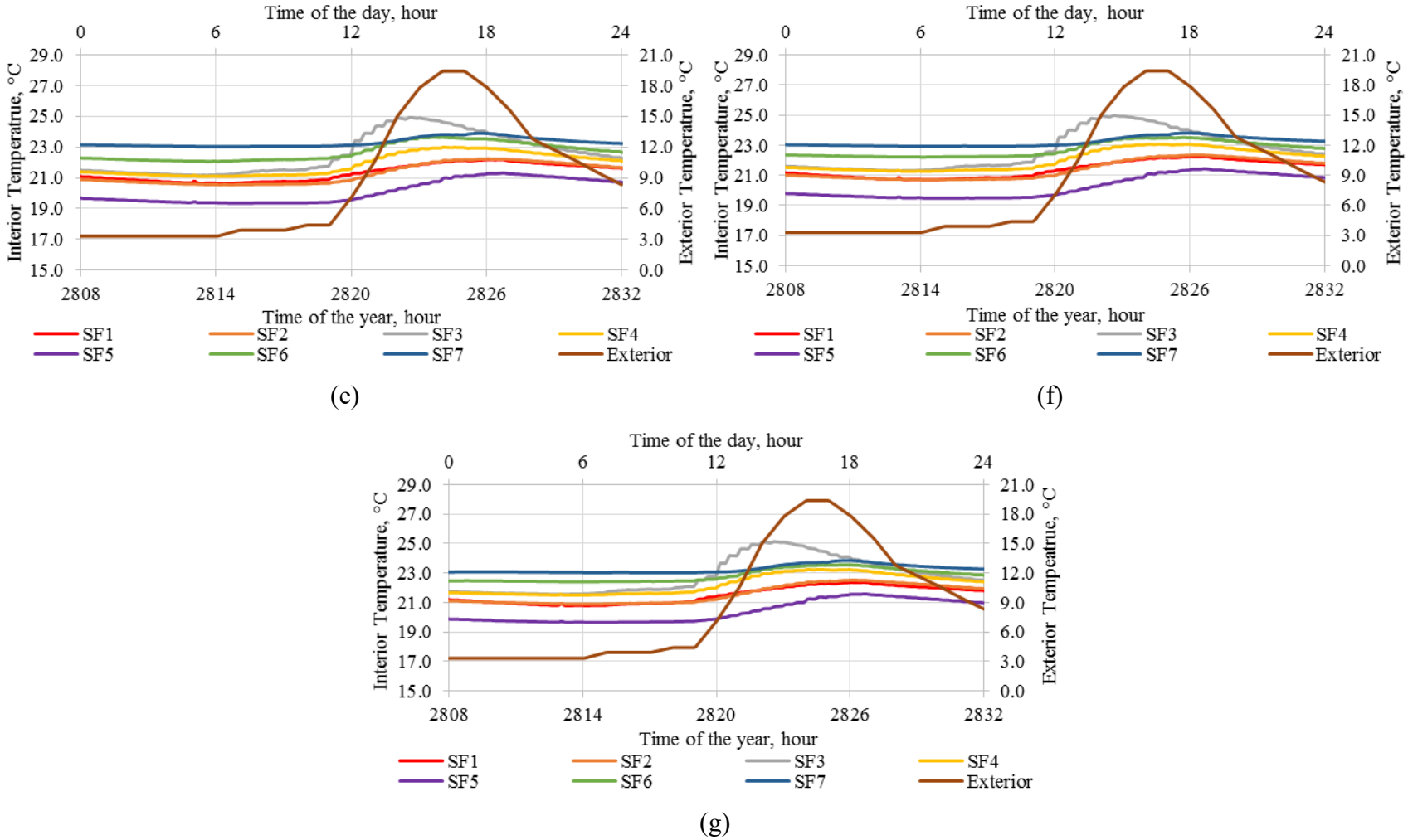

Figure 4.11: The air temperature of rooms in the second floor during the warmest day (April 27th, 2017) with the airflow rate of HES at (a) 0 CFM, (b) 100 CFM, (c) 200 CFM; (d) 300 CFM; (e) 400 CFM; (f) 500 CFM; (g) 600 CFM

Figure 4.10 and Figure 4.11 show that the interior temperature of rooms in the second floor increased by increasing the airflow rate of HES. Besides, the minimum temperature of the second floor usually occurred in room SF5, which was usually not occupied and was furthest to the outlets in SF6 and SF7.

Figure 4.10 (a) and (g)indicates that the minimum and maximum temperature among the second floor increased from around 10 °C to 16 °C and from about 16 °C to 23 °C, respectively, when increasing the airflow rate from 0 CFM (i.e. 0 $m^3.s^{-1}$) to 600 CFM (i.e. 0.28 $m^3.s^{-1}$) during the coldest day. Besides, when the HES was turned ON, the maximum temperature always occurred in room SF7 and most of time the interior temperatures of SF6 and SF7 were higher than other rooms (shown in Figure 4.10 (b) to (g)), because the hot air from B1 was directly transferred to SF6 and SF7. The reason for relative high temperature of room SF3 at noon is the high solar radiation.

Similar tendency can be observed from Figure 4.11. It need to be noted that during the warmest day with the exterior temperature ~3 °C during morning, HES at 600CFM kept all rooms in the second floor above 20 °C, as shown in Figure 4.11 (g). Therefore, when the exterior temperature is higher than 0 °C, implementing HES with 600 CFM would be able to warm the second floor of the existing house within thermal comfort.

The temperatures of second floor and basement heating power consumption under different airflow rates are summarized in Figure 4.12. The blue bars in the figure show the average power consumed by the basement ($P_{ave,basement}$, calculated based on Equation 4.1), during the simulation period under different air flow rates. Note that since the baseboards in the second floor are turned OFF, the power values represent the total power consumed by the basement and second floor under the same airflow. Due to the complexity of showing air temperature of each room at each time, the simulation results of second floor temperatures are simplified as following. The black line shows the average of mean second floor air temperature ($T_{ave,mean}$, calculated based on Equation 4.2) during the simulation period. From top to bottom, the open-high-low-close stocks show the maximum mean second floor air temperature ($T_{max,mean,}$ calculated based on Equation 4.3), followed by the maximum room temperature within the second floor ($T_{max,}$ calculated based on Equation 4.4), minimum room temperature within the second floor ($T_{min,}$ calculated based on

Equation 4.5), and minimum mean second floor air temperature ($T_{min,mean,}$ calculated based on Equation 4.6).

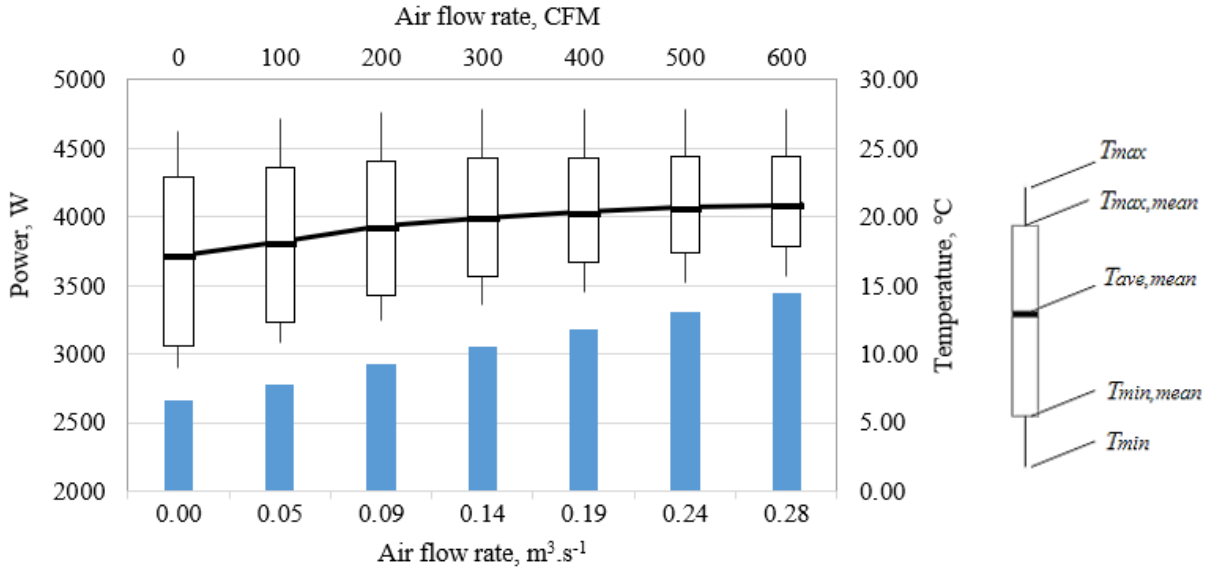

Figure 4.12: The effect of airflow rate on average basement power consumption (lower section, left axis) and the second floor temperatures (upper section, right axis)

$$P_{ave,basement} = (P_{peak,basement} * D_{peak} + P_{mid,basement} * D_{mid} + P_{off,basement} * D_{off})/24 \quad (4.1)$$

where $P_{ave,basement}$ is the average power required for heating the basement [W]; $P_{peak,basement}$, $P_{mid,basement}$, $P_{off,basement}$ is the power required for heating the basement [W]; D_{peak}, D_{mid}, D_{off} is the duration [h] during peak, mid-peak and off-peak period, respectively.

$$T_{ave,mean} = \sum_t T_{mean,t}/N \quad (4.2)$$

where $T_{ave,mean}$ is the average of mean second floor air temperature [°C]; $T_{mean,t}$ is the area weighted mean temperature of second floor at time t [°C]; N is the number of measured data points.

$$T_{max,mean} = max\ (T_{mean,t}) \quad (4.3)$$

where $T_{max,mean}$ is the maximum mean second floor air temperature [°C]; $T_{mean,t}$ is the area weighted mean temperature of second floor at time t [°C].

$$T_{min,mean} = min\ (T_{mean,t}) \quad (4.4)$$

where $T_{min,mean}$ is the minimum mean second floor air temperature [°C]; $T_{mean,t}$ is the area weighted mean temperature of second floor at time *t* [°C].

$$T_{min} = min\ (T_{in,i,t}) \tag{4.5}$$

where T_{min} is the minimum room temperature within the second floor [°C]; $T_{in,i,t}$ is the room air temperature of room *i* in second floor at time *t* [°C].

$$T_{min} = min\ (T_{in,i,t}) \tag{4.6}$$

where T_{max} is the maximum room temperature within the second floor [°C]; $T_{in,i,t}$ is the room air temperature of room *i* in second floor at time *t* [°C].

Figure 4.12 shows that increasing the airflow increased $P_{ave,basement}$ almost linearly. On the other hand, the upper section of this figure indicates that greater air flow rates increased $T_{ave,mean}$. Moreover, $T_{max,mean}$ and T_{max} increased by increasing the airflow up to 0.14 $m^3.s^{-1}$ (i.e. 300 CFM). Beyond 300 CFM, they remained almost stable, around 24.4 °C and 27.8 °C, respectively. This can be explained by the decreased source room temperature when increasing the airflow rate (shown in Figure 4.8 and Figure 4.9). On the other hand, T_{min} and $T_{min,mean}$ were almost linearly correlated to the airflow rate. This means that an air flow rate of 0.14 $m^3.s^{-1}$ would be able to keep second floor air temperature at around 20 °C in terms of $T_{ave,mean}$; however, it would not be enough to obtain an acceptable T_{min} value (i.e. 15 °C). In other words, higher airflow rate values more than 300 CFM would be needed, if the air temperature of each zone in the second floor is required to be higher than 15 °C.

4.3.1.2.The effect of outlet location

Since same airflow rate (i.e. 300 CFM) was considered for each scenario in this subsection, the source room temperature was not affected by the outlet location. Therefore, it can be considered the same as values in Figure 4.8(d) and Figure 4.9(d).

The effect of outlet location on the temperature of rooms in the second floor during coldest day and warmest day was shown in Figure 4.13 and Figure 4.14, respectively.

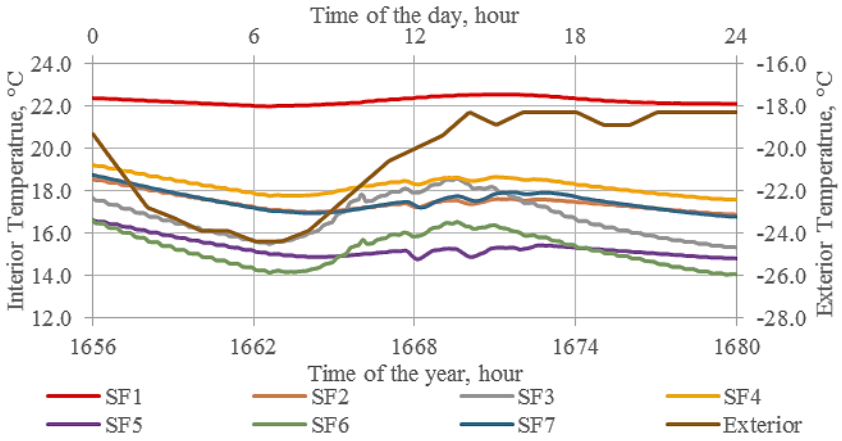
Time of the day, hour
0
6
12
18
24
Interior Temperatrue, °C
24.0
22.0
20.0
18.0
16.0
14.0
12.0
Exterior Temperatrue, °C
-16.0
-18.0
-20.0
-22.0
-24.0
-26.0
-28.0
1656
1662
1668
1674
1680
Time of the year, hour
SF1
SF2
SF3
SF4
SF5
SF6
SF7
Exterior

(a)

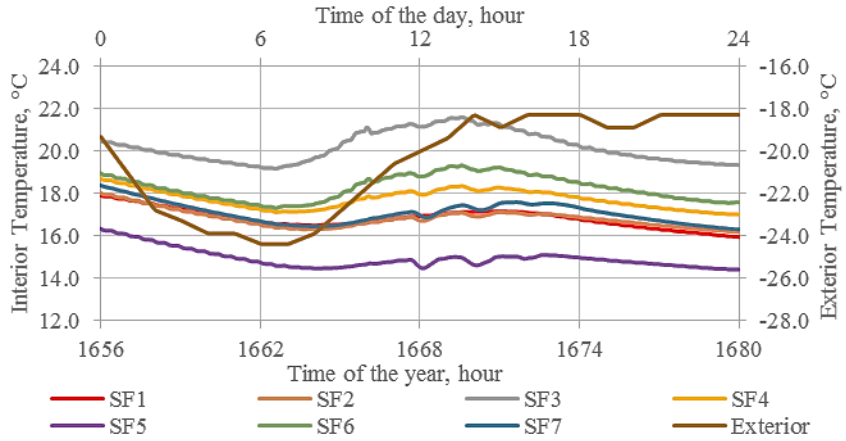
Time of the day, hour
0
6
12
18
24
Interior Temperatrue, °C
24.0
22.0
20.0
18.0
16.0
14.0
12.0
Exterior Temperatrue, °C
-16.0
-18.0
-20.0
-22.0
-24.0
-26.0
-28.0
1656
1662
1668
1674
1680
Time of the year, hour
SF1
SF2
SF3
SF4
SF5
SF6
SF7
Exterior

(b)

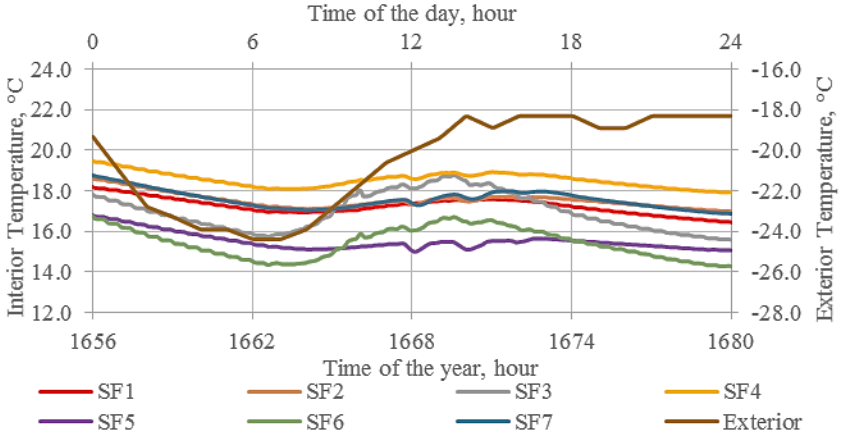
Time of the day, hour
0
6
12
18
24
Interior Temperatrue, °C
24.0
22.0
20.0
18.0
16.0
14.0
12.0
Exterior Temperatrue, °C
-16.0
-18.0
-20.0
-22.0
-24.0
-26.0
-28.0
1656
1662
1668
1674
1680
Time of the year, hour
SF1
SF2
SF3
SF4
SF5
SF6
SF7
Exterior

(c)

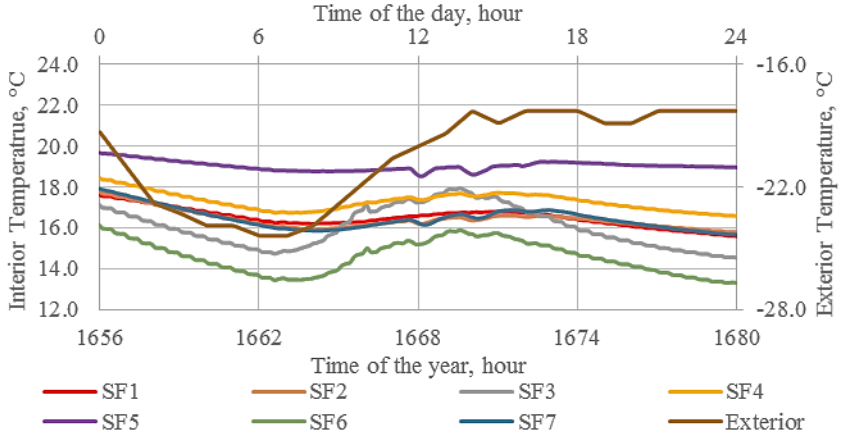
Time of the day, hour
0
6
12
18
24
Interior Temperatrue, °C
24.0
22.0
20.0
18.0
16.0
14.0
12.0
Exterior Temperatrue, °C
-16.0
-22.0
-28.0
1656
1662
1668
1674
1680
Time of the year, hour
SF1
SF2
SF3
SF4
SF5
SF6
SF7
Exterior

(d)

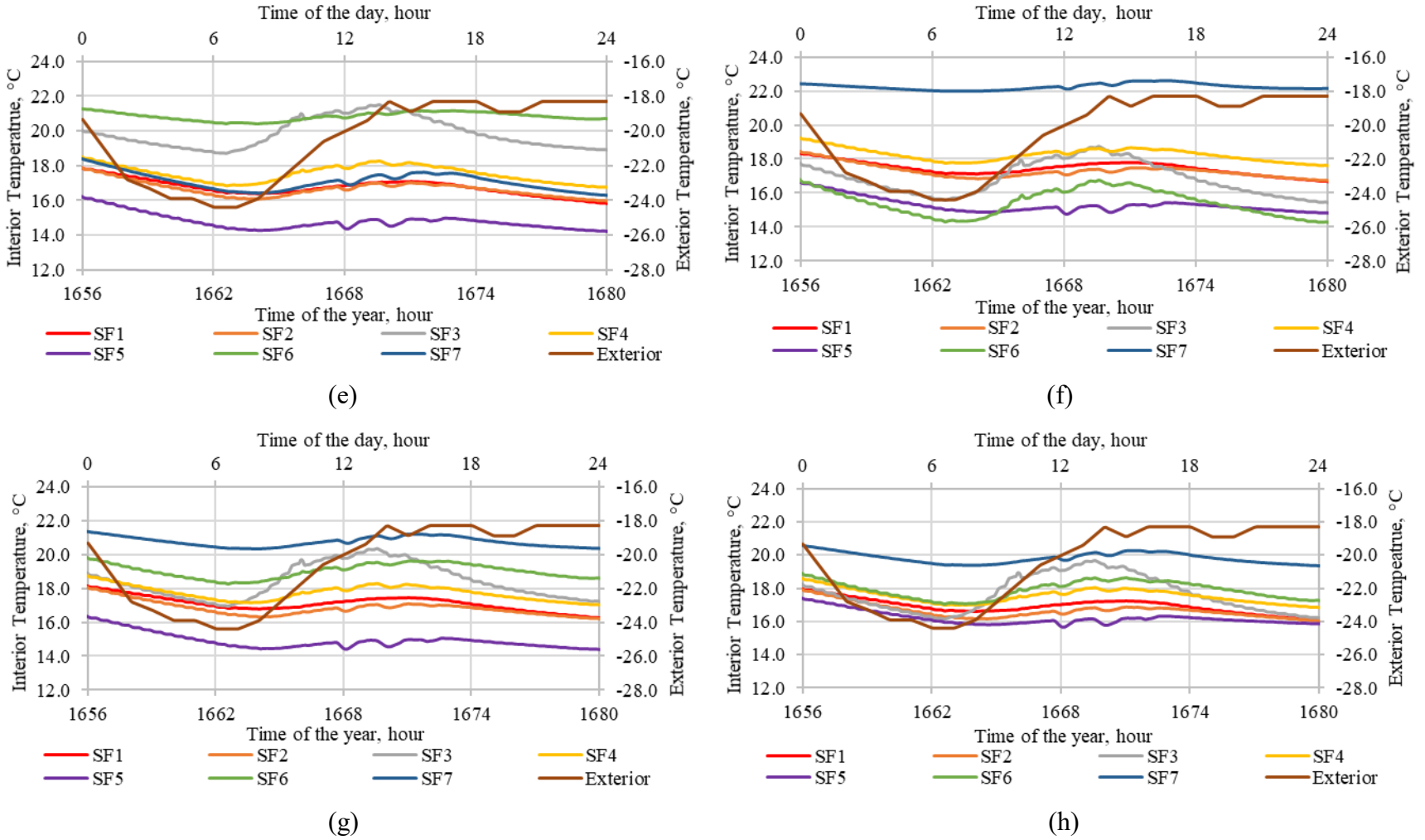

Figure 4.13: The air temperature of rooms in the second floor during the coldest day (March 10th, 2017) with the outlet located in (a) SF1, (b) SF3, (c) SF4 (d) SF5, (e)SF6, (f) SF7, (g) SF6,7, and (h) SF5,6,7.

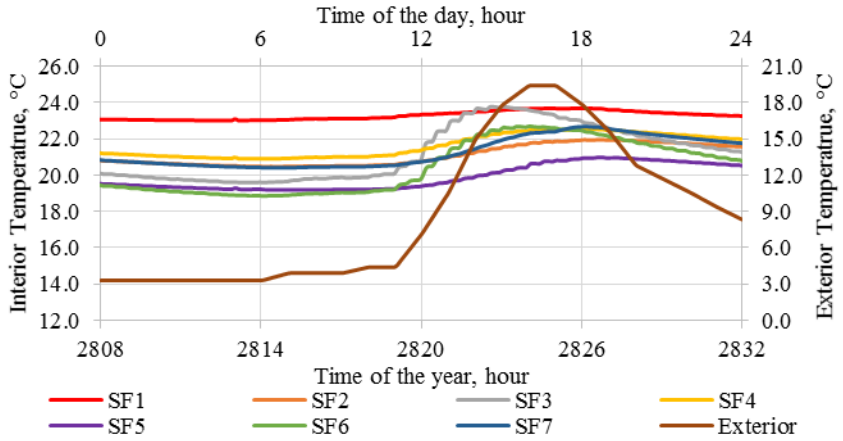
Time of the day, hour
0
6
12
18
24
Interior Temperatrue, °C
Exterior Temperatrue, °C
26.0
24.0
22.0
20.0
18.0
16.0
14.0
12.0
21.0
18.0
15.0
12.0
9.0
6.0
3.0
0.0
2808
2814
2820
2826
2832
Time of the year, hour
SF1
SF2
SF3
SF4
SF5
SF6
SF7
Exterior

(a)

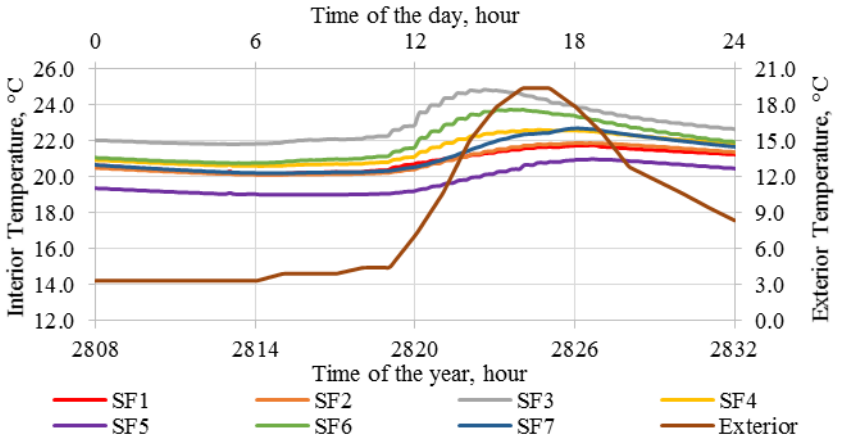
Time of the day, hour
0
6
12
18
24
Interior Temperatrue, °C
Exterior Temperatrue, °C
26.0
24.0
22.0
20.0
18.0
16.0
14.0
12.0
21.0
18.0
15.0
12.0
9.0
6.0
3.0
0.0
2808
2814
2820
2826
2832
Time of the year, hour
SF1
SF2
SF3
SF4
SF5
SF6
SF7
Exterior

(b)

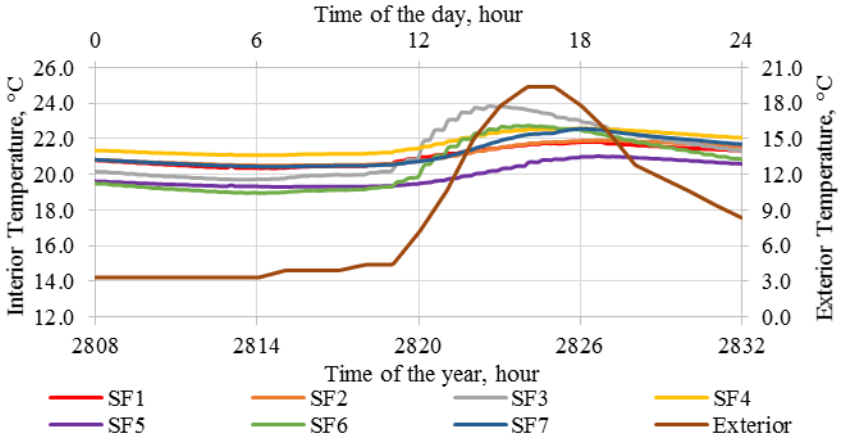
Time of the day, hour
0
6
12
18
24
Interior Temperatrue, °C
Exterior Temperatrue, °C
26.0
24.0
22.0
20.0
18.0
16.0
14.0
12.0
21.0
18.0
15.0
12.0
9.0
6.0
3.0
0.0
2808
2814
2820
2826
2832
Time of the year, hour
SF1
SF2
SF3
SF4
SF5
SF6
SF7
Exterior

(c)

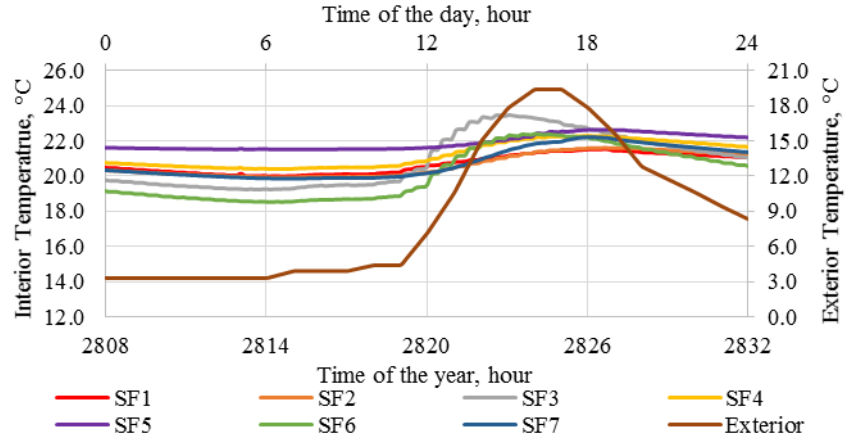
Time of the day, hour
0
6
12
18
24
Interior Temperatrue, °C
Exterior Temperatrue, °C
26.0
24.0
22.0
20.0
18.0
16.0
14.0
12.0
21.0
18.0
15.0
12.0
9.0
6.0
3.0
0.0
2808
2814
2820
2826
2832
Time of the year, hour
SF1
SF2
SF3
SF4
SF5
SF6
SF7
Exterior

(d)

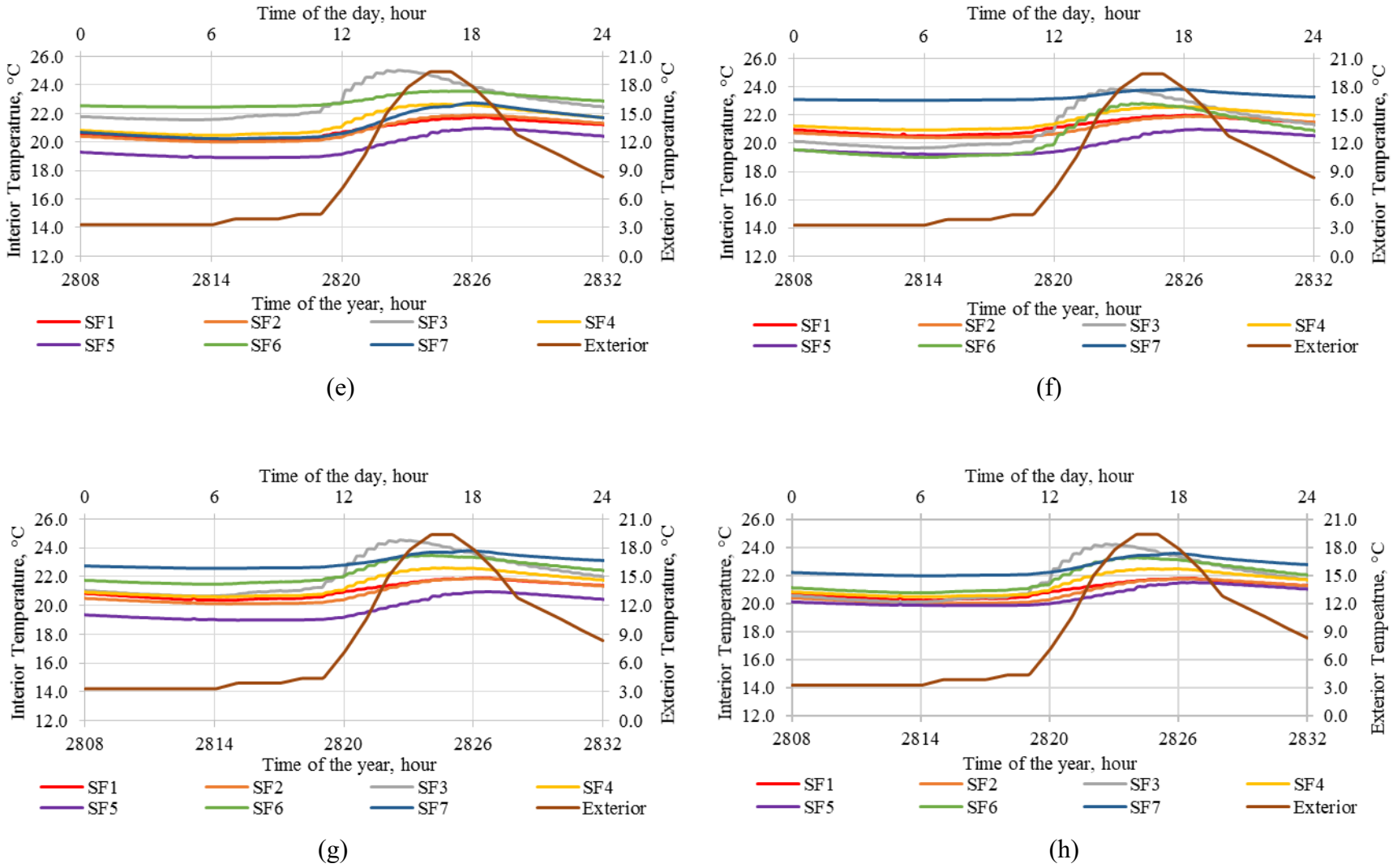

Figure 4.14: The air temperature of rooms in the second floor during the warmest day (April 27th, 2017) with the outlet located in (a) SF1, (b) SF3, (c) SF4 (d) SF5, (e) SF6, (f) SF7, (g) SF6,7, and (h) SF5,6,7.

It is obvious from Figure 4.13 and Figure 4.14 that the outlet location has a significant effect on the temperature distribution of second floor. The maximum temperature among the second floor usually occurred in the room where the hot air from basement was transferred to, while the minimum temperature among the second floor occurred in the room which is furthest to the outlet location. For instance, Figure 4.13 (a) and Figure 4.14 (a) shows that when transferring 300 CFM air to room SF1, the maximum room temperature among the second floor occurred in room SF1, while the minimum temperature among the second floor occurred in SF5 or SF6 which was not neighbored with SF1. Besides, sending air to three rooms (SF5,6,7) resulted in evenly distributed temperature (i.e. the difference between maximum and minimum temperature among the second floor was smallest when comparing to other cases). Figure 4.13 shows that during the coldest day, HES with 300 CFM airflow rate and outlets located in SF5,6,7 kept the temperature of rooms in the second floor above 15 °C, while other locations has no such ability. Further, Figure 4.14 illustrates that during the warmest day, transferring hot air directly to room SF5,6,7 could warm all rooms in the second floor to around or above 20 °C.

The temperatures of second floor and basement heating power consumption under different outlet locations are summarized in Figure 4.15. The x-axis of the figure shows the room in which the outlet is located. Note that each room had one outlet only.

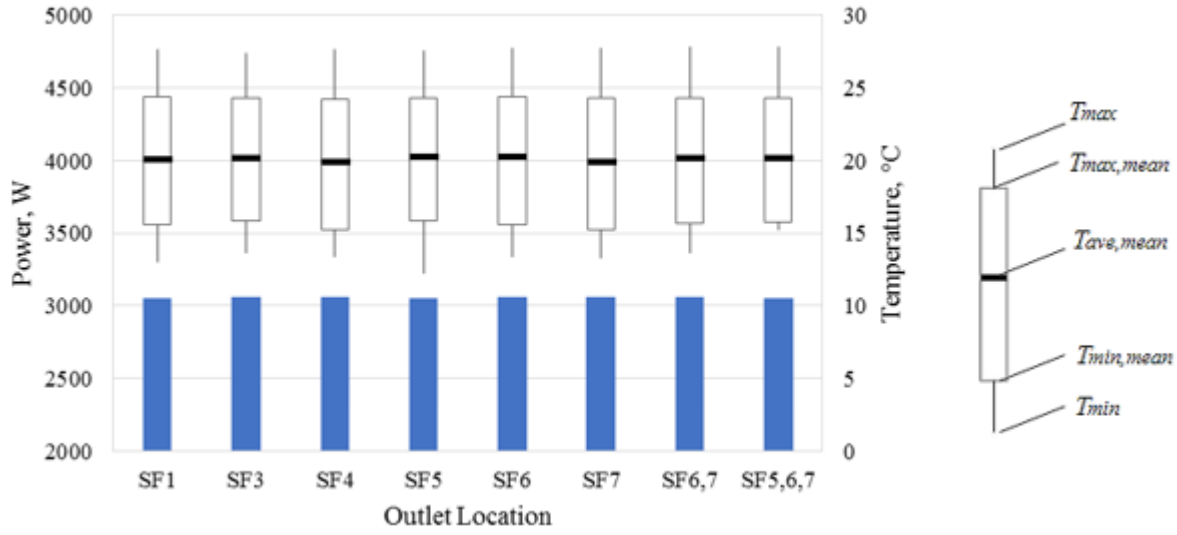

Figure 4.15: The effect of outlet location on average basement power consumption (lower section, left axis) and the second floor temperatures (upper section, right axis)

Figure 4.15 shows that the outlet location slightly affected $T_{ave,mean}$, $T_{max,mean}$, T_{max}, $T_{min,mean}$; however, its effect on T_{min} was significant. Separately supplying air into SF5, SF6, and SF7 increased T_{min} to around 15 °C. This means that separate outlets effectively transferred air to remote object rooms, such as SF5, while slightly affecting on the amount of heat extraction. Therefore, separate outlets are recommended to achieve evenly temperature distribution. However, economic factors should also be considered to select proper outlets during implementation.

4.3.2. PEAK SHIFTING EXTENDING PERFORMANCE OF HES

Due to the same airflow rate (600 CFM) between Scenario 1 and Scenario 2 (for details pertaining to scenarios, please refer Table 3.7), the source room (B1) temperature was almost the same between these two scenarios. This situation also occurred between Scenario 3 and Scenario 4. Therefore, this investigation compared the interior air temperature of room B1 for Scenario 1, Scenario 3 and the reference case. The comparison during the coldest day and the warmest day was shown in Figure 4.16 and Figure 4.17, respectively.

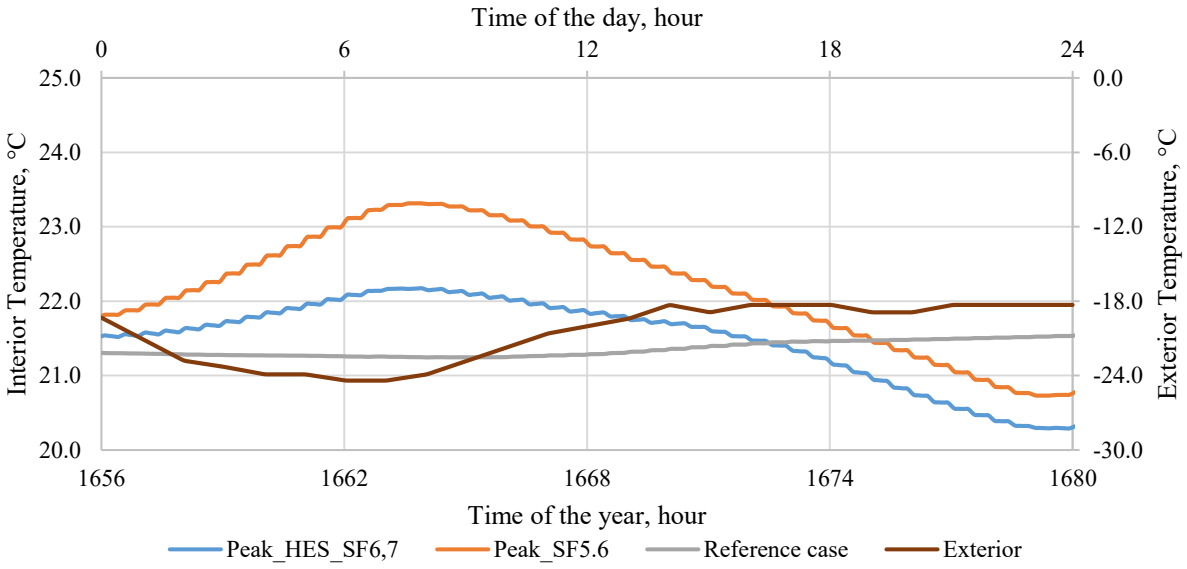

Figure 4.16: Temperature of source room (B1) for Scenario 1 (Peak_HES_SF6,7), Scenario 3 (Peak_SF6,7) and the reference case during the coldest day (March 10th, 2017)

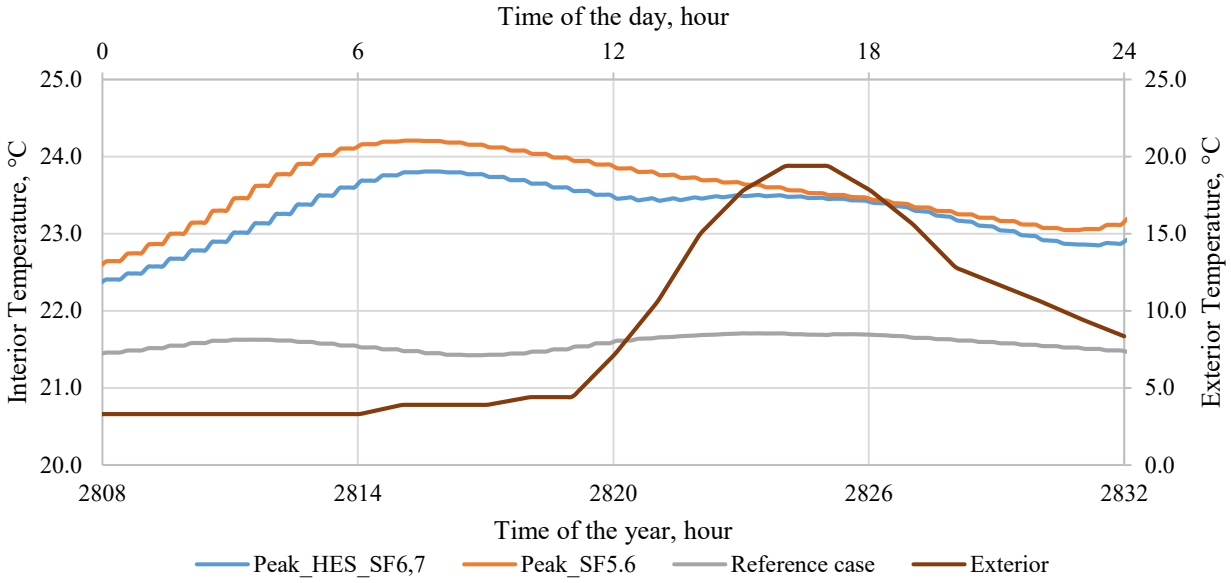

Figure 4.17: Temperature of source room (B1) for Scenario 1 (Peak_HES_SF6,7), Scenario 3 (Peak_SF6,7) and the reference case during the warmest day (April 27th, 2017)

Figure 4.16 depicts that implementing HES (i.e. Scenario 1) decreased the temperature of source room, compared with no such practice (i.e. Scenario 3). However, the source room temperature was kept always higher than 20°C in both scenarios. Thus, in this study, HES did not affect the thermal comfort of source room.

Also, the air temperature of room B1 increased above 24°C at the end of off-peak period (i.e. 6 a.m.) for Scenario 3 during the warmest day, as shown in Figure 4.17. The issue of overheating occurred. However, because of air returned from the ground floor with temperature at 21°C, the operating of HES eased this issue.

As shown in Table 3.7, only two kinds of second floor temperature (obtained from Scenario 1: Peak_HES_SF6,7 and Scenario 2: Peak_HES_SF5,6,7) were considered in this subsection. These temperatures during the coldest day and the warmest day is shown in Figure 4.18 and Figure 4.19, respectively.

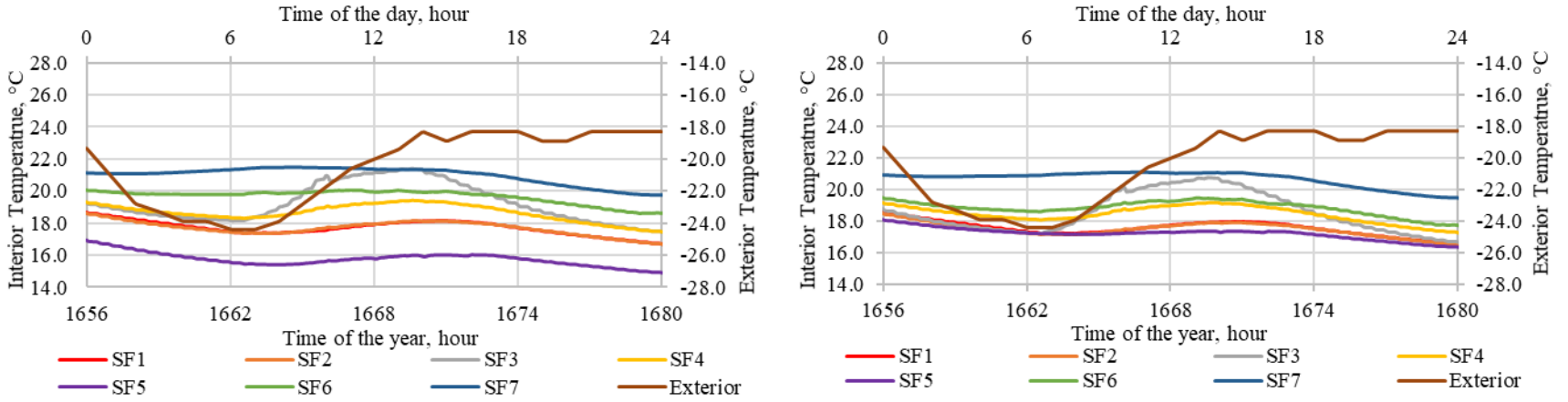

(a) (b)

Figure 4.18: The air temperature of rooms in the second floor during the coldest day (March 10th, 2017) under (a) Scenario 1: Peak_HES_SF6,7 and (b) Scenario 2: Peak_HES_SF5,6,7

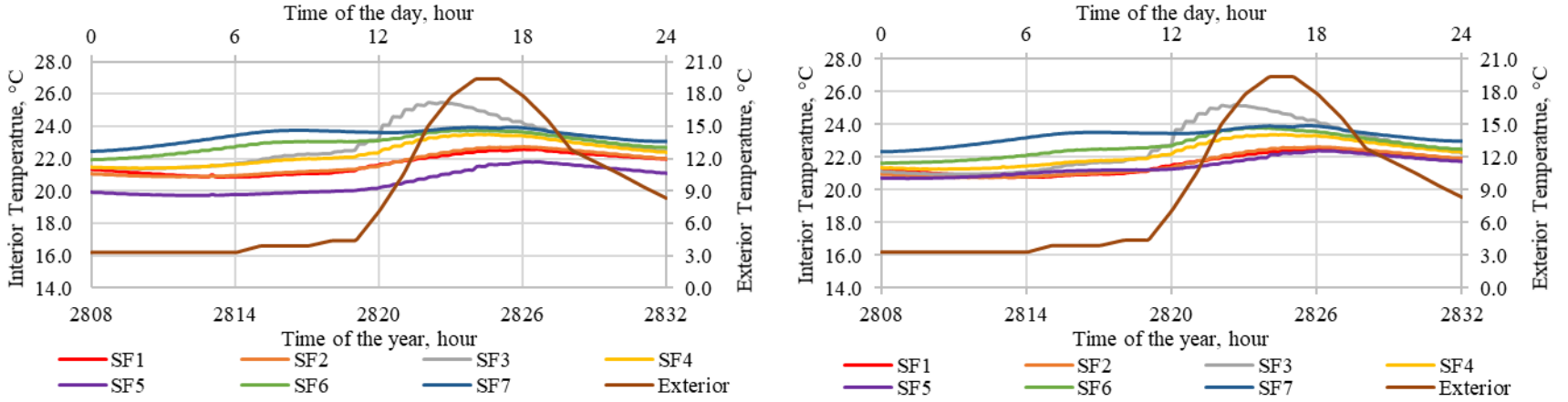

(a) (b)

Figure 4.19: The air temperature of rooms in the second floor during the warmest day (April 27th, 2017) under (a) Scenario 1: Peak_HES_SF6,7 and Scenario 2: Peak_HES_SF5,6,7

From Figure 4.18, applying PSS to EHF in the basement and sending hot air to SF6 and SF7 by HES at 600 CFM could not keep the temperature of rooms in the second floor always higher than 15 °C during the coldest day, while sending air to SF5,6,7 could achieve it. However, if higher interior temperature is required by occupants, additional heating system (such as the existing conventional baseboards) should be operated to supply more heat to the second floor. Besides, the decreasing of interior temperatures between 6 p.m. and midnight in Figure 4.18 was caused by the decreasing of source room temperature (shown in Figure 4.16). On the other hand, Figure 4.19 infers that if the exterior temperature was higher than 0 °C, Scenario 2: Peak_HES_SF5,6,7 would be enough to warm rooms in the second floor above 20°C.

The second-floor temperatures and average basement power consumption for these two scenarios are further summarized in Figure 4.20.

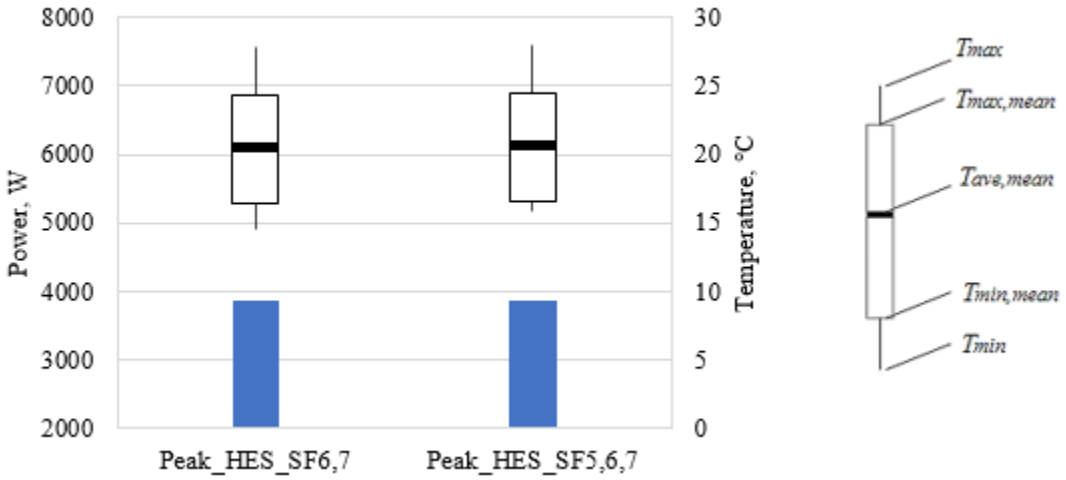

Figure 4.20: Average basement power consumption (lower section, left axis) and the second-floor temperatures (upper section, right axis) for Scenario 1(Peak_HES_SF6,7) and Scenario 2 (Peak_HES_SF5,6,7)

It is inferred from the Figure 4.20 that $T_{max,\ mean}$, T_{max}, $T_{ave,\ mean}$, $T_{min,\ mean}$ and $P_{avg,\ basement}$ were almost the same for scenarios 1 and 2. However, T_{min} was higher with three outlets than with two outlets. Though the power consumption of the HES with two and three outlets was the same, the variation between the T_{max} and T_{min} was minimum for three outlets. Note that, similar trend of results were discussed in Section 4.3.1.2. This again confirms that in order to have an evenly temperature distribution, having the dedicated (separate) outlet is recommended.

The heating power consumption for all the 5 scenarios are compared in Figure 4.21 (left axis). It can be seen from the figure that the number of outlet locations has negligible effect on the heating power consumed by the basement and the second floor, when comparing the average heating power consumed during off-peak, mid-peak and peak periods between Scenario 1: Peak_HES_SF6,7 and Scenario 2: Peak_HES_SF5,6,7; Scenario 3: Peak_SF5,6,7 and Scenario 4: Peak_SF5,6,7, respectively.

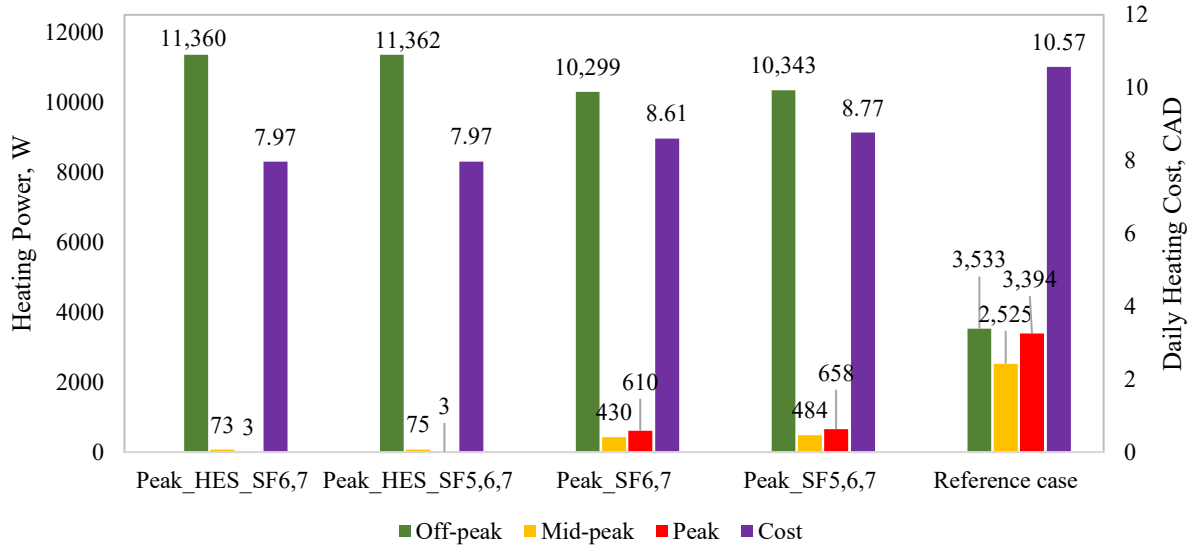

Figure 4.21: Average heating power consumed by the basement and the second floor during the off-peak period, mid-peak period and peak period (left axis) and daily heating cost (right axis)

It is worth stating that the proposed strategy (the integration of HES with EHF) could pave way for the utility companies to further shift the peak load. Figure 4.21 depicts that the decrease in peak consumption for the scenarios Peak_SF6,7 and Peak_SF5,6,7 compared to the reference case was 82.0% and 80.6%, respectively, while the reduction in mid-peak consumption was 83.0% and 80.8%. However, the combination of HES and peak shifting control (Peak_HES_SF6,7 and Peak_HES_SF5,6,7) almost completely decreased the peak consumption and 97% of the mid-peak consumption when comparing to the reference case. Thus it is construed that HES further extended the peak shifting capability of the EHF from ~80% to ~100%. However, note that compared with the reference case, due to prolonged heating during off-peak period in peak shifting control strategy, the daily energy consumed by space heating could be increased by around 18.1%.

On the other hand, it should be noted that the increased energy consumption will increase the heating cost to consumers (like Québec) where the electricity price does not vary for peak and off-peak periods. In order to analyze the effect of peak shifting on heating cost after considering the time-of use tariff, daily heating cost of these five scenarios are compared in Figure 4.21 based on time of use electricity price applicable to Ontario (HydroOne, 2017). It shows that Peak_SF6,7 and Peak_SF5,6,7 could decrease the daily electric heating fee by 18.6% and 17.0% respectively, while combining of HES and peak shifting strategy (Case I in Table 3.7) could decrease the daily heating fee by around 24.6%.

CHAPTER FIVE: CONCLUSION

5.1. SUMMARY AND CONCLUSION

The literature review on BITES for peak load shifting illustrated that both passive and active BITES system has the potential to completely shift the peak load. Both passive and active BITES system have its own advantages and disadvantages. The passive BITES system usually takes the advantage of local weather conditions for its operation instead of utilizing the external appliances (e.g. electrical heater for heating). However, in a passive BITES system, the processes of charging/discharging as well as peak shifting are hard to control. By contrast, the process of charging/discharging can be controlled (can be accelerated and decelerated) based on the requirements in an active BITES system. Besides, monitoring the active BITES is easier than the passive BITES. But the active BITES system depends on the external devices for their operation. In the recent years several advancements had been made in the BITES systems and the active BITES systems, such as EHF, HHF have gained more attention in building sector for their appreciable peak shifting and shaving abilities. Compared with passive systems, active BITES systems, especially EHF, are more suitable to shift heating load due to the convenience of charging controlling.

It should be mentioned that in most of the North American residential buildings, BITES systems such as EHF, HHF or PCM are only partially installed due to the practical constraints in the construction structure of such houses. To be more specific, most of the residential buildings in North America are built with wood and the basement is the only zone with the facility for having concrete slabs which can be utilized for TES. This challenge the installation of BITES system in all zones of a residential building. Further, if the partially installed BITES show the ability of providing enough heating/cooling and the potential of completely shifting the peak load of the room in which it is located, it can be extracted to heat other rooms without BITES system in the same building.

Considering the above challenge and the potential of BITES in peak shifting, the objective of this research is devised to investigate the possibilities of extending the heating and peak shifting

capacity of an existing BITES system - electrically heated floor (EHF) in residential buildings through the integration of heat extraction system (HES). Before implementing the HES in a residential building, it is first important to ensure that the existing BITES system (EHF) has the capability to store excessive energy within it. Hence, initially in this work, the peak shifting potential of an existing EHF (which was installed in the basement of a residential house, located in Québec, Canada) was investigated under different heating strategies by performing several simulation studies. Later, the ability of HES toward transferring the hot air from the basement to the second floor is investigated for various air flow rate and number of outlet locations.

In the present study, a multi-zone building model is initially developed in TRNSYS to perform the simulation studies. However, prediction of dynamic air flow in the zones was challenging in TRNSYS and hence, another multi-zone building model which called TRNSYS-CONTAM model was developed in TRNSYS with a link to CONTAM. Among the two developed models, the TRNSYS-CONTAM showed good agreement with measured data and thus the integrated TRNSYS-CONTAM model was considered as validated to predict the temperature distribution and energy consumption in an experimental house. It is found from the validation results that considering inter-zonal airflow in TRNSYS-CONTAM model increased the simulation accuracy of temperature and energy prediction, compared to the pure building energy (TRNSYS) model, in which the inter-zonal airflow was ignored due to the limitation in predicting it dynamically.

Later, the validated TRNSYS-CONTAM model was utilized to investigate the peak shifting potential of EHF based on two kinds of heating strategies: night-running strategy (NRS) and peak shifting strategy (PSS). The investigation results showed that both NRS and PSS can be implemented to charge the EHF to shift the peak load. The inference from the simulation results is that the NRS could take more advantageous of time of use tariff compared with PSS with the same set-point temperature for off-peak. However, it could not maintain the basement temperature above 20°C during late afternoon peak period in extremely cold days when its setpoint for off-peak period was 22 °C. On the other hand, PSS resolved the previous issue through recharging the EHF during mid peak-period. Besides, PSS with proper set-point temperature during off-peak period (e.g. 23°C or 24°C) almost completely shifted the power consumption (for heating) of basement from peak period to other periods. However, it should be noted that the existing EHF

system could only shift the power consumption of basement. Though the existing EHF possess the capacity to store the heat energy at higher temperature, it cannot be utilized to shift the peak load of the adjacent zones (ground, second floor).

In this regard, the HES was proposed and was found to be reliable to extract the heat from the EHF installed in the basement to the heat extendable areas of the same building. For the considered experimental house, if the source room (B1) was heated at the set-point temperature of 24 °C, a minimum air flow rate of 0.14 $m^3.s^{-1}$ (300 CFM) is sufficient to maintain $T_{ave,mean}$ at around 20 °C, while higher airflow would be needed to ensure that T_{min} remains higher than 15 °C. Beside airflow rate, the outlet location is another factor that should be considered when designing the HES. Separated outlets is recommended because it could result in better temperature distribution among the object rooms with almost the same power consumption compared with a single outlet.

The proposed integrated system (EHF + HES) would be beneficial for both the utility companies and the end user. The utility companies could take advantage of combining HES with EHFs from peak shifting perspective. Heating the basement based on a peak shifting control strategy and warming the second floor through the heat extraction system completely decreased the peak consumption of the basement and second floor, which was around 19% higher when heat extraction system was not considered. On the other hand, it is also inferred that the proposed methodology increases the energy consumption by 18% but decreases the daily heating cost by 24%. This reduction in daily heating cost will be a benefit to the consumers. It should be mentioned that the increase in energy consumption is due to the prolonged operation of the basement EHF during the off-peak period and the decrease in energy cost is because of shifting the peak to the off-peak period.

The Novelties of this research are :

• An HES was proposed to extend the heating and peak shifting capacity of an existing EHF in residential buildings.

• The influence of inter-zonal airflow on model accuracy is studied.

• The peak shifting potential of the existing EHF is studied based on both night-running and peak shifting strategy.

5.2. FUTURE WORK AND RECOMMENDATIONS

Based on the advancements of limitations of this present study, future work on the proposed HES to extend the peak shifting potential of BITES is recommended as followings:

- Experimental studies are required in order to verify the heating and peak shifting performance of proposed HES.
- The effect of HES on interior air quality can be studied.
- A control strategy can be designed to change the speed of fan in the HES system to control transferred air flow rate, in order to keep the interior temperature of the object room within an acceptable range with considering the effect on the total heating cost.
- The control of EHF should take into consider the dynamic change of heat extraction speed.

REFERENCES

Alaidroos, A., & Krarti, M. (2016). Numerical modeling of ventilated wall cavities with spray evaporative cooling system. *Energy and Buildings, 130*, 350-365. doi: https://doi.org/10.1016/j.enbuild.2016.08.046

Alaidroos, A., & Krarti, M. (2017). Optimized controls for ventilated wall cavities with spray evaporative cooling systems. *Energy and Buildings, 154*, 356-372. doi: https://doi.org/10.1016/j.enbuild.2017.08.076

Alva, G., Lin, Y., & Fang, G. (2018). An overview of thermal energy storage systems. *Energy, 144*, 341-378. doi: https://doi.org/10.1016/j.energy.2017.12.037

Amir, M., Lacroix, M., & Galanis, N. (1999). Comportement thermique de dalles chauffantes électriques pour le stockage quotidien. *International journal of thermal sciences, 38*(2), 121-131.

ANSI/BPI. (2015). Standard 2400-S-2015: Standard Practice for Standardized Qualification of Whole House Energy Savings Predictions by Calibration to Energy Use History.

ASHRAE. (2002). Guideline 14-2002: Measurement of Energy and Demand Savings, ASHRAE. *Atlanta*.

ASHRAE. (2014). Guideline 14-2014 *Measurement of energy, demand, and water savings*.

ASTM. (1999). Standard Test Methods for Determining Airtightness of Building Using an Orifice Blower Door: Annual Book of ASTM Standards (Volume 04.11) West Conshohocken.

Athienitis, A. K., Liu, C., Hawes, D., Banu, D., & Feldman, D. (1997). Investigation of the thermal performance of a passive solar test-room with wall latent heat storage. *Building and Environment, 32*(5), 405-410. doi: https://doi.org/10.1016/S0360-1323(97)00009-7

Barrio, M., Font, J., López, D. O., Muntasell, J., & Tamarit, J. L. (1992). Floor radiant system with heat storage by a solid-solid phase transition material. *Solar Energy Materials and Solar Cells, 27*(2), 127-133. doi: https://doi.org/10.1016/0927-0248(92)90115-6

Barzin, R., Chen, J. J. J., Young, B. R., & Farid, M. M. (2015). Peak load shifting with energy storage and price-based control system. *Energy, 92*, 505-514. doi: https://doi.org/10.1016/j.energy.2015.05.144

Bečkovský, D., Ostrý, M., & Kalábová, T. (2011). Thermal stability of attic spaces with integrated PCMin light building constructions during the climatic year. *KSI Trans, 4*(3), 54-57.

Bragança, L., Russo Ermolli, S., & Koukkari, H. (2011). Phase changing materials in buildings. *International Journal of Sustainable Building Technology and Urban Development, 2*(1), 43-51.

Buratti, C., Palladino, D., Moretti, E., & Palma, R. D. (2018). Development and optimization of a new ventilated brick wall: CFD analysis and experimental validation. *Energy and Buildings, 168*, 284-297. doi: https://doi.org/10.1016/j.enbuild.2018.03.041

Cabeza, L. F., Castellon, C., Nogues, M., Medrano, M., Leppers, R., & Zubillaga, O. (2007). Use of microencapsulated PCM in concrete walls for energy savings. *Energy and Buildings, 39*(2), 113-119.

Cabeza, L. F., Castellón, C., Nogués, M., Medrano, M., Leppers, R., & Zubillaga, O. (2007). Use of microencapsulated PCM in concrete walls for energy savings. *Energy and Buildings, 39*(2), 113-119. doi: https://doi.org/10.1016/j.enbuild.2006.03.030

Cabeza, L. F., Medrano Martorell, M., Castellón, C., Castell, A., Solé, C., Roca Enrich, J., & Nogués Aymamí, M. (2007). Thermal energy storage with phase change materials in building envelopes. *Contributions to Science, 2007, vol. 3, núm. 4, p. 501–510*.

Castell, A., Martorell, I., Medrano, M., Pérez, G., & Cabeza, L. F. (2010). Experimental study of using PCM in brick constructive solutions for passive cooling. *Energy and Buildings, 42*(4), 534-540.

Castellón, C., Castell, A., Medrano, M., Martorell, I., & Cabeza, L. (2009). Experimental study of PCM inclusion in different building envelopes. *Journal of Solar Energy Engineering, 131*(4), 041006.

Chae, Y. T., & Strand, R. K. (2013). Modeling ventilated slab systems using a hollow core slab: Implementation in a whole building energy simulation program. *Energy and Buildings, 57*, 165-175. doi: https://doi.org/10.1016/j.enbuild.2012.10.036

Chen, C., Ling, H., Yu, N., Li, N., Zhang, M., & Li, Y. (2016). Numerical Modelling of Thermal Performance of Active-passive Ventilation Wall with Phase Change Material. *Energy Procedia, 103*, 22-27. doi: https://doi.org/10.1016/j.egypro.2016.11.243

Chen, C., Ling, H., Zhai, Z., Li, Y., Yang, F., Han, F., & Wei, S. (2018). Thermal performance of an active-passive ventilation wall with phase change material in solar greenhouses. *Applied Energy, 216*, 602-612. doi: https://doi.org/10.1016/j.apenergy.2018.02.130

Chen, Y., Athienitis, A., & Galal, K. (2012). Thermal performance and charge control strategy of a ventilated concrete slab (VCS) with active cooling using outdoor air. *ASHRAE Transactions, 118*, 556.

Chen, Y., Galal, K., & Athienitis, A. K. (2010). Modeling, design and thermal performance of a BIPV/T system thermally coupled with a ventilated concrete slab in a low energy solar house: Part 2, ventilated concrete slab. *Solar Energy, 84*(11), 1908-1919. doi: https://doi.org/10.1016/j.solener.2010.06.012

Chen, Y., Galal, K. E., & Athienitis, A. K. (2014). Design and operation methodology for active building-integrated thermal energy storage systems. *Energy and Buildings, 84*, 575-585. doi: https://doi.org/10.1016/j.enbuild.2014.08.013

Chen, Y., Galal, K. E., & Athienitis, A. K. (2016). Integrating hollow-core masonry walls and precast concrete slabs into building space heating and cooling. *Journal of Building Engineering, 5*, 277-287.

Crawley, D. B., Hand, J. W., Kummert, M., & Griffith, B. T. (2008). Contrasting the capabilities of building energy performance simulation programs. *Building and Environment, 43*(4), 661-673. doi: https://doi.org/10.1016/j.buildenv.2006.10.027

Crawley, M. (2016). Ontario's smart meters failing to cut electricity demand. *[Online]. Avaliable:* http://www.cbc.ca/news/canada/toronto/smart-meters-hydro-bills-ontario-time-of-use-pricing-1.3862462.

Defraeye, T., Blocken, B., & Carmeliet, J. (2010). CFD analysis of convective heat transfer at the surfaces of a cube immersed in a turbulent boundary layer. *International Journal of Heat and Mass Transfer, 53*(1), 297-308.

Dols, W. S., Emmerich, S. J., & Polidoro, B. J. (2016). Using coupled energy, airflow and indoor air quality software (TRNSYS/CONTAM) to evaluate building ventilation strategies. *Building Services Engineering Research and Technology, 37*(2), 163-175.

Dols, W. S., & Polidoro, B. J. (2015). CONTAM User Guide and Program Documentation Version 3.2. *Technical Note (NIST TN)-1887*(1).

El Mays, A., Ammar, R., Hawa, M., Akroush, M. A., Hachem, F., Khaled, M., & Ramadan, M. (2017). Using phase change material in under floor heating. *Energy Procedia, 119*, 806-811. doi: https://doi.org/10.1016/j.egypro.2017.07.101

Emmerich, S., Howard-Reed, C., & Nabinger, S. (2004). Validation of multizone IAQ model predictions for tracer gas in a townhouse. *Building Services Engineering Research and Technology, 25*(4), 305-316.

Fallahi, A., Haghighat, F., & Elsadi, H. (2010). Energy performance assessment of double-skin façade with thermal mass. *Energy and Buildings, 42*(9), 1499-1509. doi: https://doi.org/10.1016/j.enbuild.2010.03.020

Farid, M., & Chen, X. (1999). Domestic electrical space heating with heat storage. *Proceedings of the Institution of Mechanical Engineers, Part A: Journal of Power and Energy, 213*(2), 83-92.

Fateh, A., Klinker, F., Brütting, M., Weinläder, H., & Devia, F. (2017). Numerical and experimental investigation of an insulation layer with phase change materials (PCMs). *Energy and Buildings, 153*, 231-240. doi: https://doi.org/10.1016/j.enbuild.2017.08.007

FEMP. (2015). M&V Guidelines: Measurement and Verification for Performance-Based Contracts: Version 4.0, Technical Report. U.S. Department of Energy Federal Energy Management Program.

Freris, L., & Infield, D. (2013). *Les énergies renouvelables pour la production d'électricité*: Dunod.

Guarino, F., Athienitis, A., Cellura, M., & Bastien, D. (2017). PCM thermal storage design in buildings: Experimental studies and applications to solaria in cold climates. *Applied Energy, 185*, 95-106. doi: https://doi.org/10.1016/j.apenergy.2016.10.046

Guerassimoff, G., & Maïzi, N. (2012). *Smart grids: au-delà du concept, comment rendre les réseaux plus intelligents*: Presses des MINES.

Haghighat, F., Jiang, Z., & Wang, J. (1991). A CFD Analysis of Ventilation Effectiveness in a Partitioned Room. *Indoor Air, 1*(4), 606-615. doi: doi:10.1111/j.1600-0668.1991.00022.x

Haghighat, F., & Megri, A. C. (1996). A Comprehensive Validation of Two Airflow Models — COMIS and CONTAM. *Indoor Air, 6*(4), 278-288. doi: 10.1111/j.1600-0668.1996.00007.x

HeavenlyHeat. (2018). "Radiant Floor Heating Solutions." [Online]. Avaliable: https://www.floorheatingsystemsinc.com/radiant-floor-heaters-toronto/radiant-floor-heating-electric-vs-hydronic-systems/.

Hydro-Québec. (2017). "Capacity and energy needs." *[Online]. Avaliable:* http://www.hydroquebec.com/sustainable-development/energy-environment/capacity-energy-needs.html.

HydroOne. (2017). Time-of-Use Demand Periods and Prices. [Online] Availiable: https://www.hydroone.com/rates-and-billing/rates-and-charges/electricity-pricing-and-costs.

Ip, K., & Miller, A. (2009). Thermal behaviour of an earth-sheltered autonomous building – The Brighton Earthship. *Renewable Energy, 34*(9), 2037-2043. doi: https://doi.org/10.1016/j.renene.2009.02.006

IPMVP. (2001). International Performance Measurement and Verification Protocol: Concepts and Options for Determining Energy and Water Savings, Volume I: National Renewable Energy Lab., Golden, CO (US).

Ismail, K., & Castro, J. (1997). PCM thermal insulation in buildings. *International Journal of Energy Research, 21*(14), 1281-1296.

Jiang, Z. (1990). *Intra-and inter-zone airflow with heat and mass transfer in multi-zone buildings.* Concordia University.

Jin, X., & Zhang, X. (2011). Thermal analysis of a double layer phase change material floor. *Applied Thermal Engineering, 31*(10), 1576-1581. doi: https://doi.org/10.1016/j.applthermaleng.2011.01.023

Kenisarin, M., & Mahkamov, K. (2016). Passive thermal control in residential buildings using phase change materials. *Renewable and Sustainable Energy Reviews, 55*, 371-398. doi: https://doi.org/10.1016/j.rser.2015.10.128

Khudhair, A., & Farid, M. (2009). *Use of phase change materials for thermal comfort and electrical energy peak load shifting: experimental investigations.* Paper presented at the International Conference on Solar energy and human settlement, Springer Berlin Heidelberg.

Kondo, T., Ibamoto, T., Tsubota, Y., & Kamata, M. (2001). Research on the thermal storage of PCM (Phase Change Material) Wallboard: The measurements of the thermal behavior and the effect of application as room side wall. *Journal of Architecture and Planning (Transactions of AIJ), 66*(540), 23-29. doi: 10.3130/aija.66.23_2

Konuklu, Y., & Paksoy, H. Ö. (2009). Phase change material sandwich panels for managing solar gain in buildings. *Journal of Solar Energy Engineering, 131*(4), 041012.

Koschenz, M., & Lehmann, B. (2004). Development of a thermally activated ceiling panel with PCM for application in lightweight and retrofitted buildings. *Energy and Buildings, 36*(6), 567-578. doi: https://doi.org/10.1016/j.enbuild.2004.01.029

Kosny, J., Kossecka, E., Brzezinski, A., Tleoubaev, A., & Yarbrough, D. (2012). Dynamic thermal performance analysis of fiber insulations containing bio-based phase change materials (PCMs). *Energy and Buildings, 52*, 122-131. doi: https://doi.org/10.1016/j.enbuild.2012.05.021

Krzaczek, M., & Kowalczuk, Z. (2011). Thermal Barrier as a technique of indirect heating and cooling for residential buildings. *Energy and Buildings, 43*(4), 823-837. doi: https://doi.org/10.1016/j.enbuild.2010.12.002

Kuznik, F., & Virgone, J. (2009a). Experimental assessment of a phase change material for wall building use. *Applied energy, 86*(10), 2038-2046.

Kuznik, F., & Virgone, J. (2009b). Experimental investigation of wallboard containing phase change material: Data for validation of numerical modeling. *Energy and Buildings, 41*(5), 561-570.

Kuznik, F., Virgone, J., & Roux, J.-J. (2008). Energetic efficiency of room wall containing PCM wallboard: A full-scale experimental investigation. *Energy and Buildings, 40*(2), 148-156.

Lanoue, R., & Mousseau, N. (2014). Maîtriser notre avenir énergétique. *Government of Quebec: Commission sur les enjeux energetiques du Quebec*.

Lansari, A., Streicher, J. J., Huber, A. H., Crescenti, G. H., Zweidinger, R. B., Duncan, J. W., . . . Burton, R. M. (1996). Dispersion of automotive alternative fuel vapors within a residence and its attached garage. *Indoor Air, 6*(2), 118-126.

Le Dréau, J., & Heiselberg, P. (2016). Energy flexibility of residential buildings using short term heat storage in the thermal mass. *Energy, 111*, 991-1002. doi: https://doi.org/10.1016/j.energy.2016.05.076

Lee, K. O., Medina, M. A., Raith, E., & Sun, X. (2015). Assessing the integration of a thin phase change material (PCM) layer in a residential building wall for heat transfer reduction and management. *Applied Energy, 137*, 699-706. doi: https://doi.org/10.1016/j.apenergy.2014.09.003

Lee, K. O., Medina, M. A., Sun, X., & Jin, X. (2018). Thermal performance of phase change materials (PCM)-enhanced cellulose insulation in passive solar residential building walls. *Solar Energy, 163*, 113-121. doi: https://doi.org/10.1016/j.solener.2018.01.086

Li, H. (2002). *Validation of three multi-zone airflow models.* Concordia University.

Lin, K., Zhang, Y., Xu, X., Di, H., Yang, R., & Qin, P. (2004). Modeling and simulation of under-floor electric heating system with shape-stabilized PCM plates. *Building and Environment, 39*(12), 1427-1434. doi: https://doi.org/10.1016/j.buildenv.2004.04.005

Lin, Z.-g., Zhang, S.-y., Fu, X.-z., & Wang, Y. (2006). Investigation of floor heating with thermal storage. *Journal of Central South University of Technology, 13*(4), 399-403.

Mandilaras, I., Stamatiadou, M., Katsourinis, D., Zannis, G., & Founti, M. (2013). Experimental thermal characterization of a Mediterranean residential building with PCM gypsum board walls. *Building and Environment, 61*, 93-103. doi: https://doi.org/10.1016/j.buildenv.2012.12.007

Mazo, J., Delgado, M., Marin, J. M., & Zalba, B. (2012). Modeling a radiant floor system with Phase Change Material (PCM) integrated into a building simulation tool: Analysis of a case study of a floor heating system coupled to a heat pump. *Energy and Buildings, 47*, 458-466. doi: https://doi.org/10.1016/j.enbuild.2011.12.022

. National Energy Code of Canada for Buildings, 2015. (2015) (3rd edition. ed.). Ottawa, ON: National Research Council.

Navarro, L., de Gracia, A., Castell, A., Álvarez, S., & Cabeza, L. F. (2015). PCM incorporation in a concrete core slab as a thermal storage and supply system: Proof of concept. *Energy and Buildings, 103*, 70-82. doi: https://doi.org/10.1016/j.enbuild.2015.06.028

Navarro, L., de Gracia, A., Colclough, S., Browne, M., McCormack, S. J., Griffiths, P., & Cabeza, L. F. (2016). Thermal energy storage in building integrated thermal systems: A review. Part 1. active storage systems. *Renewable Energy, 88*, 526-547. doi: https://doi.org/10.1016/j.renene.2015.11.040

Nirvan, G. (2011). *The Impact of Garage–House Interface Leakage on Contaminant Transport.* Concordia University.

NRCAN. (2016). Energy Efficiency Trends in Canada 1990 to 2013: Canada.

Olsthoorn, D. (2017). *Key Parameters and Guidelines for the Design of an Electrically Activated Concrete Slab for Peak Shifting in a Light-Weight Residential Building in a Northern Climate.* Concordia University.

Olsthoorn, D., Haghighat, F., Moreau, A., & Lacroix, G. (2017). Abilities and limitations of thermal mass activation for thermal comfort, peak shifting and shaving: A review. *Building and Environment, 118*, 113-127. doi: https://doi.org/10.1016/j.buildenv.2017.03.029

Orme, M., Liddament, M., & Wilson, A. (1994). An analysis and data summary of the AIVC's numerical database. Technical note AIVC, 44.

Ostrý, M., Bečkovský, D., & Charvat, P. (2011). Potential of passive cooling for cooling for office buildings. *KSI Trans, 4*(3), 52-53.

Pan, Y., Huang, Z., & Wu, G. (2007). Calibrated building energy simulation and its application in a high-rise commercial building in Shanghai. *Energy and Buildings, 39*(6), 651-657. doi: https://doi.org/10.1016/j.enbuild.2006.09.013

Pomianowski, M., Heiselberg, P., & Jensen, R. L. (2012). Dynamic heat storage and cooling capacity of a concrete deck with PCM and thermally activated building system. *Energy and Buildings, 53*, 96-107.

Principi, P., Di Perna, C., Borrelli, G., & Carbonari, A. (2005). *Experimental energetic evaluation of changeable thermal inertia PCM containing walls.* Paper presented at the International Conference on Passive and Low Energy Cooling for the Built Environment, Greece.

Prívara, S., Široký, J., Ferkl, L., & Cigler, J. (2011). Model predictive control of a building heating system: The first experience. *Energy and Buildings, 43*(2), 564-572. doi: https://doi.org/10.1016/j.enbuild.2010.10.022

Qian, B., Gregorich, E. G., Gameda, S., Hopkins, D. W., & Wang, X. L. (2011). Observed soil temperature trends associated with climate change in Canada. *Journal of Geophysical Research: Atmospheres, 116*(D2).

Raymer, P. (2009). *Residential ventilation handbook: ventilation to improve indoor air quality*: McGraw Hill Professional.

Rettino-Parazelli, K. (2017). Hydro-Québec offrira une tarification variable, *Le Devoir*.

Robertson, J., Polly, B., & Collis, J. (2013). *Evaluation of automated model calibration techniques for residential building energy simulation*: National Renewable Energy Laboratory.

Robillart, M., Schalbart, P., Chaplais, F., & Peuportier, B. (2018). Model reduction and model predictive control of energy-efficient buildings for electrical heating load shifting. *Journal of Process Control*. doi: https://doi.org/10.1016/j.jprocont.2018.03.007

Romanchenko, D., Kensby, J., Odenberger, M., & Johnsson, F. (2018). Thermal energy storage in district heating: Centralised storage vs. storage in thermal inertia of buildings. *Energy Conversion and Management, 162*, 26-38. doi: https://doi.org/10.1016/j.enconman.2018.01.068

Romaní, J., Belusko, M., Alemu, A., Cabeza, L. F., de Gracia, A., & Bruno, F. (2018). Control concepts of a radiant wall working as thermal energy storage for peak load shifting of a heat pump coupled to a PV array. *Renewable Energy, 118*, 489-501. doi: https://doi.org/10.1016/j.renene.2017.11.036

Romaní, J., Cabeza, L. F., & de Gracia, A. (2018). Development and experimental validation of a transient 2D numeric model for radiant walls. *Renewable Energy, 115*, 859-870. doi: https://doi.org/10.1016/j.renene.2017.08.019

Romaní, J., Pérez, G., & de Gracia, A. (2016). Experimental evaluation of a cooling radiant wall coupled to a ground heat exchanger. *Energy and Buildings, 129*, 484-490. doi: https://doi.org/10.1016/j.enbuild.2016.08.028

Rudd, A. F. (1993). Phase-change material wallboard for distributed thermal storage in buildings. *Transactions - American Society of Heating, Refrigerating and Air-Conditioning Engineers, 99*, 339-339.

Ruiz, G. R., & Bandera, C. F. (2017). Validation of Calibrated Energy Models: Common Errors. *Energies, 10*(10), 1587.

Saelens, D., Parys, W., & Baetens, R. (2011). Energy and comfort performance of thermally activated building systems including occupant behavior. *Building and Environment, 46*(4), 835-848.

Scalat, S., Banu, D., Hawes, D., Parish, J., Haghighata, F., & Feldman, D. (1996). Full scale thermal testing of latent heat storage in wallboard. *Solar Energy Materials and Solar Cells, 44*(1), 49-61.

Schossig, P., Henning, H.-M., Gschwander, S., & Haussmann, T. (2005). Micro-encapsulated phase-change materials integrated into construction materials. *Solar Energy Materials and Solar Cells, 89*(2-3), 297-306.

Shilei, L., Guohui, F., Neng, Z., & Li, D. (2007). Experimental study and evaluation of latent heat storage in phase change materials wallboards. *Energy and buildings, 39*(10), 1088-1091.

Shilei, L., Neng, Z., & Guohui, F. (2006). Impact of phase change wall room on indoor thermal environment in winter. *Energy and buildings, 38*(1), 18-24.

Thieblemont, H. (2017). *Simplified Predictive Control for Load Management: A Self-Learning Approach Applied to Electrically Heated Floor.* Concordia University.

Thieblemont, H., Haghighat, F., & Moreau, A. (2016). Thermal Energy Storage for Building Load Management: Application to Electrically Heated Floor. *Applied Sciences, 6*(7), 194.

Thieblemont, H., Haghighat, F., Moreau, A., Bastani, A., & Kuznik, F. (2016). *Alternative Method to Integrate Electrically Heated Floor in TRNSYS: Load Management*.

Thieblemont, H., Haghighat, F., Moreau, A., & Lacroix, G. (2018). Control of electrically heated floor for building load management: A simplified self-learning predictive control approach. *Energy and Buildings*. doi: https://doi.org/10.1016/j.enbuild.2018.04.042

Thieblemont, H., Moreau, A., Lacroix, G., & Haghighat, F. (2017). *Simplified Anticipatory control for Load Management: Application to Electrically Heated Floor*. Paper presented at the Internation Conference & Workshop REMOO 2017, Venice, Italy.

Turner, C., & Tovey, N. (2006). Case Study on the Energy Performance of the Zuckerman Institute for Connective Environmental Research (ZICER) Building. *ASHRAE transactions, 112*(2).

Ünalan, S., & Özrahat, E. (2014). The concrete columns as a sensible thermal energy storage medium and a heater. *Heat and Mass Transfer, 50*(8), 1037-1052. doi: 10.1007/s00231-014-1313-5

Voelker, C., Kornadt, O., & Ostry, M. (2008). Temperature reduction due to the application of phase change materials. *Energy and Buildings, 40*(5), 937-944.

Wang, S., & Xu, X. (2006). Simplified building model for transient thermal performance estimation using GA-based parameter identification. *International Journal of Thermal Sciences, 45*(4), 419-432. doi: https://doi.org/10.1016/j.ijthermalsci.2005.06.009

Xia, Y., & Zhang, X.-S. (2016). Experimental research on a double-layer radiant floor system with phase change material under heating mode. *Applied Thermal Engineering, 96*, 600-606. doi: https://doi.org/10.1016/j.applthermaleng.2015.11.133

Yang, L., Dong, C., Wan, C. L. J., & Ng, C. T. (2013). Electricity time-of-use tariff with consumer behavior consideration. *International Journal of Production Economics, 146*(2), 402-410. doi: https://doi.org/10.1016/j.ijpe.2013.03.006

Yu, J., Ye, H., Xu, X., Huang, J., Liu, Y., & Wang, J. (2018). Experimental study on the thermal performance of a hollow block ventilation wall. *Renewable Energy, 122*, 619-631. doi: https://doi.org/10.1016/j.renene.2018.01.126

Zhang, M., Medina, M. A., & King, J. B. (2005). Development of a thermally enhanced frame wall with phase-change materials for on-peak air conditioning demand reduction and energy savings in residential buildings. *International Journal of Energy Research, 29*(9), 795-809. doi: doi:10.1002/er.1082

Zhou, G., & He, J. (2015). Thermal performance of a radiant floor heating system with different heat storage materials and heating pipes. *Applied Energy, 138*, 648-660. doi: https://doi.org/10.1016/j.apenergy.2014.10.058

Zhu, L., Hurt, R., Correia, D., & Boehm, R. (2009). Detailed energy saving performance analyses on thermal mass walls demonstrated in a zero energy house. *Energy and Buildings, 41*(3), 303-310. doi: https://doi.org/10.1016/j.enbuild.2008.10.003

APPENDIX A - BUILDING INFORMATION

A.1. Elevation view

A.1.1. Front elevation

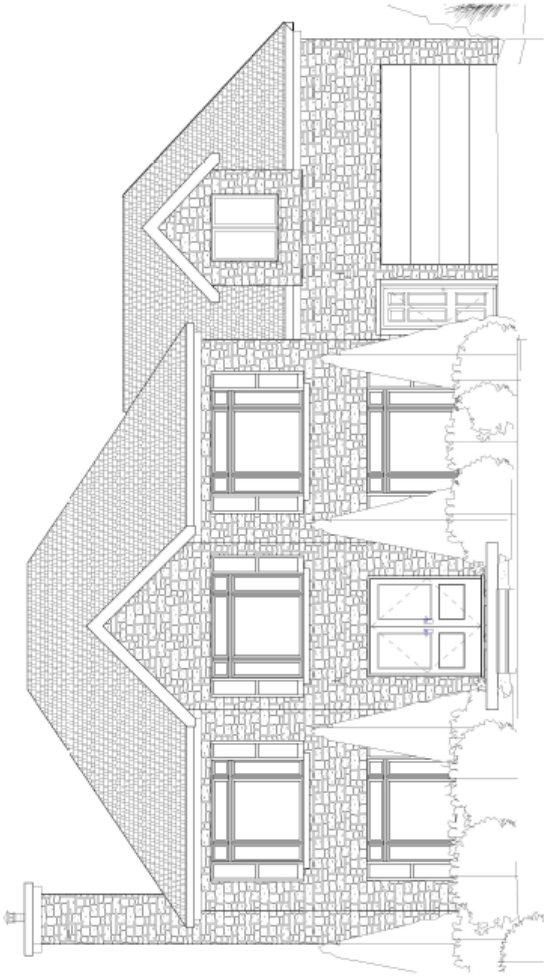

A.1.2. Right elevation

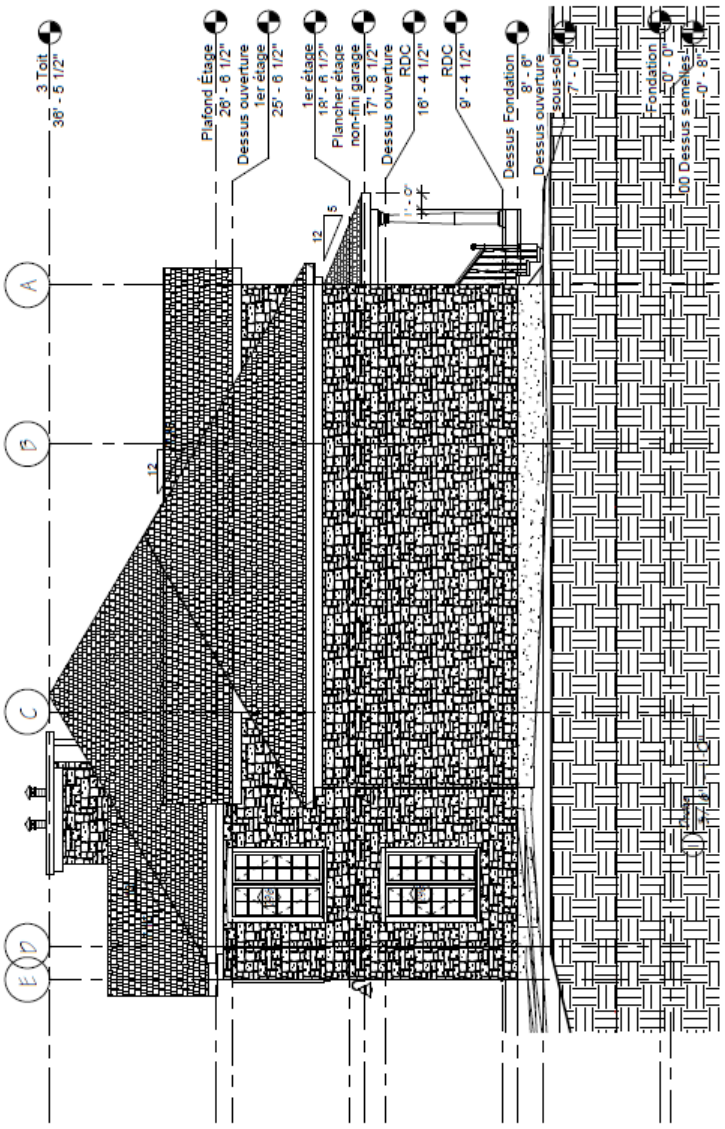

A.1.3. Back elevation

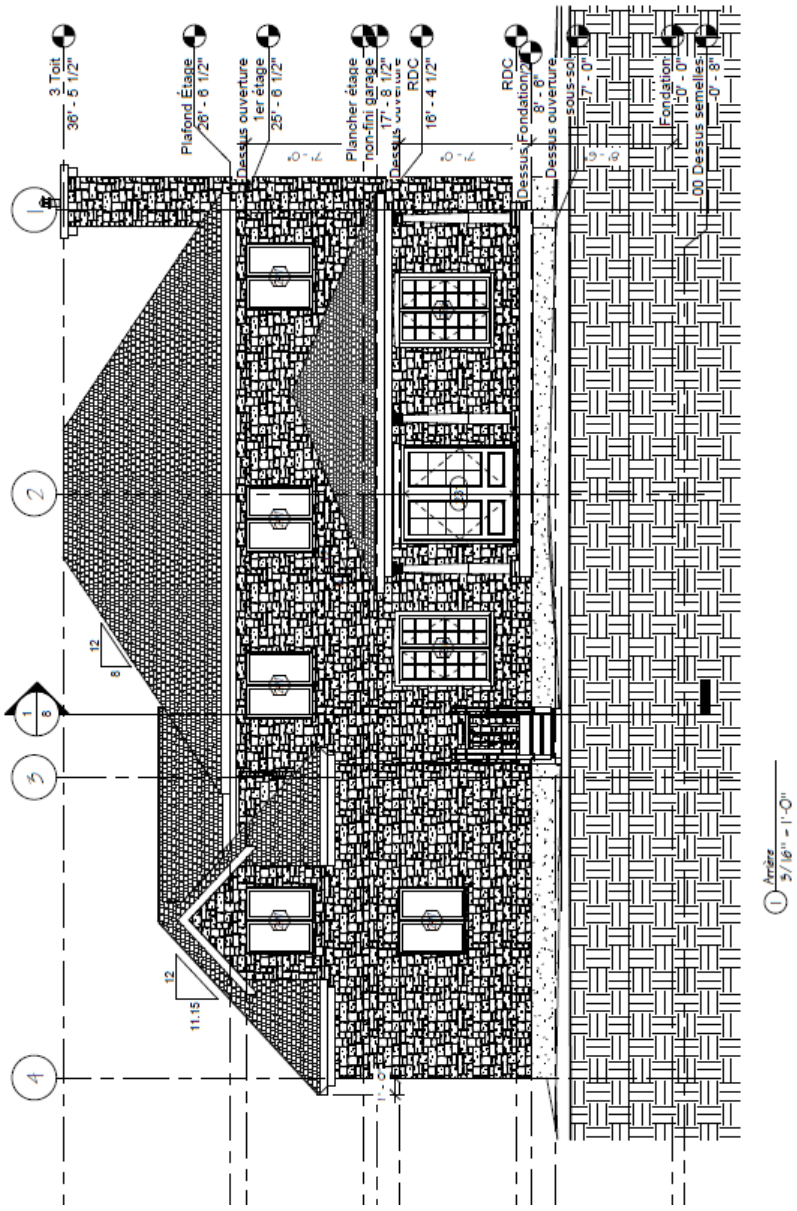

A.1.4. Left elevation

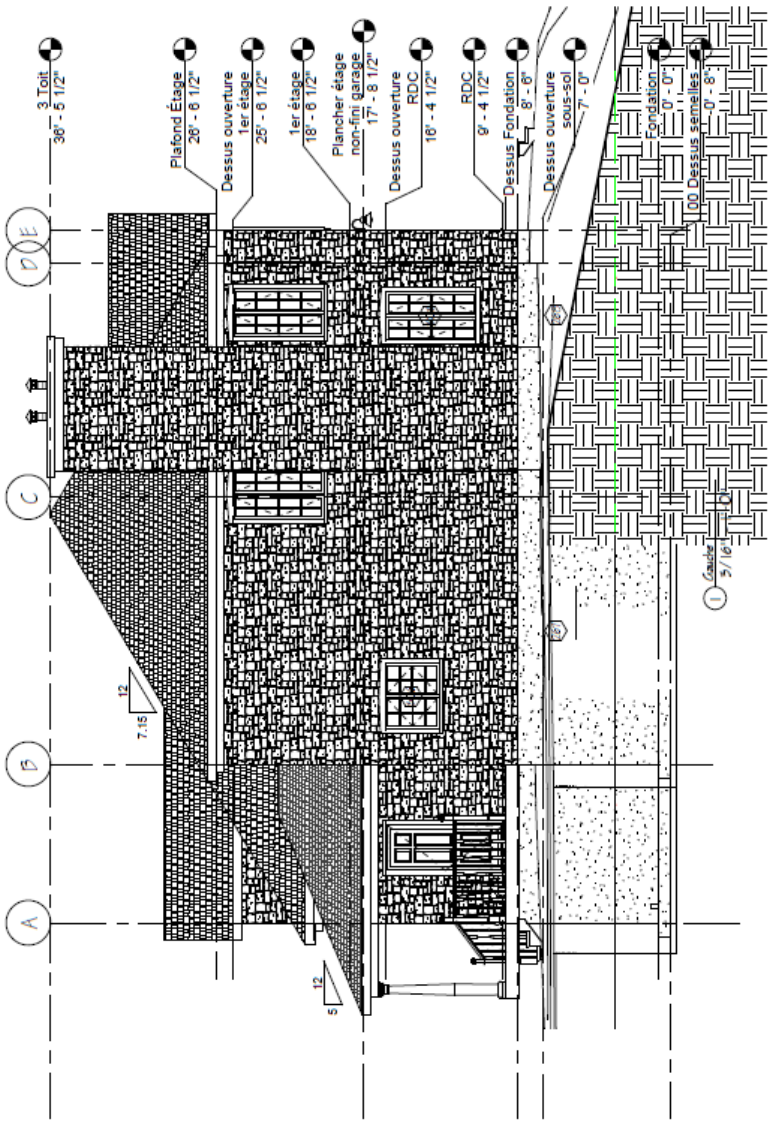

A.2. Materials and their properties of building envelopes

Wall Name	Description	Materials	L [m]	ρ [kg/m^3]	c_p [kJ/kg·K]	k [kJ/h·m·K]
FLOOR_BAS_BOT	Basement slab below heating wires	Concrete	0.1143	2240	0.9	7.02
		Extruded Polystyrene	0.05	25	1.47	0.1023
FLOOR_BAS_TOP	Basement slab above heating wires	Stratified wood flooring	0.0095	650	1.2	0.504
		Concrete	0.1143	2240	0.9	7.02
FLOOR_BAS_TOP_SDB	Basement slab above heating wires in bathroom	Porcelain Tiles	0.0064	2000	1	4.32
		Ceramic adhesive	0.0064	1920	0.84	5.04
		Concrete	0.1143	2240	0.9	7.02
EXT_EARTH	Foundation wall in contact with earth	Concrete	0.254	2240	0.9	7.02
		Expanded polystyrene	0.0508	16	1.2	0.144
		Air space	0.0159	-	-	0.3378
		Gypsum panel	0.0127	480	1.09	0.571
EXT	Foundation wall adjacent to exterior	Stucco	0.0064	1857	0.9	2.592
		Concrete	0.254	2240	0.9	7.02
		Expanded polystyrene	0.0508	16	1.2	0.144
		Air space with furring strips	0.0159	-	-	0.3378
		Gypsum panel	0.0127	480	1.09	0.571
GYPSE1	Interior wall, 2x6 assembly	Gypsum panel	0.0127	480	1.09	0.571
		Air space with 2x6 @ 0.406m	0.1397	54.86	1.047	1.264
		Gypsum panel	0.0127	480	1.09	0.571
GYPSE2	Interior wall, 2x4 assembly	Gypsum panel	0.0127	480	1.09	0.571
		Air space with 2x4 @ 0.406m	0.0889	54.86	1.047	0.161
		Gypsum panel	0.0127	480	1.09	0.571
NOTHING	Fictitious division of concave room to convex room	Massless Layer	-	-	-	-
FLOOR_LIV	Floor assembly with hardwood cover	Hardwood flooring	0.0191	670	1.63	0.5904
		Tung and groove plywood	0.0159	800	1.2	0.5400
		Air space with wood open-web joists @ 0.406m	0.3937	126.41	1.092	1.546
		Acoustic tile	0.0127	288	1.34	0.206
FLOOR_KIT	Floor assembly with ceramic cover, heated floor	Porcelain tile	0.0064	2000	1	4.32
		Ceramic adhesive	0.0064	1920	0.84	5.04
		Self-leveling concrete with heated wires	0.0064	400	0.84	0.36
		Tung and groove plywood	0.0318	800	1.2	0.5400
		Air space with wood open-web joists @ 0.406m	0.3937	126.41	1.092	1.546
		Acoustic tile	0.0127	288	1.34	0.206
CON_INT	Structural concrete wall	Gypsum panel	0.0127	480	1.09	0.571
		Air space	0.0159	-	-	0.3378
		Concrete	0.254	2240	0.9	7.02
FLOOR_BATH_2ND	2nd storey floor assembly, ceramic cover	Porcelain tile	0.0064	2000	1	4.32
		Ceramic adhesive	0.0064	1920	0.84	5.04
		Self-leveling concrete with heated wires	0.0064	400	0.84	0.36
		Tung and groove plywood	0.0318	800	1.2	0.5400

Wall Name	Description	Materials	L [m]	ρ [kg/m^3]	c_p [kJ/kg·K]	k [kJ/h·m·K]
		Air space with wood open-web joists @ 0.406m	0.3366	126.41	1.092	1.500
		Gypsum panel	0.0127	480	1.09	0.571
FLOOR_WOOD	2nd storey floor assembly, hard wood cover	Hardwood flooring	0.0191	670	1.63	0.5904
		Tung and groove plywood	0.0159	800	1.2	0.5400
		Air space with wood open-web joists @ 0.406m	0.3366	126.41	1.092	1.500
		Gypsum panel	0.0127	480	1.09	0.571
FLOOR_BATH_RDC	Floor assembly, ceramic cover, no heated floor	Porcelain tile	0.0064	2000	1	4.32
		Ceramic adhesive	0.0064	1920	0.84	5.04
		Tung and groove plywood	0.0318	800	1.2	0.5400
		Air space with wood open-web joists @ 0.406m	0.3937	126.41	1.092	1.546
		Acoustic tile	0.0127	288	1.34	0.206
FLOOR_GAR	Garage structural concrete floor	Concrete	0.2286	2240	0.9	7.02
		Extruded Polystyrene	0.0254	25	1.47	0.1023
		Air space	0.0159	-	-	0.4293
		Gypsum panel	0.0127	480	1.09	0.571
SHOWER_2ND	Interior division, ceramic cover on one side	Porcelain tile	0.0064	2000	1	4.32
		Ceramic adhesive	0.0064	1920	0.84	5.04
		Gypsum Panel	0.0127	800	1.09	0.5787
		Air space with 2x4 @ 0.406m	0.0889	54.86	1.047	0.161
		Gypsum panel	0.0127	480	1.09	0.571
FLOOR_ATTIC	Attic floor	Mineral Wool with 2x4@0.609m	0.254	-	-	0.01398
		BP Enermax & airspace	0.0286	-	-	0.0376
		Gypsum panel	0.0127	480	1.09	0.571
ROOF_INS	Cathedral ceiling	Asphalt Shingles	-	-	-	0.0214
		Roofing O.S.B.	0.0110	-	-	0.468
		Airspace with stud @ 0.609m	0.0254	36.94	1.035	0.188
		Mineral wool & joist @ 0.609m	0.254	44.81	0.874	0.166
		BP Enermax & airspace	0.0286	-	-	0.0376
		Gypsum panel	0.0127	480	1.09	0.571
WALL_EXT	Uninsulated exterior wall	Brick	0.0889	2002	0.92	4.8
		Air space	0.0254	-	-	0.439[3]
		Asphalt impregnated fiber board	0.0127	288	1.3	0.547
EXTERIOR	Insulated exterior wall	Brick	0.0889	2002	0.92	4.8
		Air space	0.0254	-	-	0.439
		Asphalt impregnated fiber board	0.0127	288	1.3	0.547
		Mineral wool with 2x6 @ 0.4064m	0.1397	62.42	0.891	0.170
		BP Enermax & airspace	0.0286	-	-	0.0376
		Gypsum panel	0.0127	480	1.09	0.571
ROOF_EXT	Attic roof	Asphalt Shingles	-	-	-	0.0214
		Roofing O.S.B.	0.0110	-	-	0.468

APPENDIX B - AIR LEAKAGE PERFORMANCE OF EACH COMPONENT

Based on National Energy Code of Canada for Buildings (2015)								
Stairs	Room	Type	Area m^2	$Q_{i,75Pa}$ L	$n_{i,lit}$	$K_{i,lit}$ $L/(s.m^2.Pa^n)$	$Q_{i,lit}$ L/s	C_i $L/(s.Pa^n)$
External door dimension								
Ground floor	GF2	Main entry exterior doors	3.855	5	0.600	0.375	5.755	1.445
	GF3	Other exterior doors	1.714	0.5	0.600	0.037	0.256	0.064
		Other exterior doors	1.734	0.5	0.600	0.037	0.259	0.065
		Main entry exterior doors	7.804	5	0.600	0.375	11.648	2.926
	GF1	Main entry exterior doors	3.829	5	0.600	0.375	5.715	1.435
Window								
Basement	B1	Operable windows	0.557	0.5	0.600	0.037	0.083	0.021
	B2	Operable windows	0.743	0.5	0.600	0.037	0.111	0.028
	B3	Operable windows	0.743	0.5	0.600	0.037	0.111	0.028
	B5	Operable windows	0.743	0.5	0.600	0.037	0.111	0.028
	B4	Operable windows	0.557	0.5	0.600	0.037	0.083	0.021
Ground floor	GF2	Operable windows	3.194	0.5	0.600	0.037	0.477	0.120
		Operable windows	3.194	0.5	0.600	0.037	0.477	0.120
		Operable windows	2.044	0.5	0.600	0.037	0.305	0.077
		Operable windows	1.533	0.5	0.600	0.037	0.229	0.057
	GF1	Operable windows	3.829	0.5	0.600	0.037	0.571	0.144
		Operable windows	2.044	0.5	0.600	0.037	0.305	0.077
		Operable windows	2.044	0.5	0.600	0.037	0.305	0.077
	GF3	Operable windows	1.486	0.5	0.600	0.037	0.222	0.056
Second floor	SF1	Operable windows	1.486	0.5	0.600	0.037	0.222	0.056
	SF2	Operable windows	1.486	0.5	0.600	0.037	0.222	0.056
	SF4	Operable windows	1.486	0.5	0.600	0.037	0.222	0.056
	SF5	Operable windows	1.486	0.5	0.600	0.037	0.222	0.056
		Operable windows	1.486	0.5	0.600	0.037	0.222	0.056
	SF3	Operable windows	3.194	0.5	0.600	0.037	0.477	0.120
		Operable windows	3.194	0.5	0.600	0.037	0.477	0.120
		Operable windows	2.044	0.5	0.600	0.037	0.305	0.077
	SF6	Operable windows	3.194	0.5	0.600	0.037	0.477	0.120
		Operable windows	1.533	0.5	0.600	0.037	0.229	0.057
	SF7	Operable windows	1.533	0.5	0.600	0.037	0.229	0.057

Based on National Energy Code of Canada for Buildings (2015)								
Stairs	Room	Type	Area m^2	$Q_{i,75Pa}$ L	$n_{i,lit}$	$K_{i,lit}$ L $/(s.m^2.Pa^n)$	$Q_{i,lit}$ L/s	C_i $L/(s.Pa^n)$
Wall								
Ground floor	GF2	South	32.640	0.2	0.810	0.006	1.276	0.198
		West	14.690	0.2	0.810	0.006	0.574	0.089
		East	9.320	0.2	0.810	0.006	0.364	0.056
	GF1	West	13.160	0.2	0.810	0.006	0.515	0.080
		North	24.240	0.2	0.810	0.006	0.948	0.147
	GF3	East	23.424	0.2	0.810	0.006	0.916	0.142
		North	16.180	0.2	0.810	0.006	0.633	0.098
		West	5.700	0.2	0.810	0.006	0.223	0.035
		South	4.320	0.2	0.810	0.006	0.169	0.026
Second floor	SF6	South	12.480	0.2	0.810	0.006	0.488	0.076
		West	10.320	0.2	0.810	0.006	0.404	0.063
	SF7	West	8.550	0.2	0.810	0.006	0.334	0.052
	SF1	West	10.471	0.2	0.810	0.006	0.409	0.063
		North	10.250	0.2	0.810	0.006	0.401	0.062
	SF2	North	9.270	0.2	0.810	0.006	0.363	0.056
	SF4	North	7.100	0.2	0.810	0.006	0.278	0.043
	SF3	East	8.664	0.2	0.810	0.006	0.339	0.052
		South	21.950	0.2	0.810	0.006	0.858	0.133
	SF5	North	13.750	0.2	0.810	0.006	0.538	0.083
		East	2.338	0.2	0.810	0.006	0.091	0.014
		West	2.338	0.2	0.810	0.006	0.091	0.014
		South	13.750	0.2	0.810	0.006	0.538	0.083
		East	2.338	0.2	0.810	0.006	0.091	0.014
		West	2.338	0.2	0.810	0.006	0.091	0.014
		West	4.863	0.2	0.810	0.006	0.190	0.029
		East	9.844	0.2	0.810	0.006	0.385	0.060
Attic		North	31.530	0.200	0.810	0.006	1.221	0.189
		East	19.890	0.200	0.810	0.006	0.771	0.119
		West	24.540	0.200	0.810	0.006	0.951	0.147
		South	31.530	0.200	0.810	0.006	1.221	0.189
		North	8.390	0.200	0.810	0.006	0.325	0.050
		East	13.070	0.200	0.810	0.006	0.506	0.078
		West	9.750	0.200	0.810	0.006	0.378	0.059
		South	7.000	0.200	0.810	0.006	0.271	0.042

Based on National Energy Code of Canada for Buildings (2015)								
Stairs	Room	Type	Area m^2	$Q_{i,75Pa}$ L	$n_{i,lit}$	$K_{i,lit}$ L $/(s.m^2.Pa^n)$	$Q_{i,lit}$ L/s	C_i $L/(s.Pa^n)$
		North	1.000	0.200	0.810	0.006	0.039	0.006
		South	1.000	0.200	0.810	0.006	0.039	0.006
$Total_{wdw}$							47.55	

Based on Air Infiltration and Ventilation Centre Technical note - AIVC 44 (1994)								
Stairs	Room	Type	Perimeter m^2	$K_{i,lit}$ L $/(s.m.Pa^$	$n_{i,lit}$	$C_{i,lit}$ $L/(s.Pa^n)$	$Q_{i,lit}$ L/s	C_i $L/(s.Pa^n))$
Door/Wall								
Ground floor	GF2	caulked joint	12.090	0.003	0.600	0.030	0.120	0.446
	GF3	caulked joint	5.842	0.003	0.600	0.015	0.058	0.223
		caulked joint	5.893	0.003	0.600	0.015	0.059	0.223
		caulked joint	11.582	0.003	0.600	0.029	0.115	0.431
	GF1	caulked joint	12.065	0.003	0.600	0.030	0.120	0.446
Window/Wall								
Ground floor	GF2	caulked joint	10.516	0.003	0.600	0.026	0.105	0.387
		caulked joint	10.516	0.003	0.600	0.026	0.105	0.387
		caulked joint	9.144	0.003	0.600	0.023	0.091	0.342
		caulked joint	8.534	0.003	0.600	0.021	0.085	0.312
	GF1	caulked joint	9.144	0.003	0.600	0.023	0.091	0.342
		caulked joint	9.144	0.003	0.600	0.023	0.091	0.342
		caulked joint	6.502	0.003	0.600	0.016	0.065	0.238
	GF3	caulked joint	7.315	0.003	0.600	0.018	0.073	0.268
Second floor	SF1	caulked joint	7.315	0.003	0.600	0.018	0.073	0.268
	SF2	caulked joint	7.315	0.003	0.600	0.018	0.073	0.268
	SF4	caulked joint	7.315	0.003	0.600	0.018	0.073	0.268
	SF5	caulked joint	7.315	0.003	0.600	0.018	0.073	0.268
		caulked joint	7.315	0.003	0.600	0.018	0.073	0.268
	SF3	caulked joint	10.516	0.003	0.600	0.026	0.105	0.387
		caulked joint	10.516	0.003	0.600	0.026	0.105	0.387
		caulked joint	9.144	0.003	0.600	0.023	0.091	0.342
	SF6	caulked joint	10.516	0.003	0.600	0.026	0.105	0.387
		caulked joint	8.534	0.003	0.600	0.021	0.085	0.312
	SF7	caulked joint	8.534	0.003	0.600	0.021	0.085	0.312
wall/Ceiling and wall/floor								

Based on Air Infiltration and Ventilation Centre Technical note - AIVC 44 (1994)								
Stairs	Room	Type	Perimeter m^2	$K_{i,lit}$ $L/(s.m.Pa^1$	$n_{i,lit}$	$C_{i,lit}$ $L/(s.Pa^n)$	$Q_{i,lit}$ L/s	C_i $L/(s.Pa^n))$
Ground floor	GF2	ceiling	17.488	0.024	0.600	0.420	1.671	6.245
		floor	17.488	0.024	0.600	0.420	1.671	6.245
	GF1	ceiling	15.278	0.024	0.600	0.367	1.460	5.457
		floor	15.278	0.024	0.600	0.367	1.460	5.457
	GF3	ceiling	23.012	0.024	0.600	0.552	2.199	8.208
		floor	23.012	0.024	0.600	0.552	2.199	8.208
Second floor	SF6	ceiling	5.398	0.024	0.600	0.130	0.516	1.933
		floor	5.398	0.024	0.600	0.130	0.516	1.933
	SF7	ceiling	2.362	0.024	0.600	0.057	0.226	0.848
		floor	2.362	0.024	0.600	0.057	0.226	0.848
	SF1	ceiling	8.014	0.024	0.600	0.192	0.766	2.855
		floor	8.014	0.024	0.600	0.192	0.766	2.855
	SF2	ceiling	3.505	0.024	0.600	0.084	0.335	1.249
		floor	3.505	0.024	0.600	0.084	0.335	1.249
	SF4	ceiling	2.591	0.024	0.600	0.062	0.248	0.922
		floor	2.591	0.024	0.600	0.062	0.248	0.922
	SF3	ceiling	9.347	0.024	0.600	0.224	0.893	3.331
		floor	9.347	0.024	0.600	0.224	0.893	3.331
	SF5	ceiling	23.012	0.024	0.600	0.552	2.199	8.208
		floor	23.012	0.024	0.600	0.552	2.199	8.208
$Total_{AIVC}$							23.138	
$Total_{test}$							344.05	

APPENDIX C - INFILTRATION COMPARISON

Stairs	Room	Infiltration rate, L/s	
		TRNSYS model	TRNSYS/CONTAM model
Basement	B1	17.14	0.08
	B2	12.89	0.11
	B3	9.08	0.11
	B4	21.09	0.08
	B5	13.11	0.11
Ground floor	GF1	38.43	57.26
	GF2	51.41	66.64
	GF3	83.26	84.24
Second floor	SF1	13.08	24.83
	SF2	9.30	11.60
	SF3	34.58	33.42
	SF4	8.72	8.91
	SF5	45.62	69.94
	SF6	23.10	19.78
	SF7	11.04	8.55
Attic		0.00	5.71
Total		391.60	391.37